When does the stress-gradient hypothesis hold true in a treeline ecotone?

Master's degree programme in Environmental Sciences

Master's thesis by Jamila Gisler (20-942-579)

Supervisor: Dr. Peter Bebi
WSL Institute for Snow and Avalanche Research SLF,
Mountain Ecosystems

Co-Supervisors: Dr. Melissa Dawes and Dr. Wouter Hantson
WSL Institute for Snow and Avalanche Research SLF,
Mountain Ecosystems

Photo by Michelle Kobler

19.01.2026

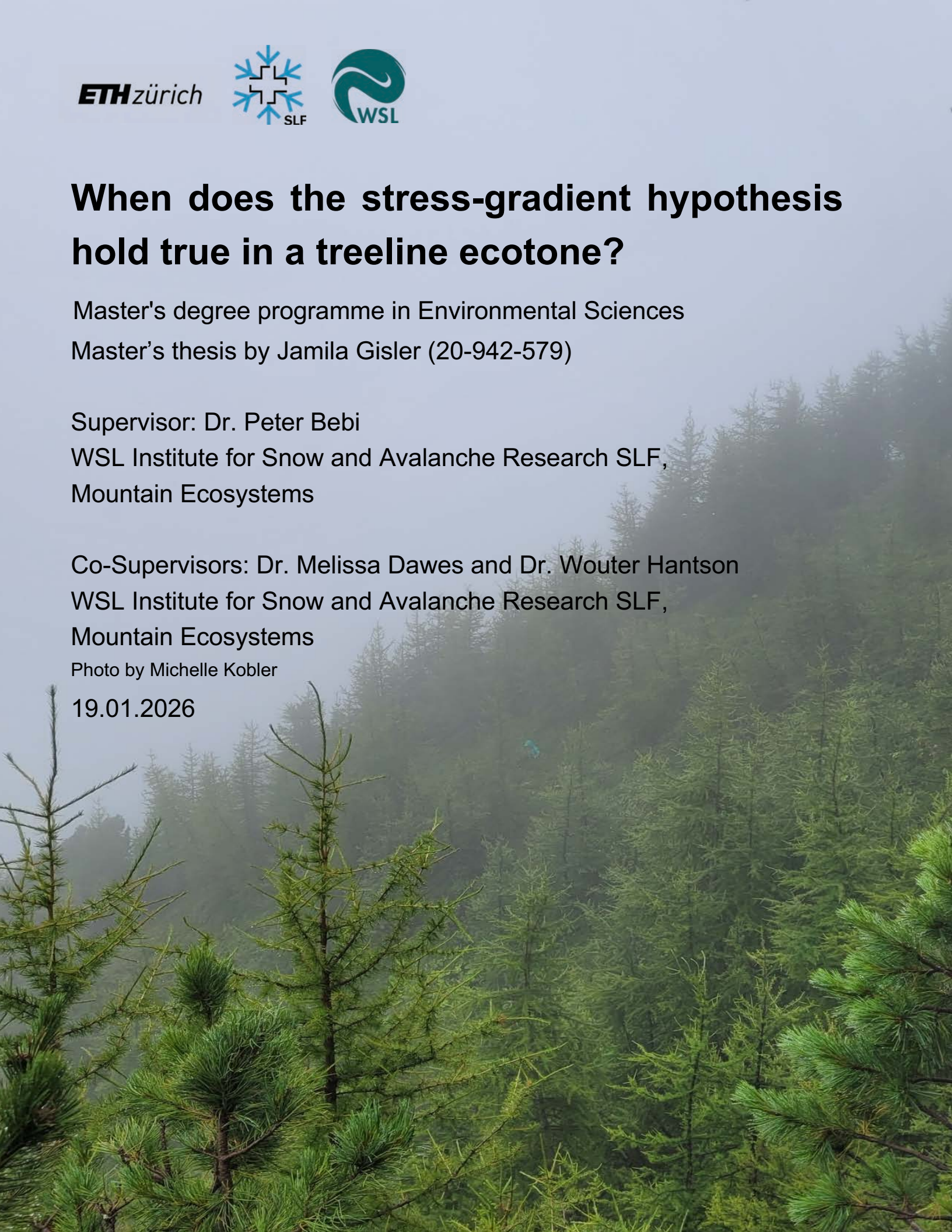

Abstract

High-elevation ecosystems are warming faster than the global average, making alpine treeline ecotones particularly sensitive to ongoing climatic warming. Treelines are already responding through upward shifts and stand densification, yet dynamics in these systems are shaped not only by climate but also by tree–tree interactions. The stress-gradient hypothesis (SGH) predicts a shift from competition under favourable conditions to facilitation under harsher conditions, and treeline ecotones provide temperature-related stress gradients along elevation for testing these predictions. Despite extensive study, support for the SGH in treeline ecotones remains mixed, with few studies comparing patterns across life stages, alternative performance metrics and species. Here, I address this gap using long-term data from the Stillberg afforestation experiment in the treeline ecotone of the Swiss Central Alps, where seedlings of *Larix decidua*, *Pinus cembra* and *Pinus mugo* subsp. *uncinata* were planted in 1975 and monitored over the subsequent 50 years. I quantified neighbour density around each focal tree within a 1.5 m radius along a ~150 m elevation gradient and related it to two tree size metrics, height and diameter at stem base, using linear mixed-effects models. Support for the SGH was conditional rather than universal across life stages, size metrics and species. In *L. decidua*, neighbour effects on height followed an SGH-like pattern during the first two decades after planting. However, competition intensified over time, with elevational contrasts converging towards the end of the 50-year period. This is likely due to reduced temperature limitation under climatic warming and increasing intraspecific competition. During the period when both size metrics were available for *L. decidua*, neighbour effects on diameter exhibited a weak, hump-shaped elevational pattern, where the lowest competitive effects were observed at mid elevations rather than at high elevations. In general, the effect of neighbours on diameter was more negative than on height, which could be because diameter growth is less limited by air temperature than height growth. SGH-like trends were clearer for *L. decidua* and *P. mugo* than for *P. cembra*. *L. decidua* experienced more positive neighbour effects than the pine species, suggesting that life-history strategies may help explain species-specific variation in the magnitude and direction of SGH-like pattern. The frequent occurrence of neutral-to-positive neighbour effects during the first few decades of establishment highlights the important role of facilitation and supports forest management approaches, such as cluster afforestation, provided that the planting designs are adapted to the local microsite conditions. Predicting treeline forest dynamics under continued climatic warming requires accounting for shifts in the magnitude and direction of neighbour effects across life stages, species and performance metrics.

Table of contents

List of figures

List of tables

1 Introduction

Treelines worldwide are shifting to higher elevations and latitudes, a trend commonly attributed to climatic warming (Hansson *et al.* 2021; Harsch *et al.* 2009). Because mountain regions are warming faster than many other parts of the globe, high-elevation ecosystems are considered particularly vulnerable (Pepin *et al.* 2022). Treeline can be defined as the upper boundary connecting the highest forest patches along a slope (Körner 1998). It is embedded within the transition zone between closed forest and low-stature vegetation, the treeline ecotone (Bader *et al.* 2021). Due to their size, trees are more closely linked to atmospheric conditions, especially air temperature, than low-stature vegetation (Körner 2012). Accordingly, the position of the alpine treeline is widely considered to be largely determined by low temperatures (Körner 2021; Körner & Paulsen 2004).

Although low temperatures strongly constrain treeline position, tree growth and survival within the treeline ecotone are also shaped by tree–tree interactions. Climatic warming can indirectly modify neighbourhood structure by increasing tree density, thereby altering interactions among trees (Wang *et al.* 2016, 2021). Evidence from forest systems beyond treeline further suggests that tree–tree interactions mediate how climatic conditions influence growth and survival (Beauchamp *et al.* 2025; Ford *et al.* 2017). This supports the expectation that tree–tree interactions near treeline may modulate the effects of warming on tree performance. These interaction-mediated effects are particularly important because treeline position and forest structure influence ecosystem carbon storage (Hansson *et al.* 2021). Moreover, climate-driven shifts in treeline species composition may alter local tree diversity, with potential consequences for the stability of mountain forest productivity (Jourdan *et al.* 2021). Consequently, studying tree–tree interactions in the treeline ecotone is essential for understanding tree performance, species distributions and range dynamics under climatic warming (Ettinger & HilleRisLambers 2013; Wang *et al.* 2016).

To understand how tree–tree interactions shape forest dynamics in the treeline ecotone, it is useful to distinguish between two opposing processes: competition and facilitation. Competition occurs when neighbouring plants reduce each other's performance, for example by lowering plant performance metrics (growth or survival) through competition for light or nutrients (Beauchamp *et al.* 2025; Coomes & Allen 2007). It can occur both within species (intraspecific) and between species (interspecific) (Kulha *et al.* 2023; Liu

et al. 2020). When neighbours are similar in size, competition tends to be more symmetric, whereas large size differences (e.g. tall adults vs juveniles) often lead to asymmetric competition, where larger individuals disproportionately suppress smaller ones (Ford *et al.* 2017; Wang *et al.* 2016). Over longer time scales, intense competition in dense, even-aged stands can lead to self-thinning, a characteristic pattern in which stand density declines as mean tree size increases (Westoby 1984).

A key consequence of density-related competition is negative density dependence (NDD), where individual performance declines as local neighbour density increases (Wang *et al.* 2016; Zheng *et al.* 2024). Neighbours can be conspecific (of the same species) or heterospecific (of different species), and the relative magnitude of interactions with each can shape community composition. NDD can promote stable coexistence when intraspecific competition is stronger than interspecific competition, because this slows or prevents competitive exclusion (Broekman *et al.* 2019). In forests, such processes have been linked to the maintenance of tree species diversity (LaManna *et al.* 2022; Wang *et al.* 2018). In particular, conspecific negative density dependence (CNDD) is often attributed to natural enemies (e.g. pathogens and insect or mammalian herbivores) that accumulate at high conspecific density and reduce the performance of nearby conspecifics (Song & Corlett 2022; Xu & Yu 2014).

In contrast, facilitation occurs when neighbours enhance performance by modifying abiotic or biotic conditions, and it can be especially important under stressful environments (Bertness & Callaway 1994). For example, conspecific krummholz-forming trees have been found to facilitate seedling survival and growth in the treeline ecotone in the Catalan Pyrenees and Andorra, particularly during winters with irregular snowpack (Batllori *et al.* 2009). Similarly, microsite features that provide overhead cover, such as branches from larger conspecifics, have been associated with higher survival (Germino *et al.* 2002), potentially by acting as a physical shelter that buffers seedlings and saplings from harsh microclimatic conditions. Facilitation can involve heterospecifics as well; in one study, seedlings and saplings growing within herbaceous ground cover survived better than those on bare soil (Germino *et al.* 2002). Competition and facilitation have been observed to operate simultaneously in boreal forests (Liu *et al.* 2020) and in treeline ecotones (Batllori *et al.* 2009), and their net balance is expected to vary with environmental conditions rather than remain constant.

A central idea linking abiotic context to the balance between competition and facilitation is the stress-gradient hypothesis (SGH). It predicts that facilitation should increase, or

competition weaken, as abiotic stress intensifies (e.g. along temperature or aridity gradients) and productivity declines (Callaway *et al.* 2002; He *et al.* 2013). Refinements of the SGH proposed that facilitative effects may diminish again under extreme stress, leading to a hump-shaped relationship between stress and the magnitude of facilitation (Michalet *et al.* 2006).

Along elevation gradients, abiotic stress increases towards higher elevations as temperatures drop. In line with this, several studies have indicated declining tree growth with increasing elevation (e.g. Barbeito *et al.* 2012). Ettinger & HilleRisLambers (2013) examined three conifer species along an elevation gradient on Mt. Rainier (WA, USA), where temperature decreased and precipitation increased with elevation. They found that growth at the upper species range edge near treeline was more sensitive to variables related to snowpack and growing-season temperature than growth at the lower range edge.

Early work on plant communities along elevation gradients led to relatively consistent support for the SGH (Callaway *et al*. 2002). In forests, studies along elevation or temperature gradients sometimes match SGH predictions (Beauchamp *et al.* 2025; Callaway 1998; Coomes & Allen 2007; Eränen & Kozlov 2008; Jourdan *et al.* 2021; LaManna *et al.* 2022). Others support a hump-shaped variant, with strongest facilitation under intermediate stress (He *et al.* 2023). However, several studies have pointed to little or no change in the magnitude or direction of species interactions along elevation gradients and thus lend no support for the SGH (Ettinger & HilleRisLambers 2013; Lyu *et al.* 2025; Okano *et al.* 2021). Together, these mixed findings suggest that the balance between competition and facilitation along elevation gradients is strongly context dependent, particularly in forested systems.

One reason SGH tests yield mixed results is that the balance of competition and facilitation can shift across plant life stages. Along subarctic elevation and seashore gradients, positive interactions were more common between adults and seedlings at high-stress sites, whereas seedling–seedling interactions were predominantly competitive (Eränen & Kozlov 2008). Near the upper elevation limit of species' climatic niches, juvenile and adult trees differed in the extent to which growth responded to climatic constraints such as snowpack and growing-season temperature (Ettinger & HilleRisLambers 2013). Further, a study examining CNDD in a temperate forest along an elevation gradient showed that its effects shifted across size classes, strongly reducing survival in small trees while primarily constraining growth in larger individuals (LaManna

et al. 2022). Similarly, at high-elevation sites in the Rocky Mountains, larger individuals of a focal species showed a stronger spatial association with a heterospecific neighbour than did seedlings of the same species (Callaway 1998). In that study, the heterospecific neighbour was considered a facilitator, as it was shown to enhance growth rates of the focal species near treeline.

Another possible reason for the inconsistent findings is that abiotic stress can have contrasting effects on different components of performance (e.g. growth versus survival), so 'stress' is not expressed uniformly across response metrics. For example, Barbeito *et al.* (2012) examined survival and height growth of three conifer species along an elevation gradient in a treeline ecotone in the Swiss Alps and found that optimal conditions for growth did not coincide with those for survival. Snowmelt timing showed opposing associations with the different responses: earlier snowmelt reduced mortality, whereas later snowmelt enhanced growth. Another example is height growth in treeline trees, which is generally more sensitive to cold, high-elevation conditions than diameter growth (Bernoulli & Körner 1999; Körner & Hiltbrunner 2024). This difference likely reflects temperature gradients above the ground rather than tissue sensitivity: apical meristems driving height growth are more exposed to cold conditions than the cambial tissue responsible for radial growth (Körner 2012). For example, along a subarctic elevation gradient, positive host–seedling interactions increased with increasing abiotic stress, but only for the leaf length of the seedlings and not for seedling height (Eränen & Kozlov 2008).

Finally, species characteristics shape sensitivity to abiotic stress and neighbourhood interactions, so SGH patterns are often species-specific. Across 33 European tree species, Beauchamp *et al.* (2025) showed that whether competition along a temperature gradient followed an SGH-like pattern varied among species even within their climatic niches. Maestre *et al.* (2009) formalised this contingency by refining the SGH to account for the life-history strategies of both benefactor and beneficiary species, drawing on Grime's CSR framework, which distinguishes among competitive (C), stress-tolerant (S) and ruderal strategies (R) (Grime 1977). Along non-resource stress gradients (e.g. temperature), Maestre *et al.* (2009) predicted that the magnitude and direction of the SGH-like pattern depends on competitive vs stress-tolerant life-history strategy of benefactor and beneficiaries (Table 1).

Table 1: Predicted net interaction outcomes along a non-resource stress gradient (e.g. temperature). Interaction outcomes depend on competitive (C) and stress-tolerant (S) benefactors and beneficiaries (table adapted from Maestre et al. *(2009)). The symbols denote the net interaction effects: ++ strong facilitation, + facilitation, 0 neutral, − competition.*

	C benefactor		S benefactor	
Stress level	C beneficiary	S beneficiary	C beneficiary	S beneficiary
Low	-	-	-	-
Medium	++	+	+	0
High	+	++	++	+

Life history strategy has been assessed for major European tree species (Brzeziecki & Kienast 1994), including several characteristic of the treeline ecotone (Körner 2012; Lingua *et al.* 2008). *Pinus cembra* is commonly classified as stress-tolerant, whereas *Larix decidua* is considered to have a mixed strategy combining competitive, stress-tolerant and ruderal characteristics (Brzeziecki & Kienast 1994). Although a formal CSR classification for *Pinus mugo* is lacking, to my knowledge, its ecology suggests a predominantly stress-tolerant strategy with some ruderal characteristics (Dullinger *et al.* 2005; Lingua *et al.* 2008; Risch *et al.* 2003). Together, these findings indicate that the magnitude and direction of tree–tree interactions along elevation gradients depend on the species' life-history strategies and context.

We still lack a systematic assessment of how the SGH behaves when species identity, life stage and performance metric vary simultaneously. Most existing studies focus on a single performance metric, often the diameter at breast height (DBH; e.g. He *et al.* 2023), and therefore provide only a partial view of how abiotic stress and neighbour effects interact. To address this gap, I analysed data from a large afforestation experiment in the treeline ecotone in the Swiss Alps. At this site, three key treeline species of the European Alps, *Larix decidua*, *Pinus cembra* and *Pinus mugo* subsp. *uncinata*, were planted as seedlings in 1975 and monitored over the last 50 years. Over the course of the experiment, survival became increasingly dominated by *Larix decidua* (Lechler *et al.* 2024). The afforestation spans an elevation gradient of approximately 150 m, with all trees established above the average treeline elevation at the time of planting, and it has been used to investigate many aspects of treeline dynamics (see Lechler *et al.* 2024 for an overview). Despite this long research history, neighbourhood interactions at the site have received relatively little attention: tree–tree interactions have so far only been briefly explored in a thinning experiment, which already indicated support for SGH-like patterns (Barbeito 2013). Long-term monitoring of an even-aged stand, with the trees of each

species originating from the same provenance, offers an ideal basis for analysing tree performance along an elevational stress gradient. Coupled with detailed neighbourhood data and measurements of multiple size metrics (i.e. height and diameter), this design allows temporal, size-metric-specific and species-specific patterns of neighbour effects to be disentangled more clearly in a treeline ecotone. Analyses involving diameter were restricted to *Larix decidua* in 2015 and 2025, because diameter was not recorded before 2015, and sample sizes for *Pinus cembra* and *Pinus mugo* were too small. Accordingly, species-specific analyses were limited to 1985 and 1995 to ensure adequate coverage of the elevation stress gradient and associated neighbour effects.

In this thesis, I addressed the following questions:

1. Temporal dimension: Do neighbour effects on tree height of *Larix decidua* follow an SGH-like pattern along the elevation gradient, and do the magnitude and direction of these effects change across life stages from 1985 to 2025?

2. Size-metric dimension: Do neighbour effects on tree height and diameter of *Larix decidua* follow an SGH-like pattern along the elevation gradient in 2015 and 2025, and do the magnitude and direction of these effects differ between the two size metrics?

3. Species dimension: Do neighbour effects on tree height of *Larix decidua*, *Pinus cembra* and *Pinus mugo* follow an SGH-like pattern along the elevation gradient in 1985 and 1995, and do the magnitude and direction of these effects differ among species?

I had the following hypotheses:

1. Neighbour effects on *Larix decidua* height will follow an SGH-like pattern along the elevation gradient, with stronger competition at low elevations and weaker competition or even facilitation at high elevations. Competitive neighbour effects will be detectable already in early life stages (1985 and 1995). Competition will intensify over time (1985–2025) at low elevations while remaining weaker at high elevations.

2. Neighbour effects will differ between height and diameter in *Larix decidua* along the elevation gradient during the period for which data on both size metrics were available (2015 and 2025). Height will follow an SGH-like pattern, with stronger competition at low elevations and weaker competition or even facilitation at high elevations. In

contrast, diameter will be affected by competition across the elevation gradient, although especially at low elevations, and overall will be more sensitive to competition than height.

3. During early life stages (1985 and 1995), neighbour effects on height will differ in magnitude and direction among *Larix decidua*, *Pinus cembra* and *Pinus mugo* along the elevation gradient. For all three species, an SGH-like pattern will emerge, with stronger competitive effects at lower elevations and weaker competition or facilitation at higher elevations. However, because *Larix decidua* has a more competitive life-history strategy, it will exhibit more positive neighbour effects across the gradient, either through stronger facilitation at high elevations or weaker competition at low elevations. In contrast, as both *Pinus cembra* and *Pinus mugo* have a more stress-tolerant life-history strategy, neighbour effects for these species will be weaker or more negative overall, reflecting reduced sensitivity to facilitation associated with greater tolerance to abiotic stress.

2 Research methodology

2.1 Literature research

For the literature review, I structured the search around three complementary topics that define the scope of this thesis (Figure 1): (i) the study organism (trees), (ii) the focal abiotic stress context (an elevation gradient) and (iii) species interactions. For each topic, I defined a set of keywords and searched the literature on Web of Science using multiple combinations of these keywords, prioritising studies that explicitly addressed the intersection of the three topics. Given the thesis' working hypotheses, I placed particular emphasis on literature related to the stress-gradient hypothesis, positioned at the intersection of abiotic stress and species interactions.

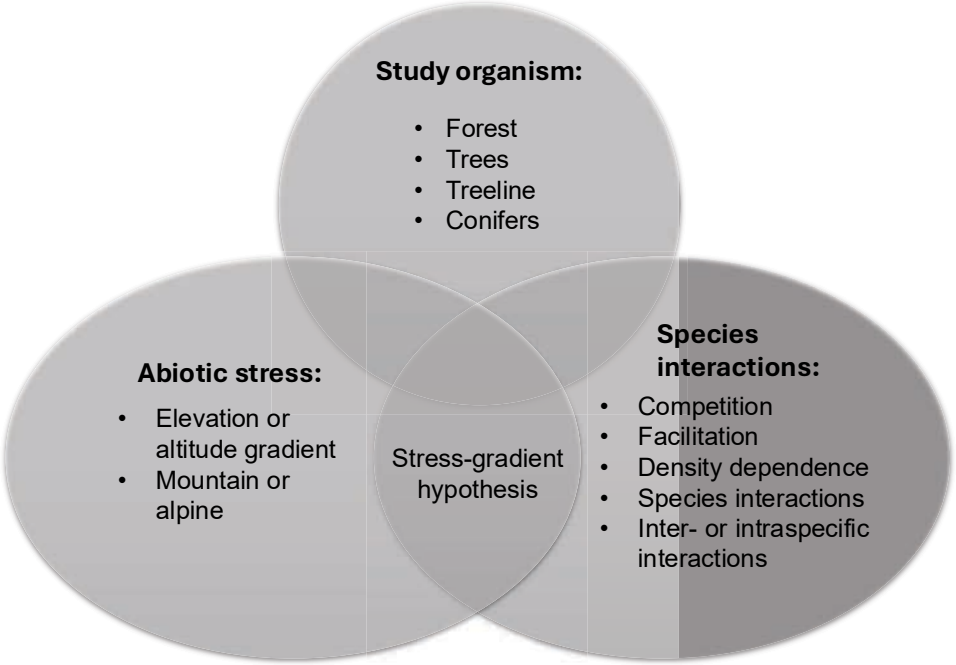

Figure 1: Conceptual overview of the literature search structure.
The literature review was organised around keywords related to three topics: study organism, abiotic stress and species interactions.

2.2 Study area

To address the research questions, I used data from the Stillberg long-term afforestation experiment. This experiment is located in the treeline ecotone of the Central Swiss Alps,

in the Dischma Valley near Davos (47°28’ N, 78°30’ E; Lechler *et al.* 2024). The research site is situated on a north-east-facing slope. In 1975, approximately 92,000 three- to four-year-old seedlings of the three most widespread conifer species in the treeline ecotone of the European Alps, European larch (*Larix decidua* L.), mountain pine (*Pinus mugo* subsp. *uncinata* Ramond, thereafter called *Pinus mugo*) and Cembran pine (*Pinus cembra* L.), were planted in a total of 4107 plots along an elevation gradient from 2075 to 2230 m a.s.l. Each plot contained 25 seedlings arranged in a regular grid with 70 cm spacing. One tree species was planted per plot, and species assignments alternated among adjacent plots in a regular pattern across the site (Figure 2). Details of the 2025 data collection campaign are provided in section 2.5.2. Elevation data for Figure 2 were obtained from the swissALTI3D digital elevation model (Federal Office of Topography swisstopo, 2024).

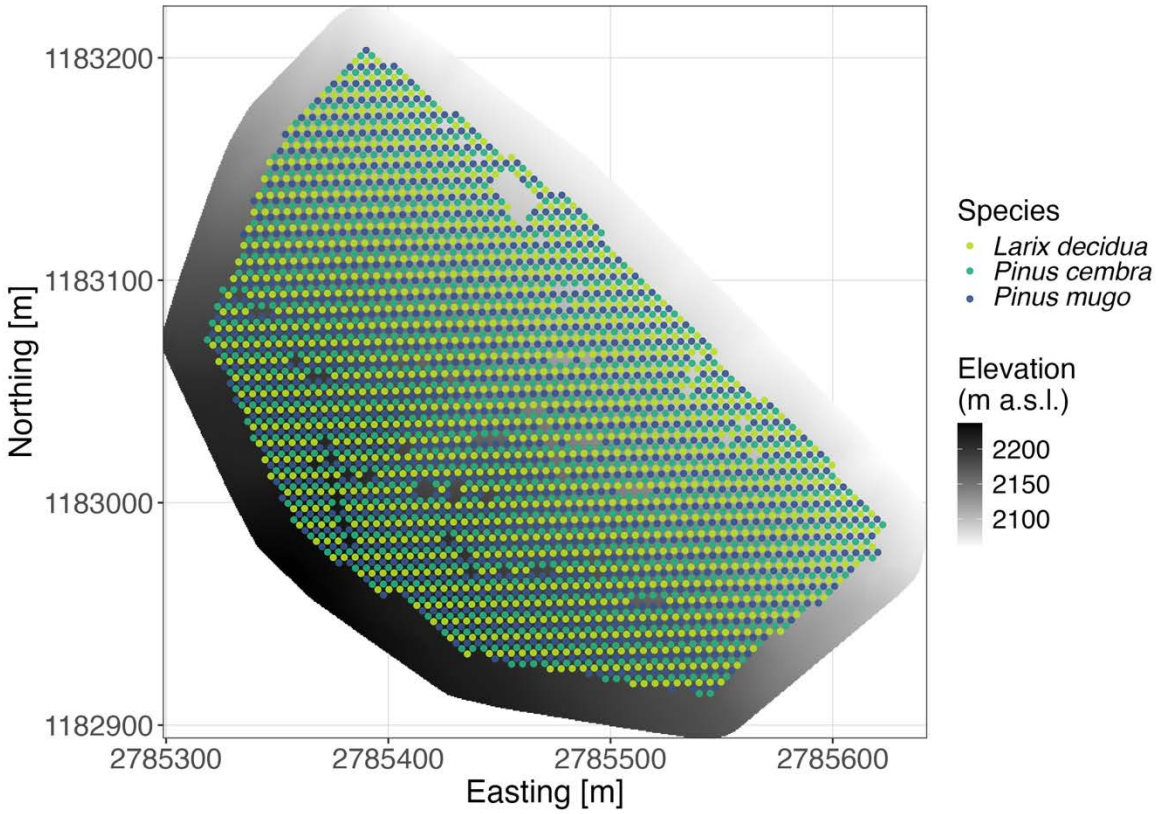

Figure 2: Plot-level planting scheme at Stillberg.
Points indicate plots planted with Larix decidua*,* Pinus cembra*, or* Pinus mugo*. Background shading represents site-scale elevation derived from a digital elevation model, with elevation increasing from light to dark shading. Coordinates are shown in the Swiss national reference system (CH1903+ / LV95). Elevation data: swissALTI3D © swisstopo.*

2.3 Data collection

The tree performance metrics survival status, height, diameter at stem base and stem architecture have been measured at the Stillberg afforestation since 1975. Tree survival status was recorded for every individual tree at 10-year intervals from 1975 to 2025. A tree was classified as alive if it retained green needles on any part of the crown or stem. Tree height was measured along the tree stem, following its curvature. Height therefore corresponds to stem length rather than vertical height. Height was measured for all trees at 10-year intervals from 1975 to 1995 and on a subset of three representative trees per plot from 2005 to 2025. One tree was located at a plot corner, one in the plot centre and one along a plot edge. This selection strategy was used to capture contrasting neighbourhood compositions created by the experimental layout. The central individual has only conspecific (from the same species) neighbours within the plot, whereas edge and corner trees additionally border neighbouring plots and therefore can have heterospecific (from a different species) neighbours (one adjacent species for edge trees; two adjacent species for corner trees). To ensure temporal consistency, the same trees as in the previous survey were measured whenever possible. If a previously selected tree had died or could not be identified with certainty, a standardised procedure was followed to select a replacement tree in a similar position within the plot (for details on tree selection see Figure 23 and Figure 24 in the Appendix 8.1). From 2015 onwards, tree diameter was measured on the same subset of trees used for height measurements. This was done at the stem base, approximately 5 cm above ground level. Stem architecture was recorded at 10-year intervals from 1995 to 2025 and classified into three categories: single stem; forked (split into two stems for >50% of total tree height); and shrublike (split into >2 stems for >50% of total tree height).

I worked as part of a core team of four, supported by additional field assistants as available, to conduct the survey in 2025. Due to the limited number of field workers and weather-related constraints, we were only able to survey approximately 50% of the afforestation experiment (for more details see section 2.5.2).

2.4 Soil temperature

2.4.1 Experimental design

I placed a total of 48 iButton temperature loggers (DS1922L-F5#; Analog Devices, Wilmington, MA, USA) across the afforestation to capture microsite variability. I buried the soil-temperature loggers at 5 cm depth using two different designs. In design one, I stratified plots by elevation (low: 2,076–2,121 m a.s.l.; high: 2,168–2,230 m a.s.l.) and by plot-level tree density (low: <4 trees; high: ≥15 trees) and installed four loggers per elevation × tree-density combination. In design two, which I implemented at intermediate elevation (2,121–2,168 m a.s.l.), I stratified plots by topography type (east-facing, north-facing, gully, ridge) and plot-level tree density and installed four loggers per topography × tree-density combination.

2.4.2 Analysis

For analysis and visualisation, I calculated plot-level mean soil temperature across the full measurement period (mid July to mid September 2025). Because soil temperature differed little among neighbour-density categories, I pooled plots across density strata when estimating mean soil temperature at the study site. I visualised differences among elevation levels and among topography types using boxplots of plot-level mean soil temperature (median and interquartile range (IQR), whiskers to 1.5 × IQR) with overlaid jittered points showing individual plot-level values and dispersion. For the elevation comparison, I grouped plots into low, mid and high elevation and produced one boxplot per elevation group. For the topography comparison, I restricted the dataset to mid elevation plots and grouped them by topography type (east-facing, north-facing, gully, ridge).

2.5 Statistical analysis

2.5.1 General information

I carried out all statistical analyses in R using the R Studio interface (R Core Team 2025). I performed data preparation and transformation with the packages tibble, dplyr and tidyr (Müller & Wickham 2025; Wickham *et al.* 2023, 2024). For visualisation, I used the ggplot2

package to create all figures (Wickham 2016) and the patchwork package to combine multiple figures into composite panels (Pedersen 2025).

I assessed statistical significance using a threshold of $p < 0.05$. To enhance readability while maintaining numerical precision, I rounded reported estimates and descriptive statistics adaptively. Specifically, I rounded values with an absolute magnitude ≥ 0.01 to two decimal places and smaller non-zero values (< 0.01) to two significant digits to avoid truncation to zero. This formatting approach provides consistency in presentation while retaining meaningful information on small effect sizes.

2.5.2 Datasets

As not all plots in the Stillberg area were surveyed in 2025, as in anterior years, I defined the dataset that covers all plots across the study area as the ‘full-area dataset’ and the dataset that only includes the reduced spatial extent as the ‘subset dataset’ (Figure 3). To avoid confounding effects of other treatments, I removed 108 plots that were included in additional experiments at the site (in addition to the afforestation experiment) from the dataset prior to analysis.

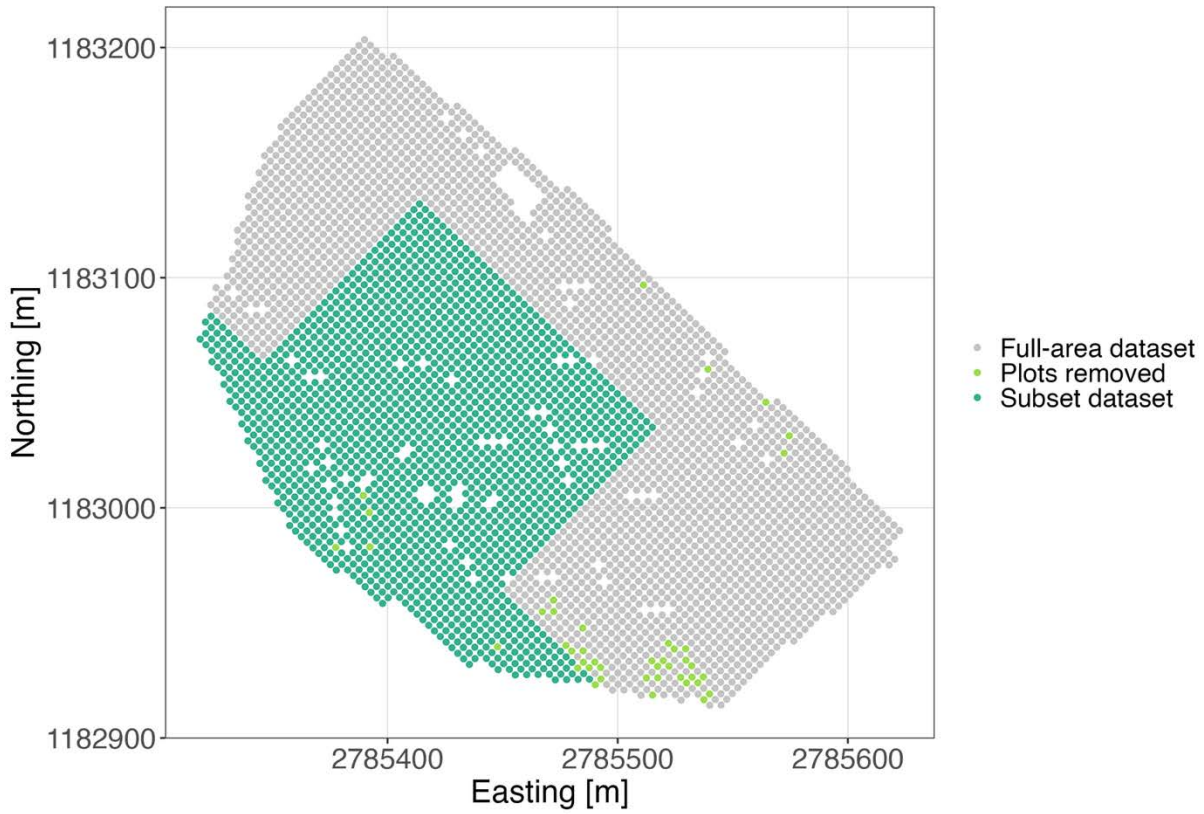

Figure 3: Overview of the two datasets used in the analyses.
Grey points indicate plots included in the full-area dataset and dark green points indicate plots included in the subset dataset (a subset of the full-area dataset). Light green points indicate plots from which trees were removed due to being part of additional experiments. Coordinates are shown in the Swiss national reference system (CH1903+ / LV95).

2.5.3 Explanatory variables used to test the stress-gradient hypothesis

2.5.3.1 Elevation

In the Swiss Alps, elevation and temperature are strongly correlated: mean air temperature decreases by ~0.6 °C per 100 m of elevation gain (Körner 2021). I therefore used elevation as a proxy for a temperature-related stress gradient, with higher elevations representing colder conditions that are generally more limiting for tree performance. In all analyses, I treated elevation as the stress-gradient explanatory variable.

However, elevation does not fully capture fine-scale heterogeneity in microsite conditions at treeline. Plot-level microsite attributes (slope angle, aspect, radiation, wind velocity and snowmelt day of the year) varied within elevation bands and showed only weak to

moderate correlations with elevation (Figure 4). This pattern indicates that microsite conditions vary largely independent of elevation. Elevation therefore remains a parsimonious proxy for the dominant temperature-related stress gradient, while the microsite variables primarily capture local heterogeneity superimposed on that gradient. These variables were recorded at the early stages of the Stillberg afforestation and may not fully represent present-day microsite conditions; details of the original site survey and documentation are provided by Schönenberger & Frey (1988).

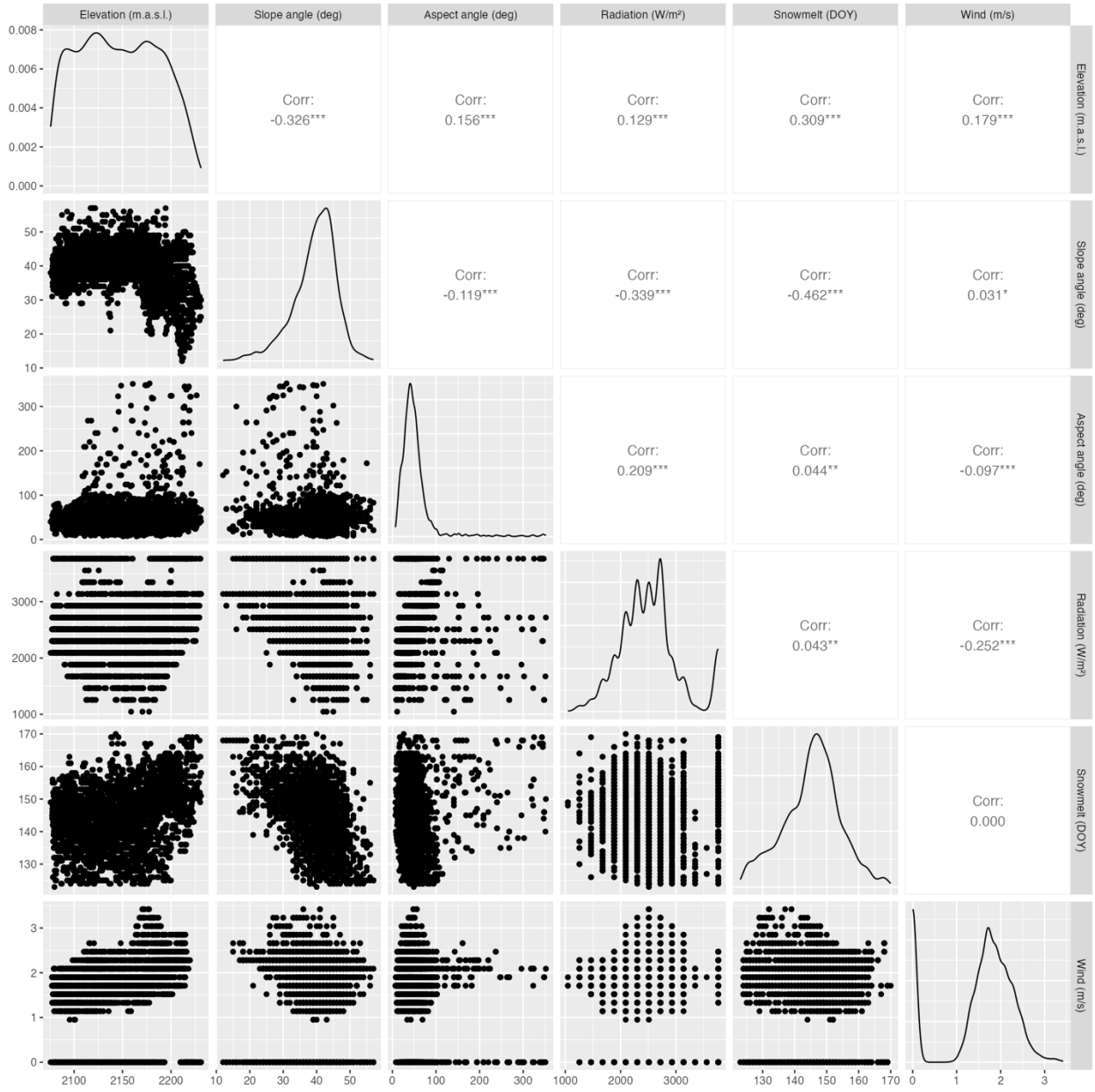

Figure 4: Pairwise scatterplot matrix of plot-level elevation and microsite variables.
Diagonal panels show the probability distribution of elevation and each microsite variable (slope angle, aspect angle, radiation, snowmelt day of the year and wind velocity), panels in the lower left show pairwise scatterplots and panels in the upper right report Pearson correlation coefficients with significance level indicated by asterisks: $p < 0.05$ *(*),* $p < 0.01$ *(**) and* $p < 0.001$ *(***).*

2.5.3.2 Neighbour density

To model the species interaction component of the SGH, I used the number of neighbouring trees (referred to as 'neighbour density' below) around each focal tree (Figure 5). For each focal tree and survey year, I counted the number of neighbours at a radius (r) of 1.5 metres distance. I defined neighbours as all conspecific and heterospecific trees within a Euclidean distance ≤ r from the focal tree. I excluded the focal tree itself, and I only counted trees that were recorded as alive in that year. For each focal tree and year, I derived counts of conspecific neighbours, heterospecific neighbours and the total number of neighbours (conspecifics + heterospecifics). I additionally derived an explanatory variable named 'conspecific proportion', defined as the proportion of conspecific neighbours relative to the total number of neighbours for each focal tree. I constructed neighbourhoods from tree coordinates (CRS: CH1903+ / LV95), and implemented radius queries via a KD-tree search using the RANN package (Jefferis *et al.* 2024).

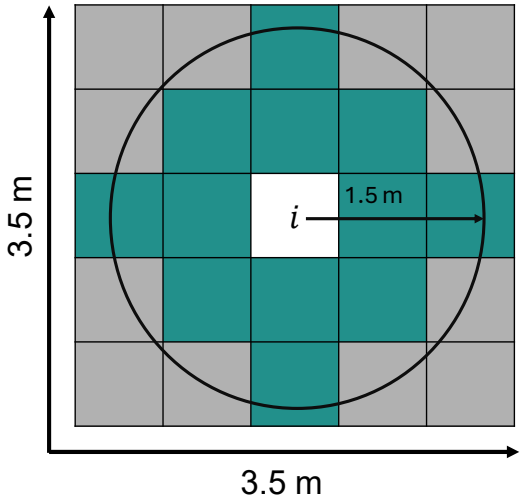

Figure 5: Schematic illustration of the neighbourhood definition around a focal tree i. The circle shows the neighbourhood radius (here 1.5 m) and coloured cells represent potential neighbours within the given radius, whereas grey cells fall outside the neighbourhood and are not counted. The focal tree itself (white cell) is excluded from all

A limitation of this approach is that trees that were present at Stillberg prior to establishment of the afforestation, as well as individuals that have subsequently colonised the area, were not included in the neighbourhood definitions. Pre-existing trees are often substantially larger than planted individuals and may therefore influence local neighbourhood conditions (e.g. shading), potentially affecting estimated neighbour effects.

2.5.4 Subsampling

Higher mortality at high elevations created an imbalance in neighbour-density observations across the abiotic stress gradient, with low neighbour densities overrepresented at high elevations and high neighbour densities overrepresented at low elevations. To reduce this imbalance and mitigate spatial autocorrelation (section 2.5.6), I applied stratified random subsampling within nine strata (Smith *et al.* 2017). I defined these strata based on equal-width bins from three elevation classes and three neighbour

density classes (example of a stratum: low elevation × high neighbour density; for the bins see Table 2 and Table 3). Within each subsampling iteration, I sampled trees without replacement from each stratum. I repeated the procedure 500 times, drawing new subsamples for each iteration and refitting the model that was selected during model selection (section 2.5.5). I then averaged the model estimates across the 500 model refits. I obtained pointwise 95% confidence intervals from the 2.5th and 97.5th percentiles of the empirical distribution of these estimates. This procedure yielded more balanced and spatially less autocorrelated model training sets and helped stabilise model estimates and predictions, consistent with the rationale described in Li *et al.* (2019).

I sampled the same number of trees per stratum within a given analysis to enhance comparability among years (Table 4; for a list of shortfalls in sample numbers see Table 23 in the Appendix 8.2). However, the chosen sample size per stratum differed among species and between analyses based on the full-area versus the subset dataset. The target number of trees per stratum was largely constrained by the minimum number of observations available in later years, which generally had fewer trees per stratum than in earlier years. Consequently, stratified subsampling in earlier years drew from a larger underlying pool and captured greater variability, whereas in later years some strata contained relatively few samples, limiting the effective sample size and reducing variability among subsamples. This imbalance is a limitation of the later years and should be kept in mind when comparing results across years, as estimates for sparsely populated strata are necessarily less variable and potentially less informative.

Table 2: Elevation bins used for the full-area dataset (left table) and for the subset dataset (right table). Elevation is given in metres above sea level. The column 'Elevation bin' lists the three bin categories, while the columns 'Minimum' and 'Maximum' give the corresponding minimum and maximum elevation values observed for each bin.

Elevation bin	Minimum	Maximum
Low	2074.83	2127.10
Mid	2127.11	2179.38
High	2179.39	2231.66

Elevation bin	Minimum	Maximum
Low	2112.11	2151.95
Mid	2151.96	2191.80
High	2191.81	2231.66

Table 3: Neighbour density bins used for the full-area and subset datasets.
Neighbour density is expressed as the total number of neighbouring trees, irrespective of species identity. The column 'Neighbour density bin' lists the three bin categories, while the columns 'Minimum' and 'Maximum' give the corresponding minimum and maximum neighbour counts observed for each bin.

Neighbour density bin	Minimum	Maximum
Low	0	4
Mid	4	8
High	8	12

Table 4: Overview of subsampling schemes, number of samples per stratum and number of subsampling iterations for the different model groups.

Model type	Data	Number of samples per stratum	Subsampling iterations
Temporal models for 1985–2015 and species models for 1985 and 1995	Full-area dataset	100	500
Temporal models for 1985–2025 and size-metric models for 2015 and 2025	Subset dataset	30	500

2.5.5 Model selection

2.5.5.1 General workflow

I decided to work with mixed-effects models to be able to account for relevant random factors. I included plot number as a random effect to account for spatial clustering of trees within plots and repeated measurements at the plot level. I fit all my models with the lme4 package (Bates *et al.* 2015). I used three groups of models to address my three hypotheses: temporal models for hypothesis 1, size-metric models for hypothesis 2 and species models for hypothesis 3 (sections 2.5.5.4, 2.5.5.5 and 2.5.5.6). I did not include year as an explanatory variable in any of the models, because preliminary analyses showed that adding year led to poor model diagnostics. Instead, I fitted all models separately for each survey year. As a result, I could analyse temporal trends only qualitatively. For all analyses, I excluded data from 1975 because the trees had just been planted and at that time neighbour or elevation effects can reasonably be assumed to be negligible.

I based my model selection on AIC and BIC and, for nested models I additionally did likelihood-ratio tests (fitted with maximum likelihood). I further evaluated model fit using simulation-based residual diagnostics in the DHARMa package (Hartig 2024). For each fitted model, I generated DHARMa residuals from 100 simulations and assessed them using the residual uniformity QQ plots and residuals-versus-predicted plots. I applied DHARMa tests for residual uniformity (Kolmogorov–Smirnov), dispersion and outliers to detect deviations from distributional assumptions and systematic lack of fit. Because these tests can be highly sensitive in large datasets, significant results were interpreted alongside visual residual patterns. To summarise diagnostics across model refits within each model type, I examined diagnostics for five randomly selected model fits per year and verified that diagnostic patterns were consistent across inspected models. For temporal models, I examined diagnostics in detail for an early and a late survey year (1985 and 2015) to capture potential differences across life stages, and then applied the selected model type consistently across the full time series. For size-metric models I inspected the years 2015 and 2025 and for species models the years 1985 and 1995.

2.5.5.2 Collinearity analyses

Before model fitting, I checked for collinearity on the unscaled and untransformed variables: height, diameter, number of *Larix decidua* neighbours, number of *Pinus cembra* neighbours, number of *Pinus mugo* neighbours, total number of neighbours and elevation. I assessed multicollinearity using three complementary diagnostics, following Zuur *et al.* (2009): pairwise scatterplots, correlation coefficients and variance inflation factors (VIFs). I generated a pairwise scatterplot matrix, combining scatterplots and correlation coefficients, using the GGally package, which enabled a visual and quantitative assessment of pairwise relationships among explanatory variables and between explanatory and response variables (Schloerke *et al.* 2025). According to these three diagnostics, collinearity was not an issue in my data (for pairwise scatterplot matrix see Figure 25 and for VIFs see Table 24 in the Appendix 8.3).

2.5.5.3 Scaling and transformation of variables

To facilitate model convergence and allow direct comparison of effect sizes, I standardised the explanatory variables neighbour density, conspecific proportion and elevation prior to analysis (the explanatory variables are hereafter represented by x). I standardised the variables by applying a z-transformation to the full dataset across

species and years using the base R function *scale(x, center = TRUE, scale = TRUE).* For each of the explanatory variables I computed

$$z_i = \frac{x_i - \bar{x}}{s_x}$$

where $\bar{x}$ is the sample mean and s_x the sample standard deviation of x. The standardised explanatory variables therefore had a mean of zero and a standard deviation of one.
I analysed tree height and diameter on the log scale. Both size metrics showed strongly right-skewed distributions and variances increasing with the mean; log-transformation reduced skewness and stabilised the variance, improving adherence to Gaussian linear mixed-effects model assumptions.

2.5.5.4 Temporal models for *Larix decidua* for 1985–2015

I fitted the temporal models twice: once using the full-area dataset from 1985 to 2015 (excluding 2025) and once using the subset dataset from 1985 to 2025 (for details on subsampling see section 2.5.4). Since the subset dataset spanned a shorter elevation gradient and had fewer samples per stratum, I fitted the temporal models for both the full-area and subset datasets. This enabled me to examine whether gradient length and subsample size influenced the inferred temporal pattern.

Table 5 summarises the models I considered during model selection. I compared a linear model with an interaction between neighbour density and elevation with a more flexible spline model with the same interaction structure. The spline model had a slightly lower AIC but a slightly higher BIC (for a summary see Table 6 and for extended results see Table 25 in the Appendix 8.4.1). Overall, model 5.1 had the lowest AIC value in both years and model 2.1 had the lowest BIC value in both years.

Likelihood-ratio tests across model refits showed that the interaction between elevation and neighbour density was supported in 1985 but not in 2015 (for summary see Table 7 and for extended results see Table 26 in the Appendix 8.4.1). Models that included conspecific proportion, either as a fixed effect or as a fixed effect plus an interaction with neighbour density and elevation, had lower AIC values compared to model 3.1. Even though that was the case, I did not include conspecific proportion, because no likelihood-ratio test was significant. Based on these comparisons, together with satisfactory

DHARMa residual diagnostics, I selected model 3.1 as the final model for testing the first hypothesis (for residual diagnostics see Figure 26 in the Appendix 8.4.1).

Table 5: Linear mixed-effects models used for temporal analysis.
Overview of the fixed- and random-effects structures for the five model types considered in the temporal model selection procedure. The response is the log-transformed height value and is applied to every model type. 'ns()' denotes natural cubic splines. Random intercepts for plot number (nr) account for spatial clustering. Interactions are indicated by '', which implies inclusion of all lower-order terms (e.g. 'neighbour density * elevation' expands to 'neighbour density + elevation + neighbour density × elevation').*

Model type	Model formula
	Log(height) ~
1.1	neighbour density * elevation + (1 | plot nr)
2.1	ns(neighbour density) + ns(elevation) + (1 | plot nr)
3.1	ns(neighbour density) * ns(elevation) + (1 | plot nr)
4.1	conspecific proportion + ns(neighbour density) * ns(elevation) + (1 | plot nr)
5.1	conspecific proportion * ns(neighbour density) * ns(elevation) + (1 | plot nr)

Table 6: Summary of model fit (AIC and BIC) for the temporal models for 1985 and 2015.
For each model type and year, the median AIC and BIC computed across all model refits are reported.

Model type	Year	Median AIC	Median BIC
1.1	1985	1496.28	1525.10
1.1	2015	1433.16	1461.67
2.1	1985	1500.12	1524.13
2.1	2015	1426.82	1450.57
3.1	1985	1489.37	1542.19
3.1	2015	1425.11	1477.37
4.1	1985	1490.70	1548.33
4.1	2015	1424.88	1481.89
5.1	1985	1477.99	1574.04
5.1	2015	1399.27	1494.29

Table 7: Results of likelihood-ratio tests for the temporal models for 1985 and 2015.
For each model comparison, the columns 'Comparison' and 'Year' identify the contrasted model types and year. The columns 'Median Chi-squared' and 'Median p*-value' report the median chi-squared statistic and median* p*-value across model refits. Significance levels are indicated using asterisks:* p *< 0.05 (*),* p *< 0.01 (**) and* p *< 0.001 (***). The columns 'Median ΔAIC' and 'Median ΔBIC' give the median differences in AIC and BIC between the more complex model and the simpler model. Negative values in 'Median ΔAIC' or 'Median ΔBIC' indicate improved fit with the more complex model.*

Comparison	Year	Median Chi-squared	Median *p*-value	Median ΔAIC	Median ΔBIC
2.1 vs 3.1	1985	19.07	0.004 **	-7.07	21.74
2.1 vs 3.1	2015	10.43	0.11	1.57	30.08
3.1 vs 4.1	1985	2.67	0.10	-0.67	4.13
3.1 vs 4.1	2015	2.00	0.16	0.00056	4.75
4.1 vs 5.1	1985	9.96	0.27	6.04	44.46
4.1 vs 5.1	2015	13.23	0.10	2.77	40.78

2.5.5.5 Size-metric models for *Larix decidua* for 2015 and 2025

Compared with the temporal models, I restructured the size-metric models so that the response variable combined both height and diameter measurements (Table 8). Additionally, I added an explanatory variable called 'size metric', with two levels (height and diameter), so I could test whether neighbour effects differed between the two metrics. Because each tree contributed multiple measurements, one for height and one for diameter, I included tree ID as a random effect to account for non-independence. Size-metric comparisons were possible for *Larix decidua* only and for 2015 and 2025 only, since diameter was not measured before 2015 and *Pinus cembra* and *Pinus mugo* had too few observations in later years to represent the full elevation and neighbour density gradients (for species survival proportions for the subset dataset see Figure 27 in the Appendix 8.4.2). I fitted these models on the subset dataset because I included data from 2025.

I fitted linear mixed-effects models with *lme4:lmer() using* restricted-maximum-likelihood optimisation. To reduce convergence issues from spline terms, higher-order interactions and repeated subsampling, I used a two-step optimiser strategy with an increased evaluation budget ($maxfun = 2 \times 10^5$). I fitted each model first with the *bobyqa* optimiser; if convergence messages occurred, I refitted the model using the *nloptwrap* optimiser. I

retained the *nloptwrap* fit only when it removed convergence messages; otherwise, I kept the *bobyqa* fit and logged all remaining convergence/ warning messages for transparency. Across model types and years, the proportion of models with convergence warnings ranged from 0.02 to 0.118, with more complex models showing a higher frequency of warnings (Table 27 in the Appendix 8.4.2). In addition, I screened all fits for boundary (singularity) issues. Across model types, the proportion of fits flagged as singular ranged from 0.02 to 0.12. In the majority of singular fits (0.8–1), the warning was attributable to the random effect 'plot number', indicating that its variance component was estimated as very close to zero. This issue was never driven by the random factor 'tree ID'. A small number of fits showed the warning for other reasons. For transparency, I recorded singularity flags systematically across all model refits (Table 28 in the Appendix 8.4.2).

Because of convergence issues in a subset of model refits, I computed all model-fit indices twice: once using all model refits and once excluding model refits with convergence warnings. Median AIC and BIC values differed marginally between these two sets, so I report results based on all model refits (for a summary see Table 9 and for extended results see Table 29 in the Appendix 8.4.2). I compared a linear model with an interaction between neighbour density and elevation with a more flexible spline model with the same interaction structure. The spline model had a slightly lower AIC but a slightly higher BIC. Overall, model 5.2 had the lowest AIC value in both years and model 2.2 had the lowest BIC value in both years.

Likelihood-ratio tests across model refits showed that the interaction between elevation and neighbour density was not supported in 2015 or 2025 (for a summary see Table 10 and for extended results see Table 30 in the Appendix 8.4.2). Including stem architecture as a fixed effect significantly improved model fit in both years. The three-way interaction between size metric, neighbour density and elevations significantly improved model fit. Based on these comparisons, together with satisfactory DHARMa residual diagnostics, I selected model 5.2 as the final model for testing the second hypothesis (for residual diagnostics see Figure 28 in the Appendix 8.4.2).

Table 8: Linear mixed-effects models used for size-metric analysis.
Overview of the fixed- and random-effects structures for the five model types considered in the size-metric model selection procedure. The response is the log-transformed size-metric value (height or diameter) and is applied to every model type. 'stem' denotes stem architecture and 'size metric' indicates whether the response corresponds to height or diameter. 'ns()' denotes natural cubic splines. Random intercepts for plot number (nr) and tree identity (ID) account for spatial clustering and multiple measurements (height and diameter) made on the same trees. Interactions are indicated by '', which implies inclusion of all lower-order terms (e.g. 'neighbour density * elevation' expands to 'neighbour density + elevation + neighbour density × elevation').*

Model type	Model formula
	Log(response) ~
1.2	size metric + neighbour density * elevation + (1 | plot nr) + (1 | tree ID)
2.2	size metric + ns(neighbour density) + ns(elevation) + (1 | plot nr) + (1 | tree ID)
3.2	size metric + ns(neighbour density) * ns(elevation) + (1 | plot nr) + (1 | tree ID)
4.2	stem + size metric + ns(neighbour density) * ns(elevation) + (1 | plot nr) + (1 | tree ID)
5.2	stem + size metric * ns(neighbour density) * ns(elevation) + (1 | plot nr) + (1 | tree ID)

Table 9: Summary of model fit (AIC and BIC) for the size-metric models for 2015 and 2025.
For each model type and year, the total number of refitted models ('Nr. of models (all)') and the number of model refits without convergence issues ('Nr. of models (nci)') are reported, together with the median AIC and BIC computed across all model refits ('Median AIC/BIC (all)') and across the subset of non-convergence-issue model refits ('Median AIC/BIC (nci)').

Model type	Year	Nr. of models (all)	Nr. of models (nci)	Median AIC (all)	Median BIC (all)	Median AIC (nci)	Median BIC (nci)
1.2	2015	500	480	524.77	559.10	524.77	559.10
1.2	2025	500	483	648.03	681.84	648.81	682.63
2.2	2015	500	490	519.94	558.57	519.94	558.57
2.2	2025	500	490	641.70	679.73	641.92	679.96
3.2	2015	500	490	517.72	573.51	517.72	573.51
3.2	2025	500	486	639.22	694.16	639.61	694.55
4.2	2015	500	469	501.78	566.15	501.64	566.01
4.2	2025	500	479	631.51	694.90	632.01	695.41
5.2	2015	500	468	493.15	591.86	493.24	591.94
5.2	2025	500	481	611.98	709.19	612.27	709.48

Table 10: Results of likelihood-ratio tests for the size-metric models for 2015 and 2025.
For each model comparison, the columns 'Comparison' and 'Year' identify the contrasted model types and year. The columns 'Median Chi-squared' and 'Median p*-value' report the median chi-squared statistic and median* p*-value across model refits. Significance levels are indicated using asterisks:* p *< 0.05 (*),* p *< 0.01 (**) and* p *< 0.001 (***). The columns 'Median ΔAIC' and 'Median ΔBIC' give the median differences in AIC and BIC between the more complex model and the simpler model. Negative values in 'Median ΔAIC' or 'Median ΔBIC' indicate improved fit with the more complex model.*

Comparison	Year	Median Chi-squared	Median *p*-value	Median ΔAIC	Median ΔBIC
2.2 vs 3.2	2015	3.84	0.43	4.16	21.33
2.2 vs 3.2	2025	2.57	0.63	5.43	22.34
3.2 vs 4.2	2015	25.73	< 0.001 ***	-21.73	-13.14
3.2 vs 4.2	2025	13.90	< 0.001 ***	-9.90	-1.45
4.2 vs 5.2	2015	35.89	< 0.001 ***	-19.89	14.44
4.2 vs 5.2	2025	44.00	< 0.001 ***	-28.00	5.81

2.5.5.6 Species models for 1985 and 1995

The species model structure was similar to that for the temporal models, but I included species as an additional explanatory variable (Table 11). As species has three levels (*Larix decidua*, *Pinus cembra* and *Pinus mugo*), I was able to test whether neighbour effects differed among the three species. I added a variable representing the type of topography, based on the categories described by Schönenberger & Frey (1988). I categorised topography into five types: east-facing, north-facing, gully, ridge and other. It was only possible to conduct species comparisons for 1985 and 1995, since there were too few observations of *Pinus cembra* and *Pinus mugo* in later years to represent the full elevation and neighbour density gradients (for species survival proportions for the full-area dataset see Figure 29 in the Appendix 8.4.3). I fitted these models to the full-area dataset. I did not include stem architecture as an explanatory variable because it was recorded from 1995 onward and was unavailable in 1985. This omission may be most consequential for *Pinus mugo*, which showed the highest within-species proportion of shrublike trees (Figure 30 in the Appendix 8.4.3). As a result, height-based analyses may not fully capture differences in growth form and allocation to lateral versus vertical growth in this species, and alternative size metrics may better represent growth patterns in *Pinus mugo*.

I compared a linear model with an interaction between neighbour density and elevation with a more flexible spline model with the same interaction structure. The spline model had a slightly lower AIC but a slightly higher BIC (for a summary see Table 12 and for extended results see Table 31 in the Appendix 8.4.3). Overall, model 5.3 had the lowest AIC value in both years, while model 2.3 had the lowest BIC value in 1985. In 1995, model 5.3 had the lowest BIC value.

Likelihood-ratio tests across model refits showed that the interaction between elevation and neighbour density was not supported in 1985 or 1995 (for a summary see Table 13 and for extended results see Table 32 in the Appendix 8.4.3). Including the three-way interaction between species, neighbour density and elevation significantly improved model fit. Including topography as a fixed effect significantly improved model fit in both years. Based on these comparisons, together with satisfactory DHARMa residual diagnostics, I selected model 5.3 as the final model for testing the third hypothesis (for residual diagnostics see Figure 31 in the Appendix 8.4.3).

Table 11: Linear mixed-effects models used for species analysis.
Overview of the fixed- and random-effects structures for the five model types considered in the species model selection procedure. The response is the log-transformed height and is applied to every model type. 'species' indicates whether the height response corresponds to Larix decidua*,* Pinus *cembra or* Pinus mugo*, and 'topography' denotes the topography type. 'ns()' denotes natural cubic splines. Random intercepts for plot number (nr) account for spatial clustering. Interactions are indicated by '*', which implies inclusion of all lower-order terms (e.g. 'neighbour density * elevation' expands to 'neighbour density + elevation + neighbour density × elevation').*

Model type	Model formula
	Log(height) ~
1.3	species + neighbour density * elevation + (1 | plot nr)
2.3	species + ns(neighbour density) + ns(elevation) + (1 | plot nr)
3.3	species + ns(neighbour density) * ns(elevation) + (1 | plot nr)
4.3	species * ns(neighbour density) * ns(elevation) + (1 | plot nr)
5.3	topography + species * ns(neighbour density) * ns(elevation) + (1 | plot nr)

Table 12: Summary of model fit (AIC and BIC) for the species models for 1985 and 1995.
For each model type and year, the median AIC and BIC computed across all model refits are reported.

Model type	Year	Median AIC	Median BIC
1.3	1985	3115.20	3162.41
1.3	1995	3068.01	3114.94
2.3	1985	3106.37	3159.48
2.3	1995	3054.23	3107.03
3.3	1985	3112.19	3188.90
3.3	1995	3057.10	3133.36
4.3	1985	3040.38	3211.51
4.3	1995	3036.58	3206.71
5.3	1985	2969.42	3164.15
5.3	1995	2908.44	3102.03

Table 13: Results of likelihood-ratio tests for the species models for 1985 and 1995.
For each model comparison, the columns 'Comparison' and 'Year' identify the contrasted model types and year. The columns 'Median Chi-squared' and 'Median p*-value' report the median chi-squared statistic and median* p*-value across model refits. Significance levels are indicated using asterisks:* p < *0.05 (*),* p < *0.01 (**) and* p < *0.001 (***). The columns 'Median ΔAIC' and 'Median ΔBIC' give the median differences in AIC and BIC between the more complex model and the simpler model. Negative values in 'Median ΔAIC' or 'Median ΔBIC' indicate improved fit with the more complex model.*

Comparison	Year	Median Chi-squared	Median *p*-value	Median ΔAIC	Median ΔBIC
2.3 vs 3.3	1985	6.41	0.17	1.59	25.20
2.3 vs 3.3	1995	8.50	0.07	-0.50	22.97
3.3 vs 4.3	1985	120.81	< 0.001 ***	-88.81	5.61
3.3 vs 4.3	1995	57.24	< 0.001 ***	-25.24	68.62
4.3 vs 5.3	1985	100.28	< 0.001 ***	-92.28	-68.67
4.3 vs 5.3	1995	159.04	< 0.001 ***	-151.04	-127.57

2.5.6 Spatial autocorrelation

Using the Moran's I test from the DHARMa package, I tested for spatial autocorrelation at the plot level (Hartig 2024). To do this, I aggregated residuals by plot and used mean plot coordinates. Due to computational constraints, I was unable to run tree-level tests. I compared spatial autocorrelation of model 3.1 when fitted once to the full dataset and when fitted 500 times to different subsamples from the full dataset. In both cases, the spatial pattern of the residuals showed that neighbouring plots tended to have similar deviations, confirming that spatial autocorrelation was not fully captured by the model based on either the full or the subsampled dataset (for the full dataset see Table 14 and for the subsampled dataset see Table 15). This is also clearly visible in Figure 6. Although the subsampling approach reduced the strength of spatial autocorrelation compared with the full-area dataset, as seen in the smaller difference between observed and expected Moran's I values, the test results remained significant for all model refits. I therefore chose to base the analysis on the subsampling method. However, I avoided using too few samples per stratum, as this would have further reduced spatial autocorrelation at the cost of statistical power and representativeness. I chose this compromise to mitigate spatial autocorrelation while maintaining the robustness of the results.

Table 14: Output of DHARMa Moran's I test for distance-based autocorrelation for the full dataset. 'Observed' is the observed Moran's I, 'Expected' is the Moran's I expected under the null hypothesis of no spatial autocorrelation. 'SD' is the standard deviation of Moran's I and 'p-value' is the p-value for the test with this null hypothesis. Significance levels are indicated using asterisks: $p < 0.05$ (*), $p < 0.01$ (**) *and* $p < 0.001$ (***).

Year	Observed	Expected	SD	*p*-value
1985	0.039	-0.00077	0.0013	< 0.001 ***
2015	0.032	-0.00078	0.0013	< 0.001 ***

Table 15: Summary of DHARMa Moran's I tests for distance-based autocorrelation for the subsampled dataset. 'Median observed' and its 2.5th and 97.5th percentiles describe the distribution of observed Moran's I across all model refits. 'Median expected' and its percentiles give the corresponding values under the null hypothesis of no spatial autocorrelation. 'Proportion of significance' indicates the fraction of the 500 model refits with a significant ($p < 0.05$) Moran's I test.0

Year	1985	2015
Median observed	0.0130	0.0180
2.5th percentile observed	0.0065	0.0090
97.5th percentile observed	0.0220	0.0290
Median expected	-0.0016	-0.0016
2.5th percentile expected	-0.0016	-0.0017
97.5th percentile expected	-0.0015	-0.0016
Proportion of significance	1	1

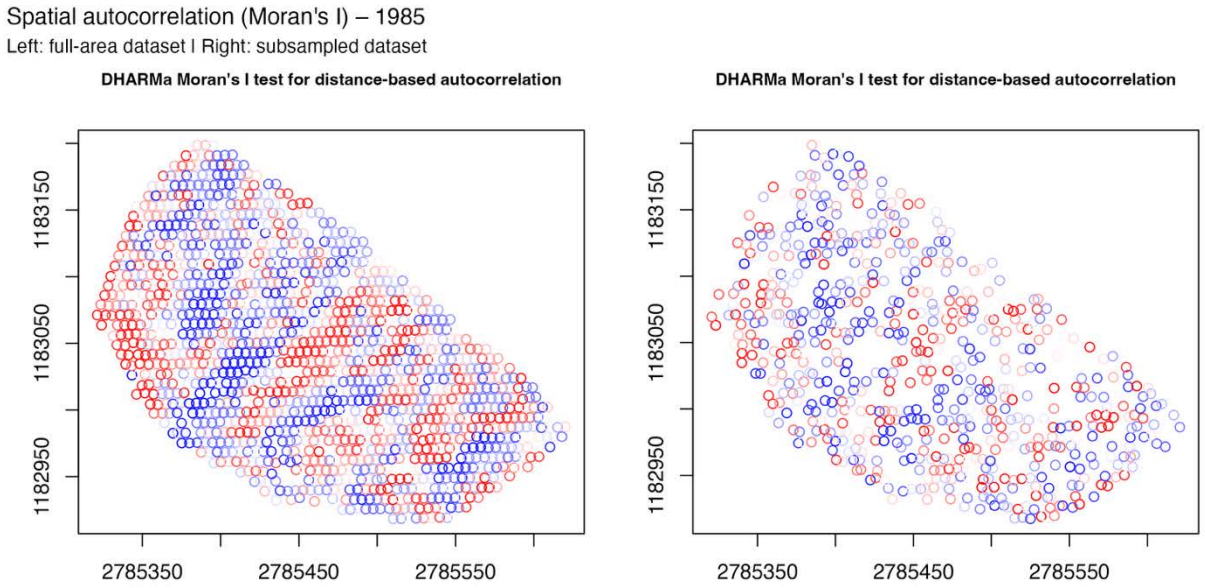

Figure 6: Spatial visualisation of DHARMa Moran's I test for residual autocorrelation for the full dataset (left) and for one randomly selected sample of the subsamples (subsample 1; right) in 1985.
Each circle represents a plot location in the Stillberg study area. The colour of a circle indicates the sign of the DHARMa standardised residual: a red circle denotes a positive residual (observed height > fitted height), and a blue circle denotes a negative residual (observed height < fitted height). Colour intensity reflects the magnitude of a residual (the darker the colour, the larger the absolute residual). Coordinates are shown in the Swiss national reference system (CH1903+ / LV95).

2.5.7 Analyses

2.5.7.1 Neighbour slope calculations and calculations of contrasts

To quantify the marginal slope of neighbour density at three distinct elevation levels (low, mid and high), I used the *emtrends* function from the package emmeans (Lenth 2025). I defined these elevation levels as the 10th, 50th and 90th percentiles of elevation within each subsample and year. This approach allowed me to evaluate how the neighbour effect on tree height varied across elevation levels. For each year, I extracted the marginal slopes associated with neighbour density across the 500 model refits. The results for each year–elevation combination included both the mean slope and a 95% confidence interval, calculated as the 2.5th and 97.5th percentiles of the neighbour slopes derived from the iterations. Since I standardised neighbour density, the resulting slopes can be interpreted as the marginal neighbour effect. Specifically, this effect represents the change in the logarithmic response variable associated with a one-standard deviation increase in neighbour density at a given elevation level, mathematically expressed as: $\partial \log(response) / \partial neighbour$). For better interpretation, I back transformed the logarithmic response. The result is a response ratio. If the ratio is one, the response variable does not change when the neighbour density increases by one standard deviation. If the ratio is greater than one, it indicates a positive neighbour effect on the response ratio. By contrast, a ratio smaller than one indicates a negative neighbour effect on the response ratio.

After estimating elevation-specific neighbour slopes for each subsample using *emtrends*, I computed pairwise contrasts between elevation levels with *pairs* from the emmeans package (Lenth 2025). Then, I summarised contrasts across subsamples using the median and the 2.5th and 97.5th percentiles of the subsample-wise contrast distribution. I assessed significance using a two-sided sign-based *p*-value across subsamples: I computed the fraction of subsample estimates that were < 0 and the fraction that were > 0 and defined the *p*-value as twice the smaller of these two fractions. Thus, the *p*-value is small when most subsample estimates lie on the same side of zero. I did not report the within-model standard errors for *emtrends* or for *pairs* because my aim was to quantify the uncertainty arising from the subsampling and the model refitting procedure. Additionally, in this setting, I expected the between-subsample variability to be much larger than the within-fit uncertainty.

2.5.7.2 Elevation × neighbour density surface

To visualise how predicted tree performance (height or diameter) varied jointly with neighbour density and elevation, I created a grid over the observed ranges of neighbour density and elevation for each year. For each grid point, I predicted tree height and diameter from each of the 500 model refits using the base R function *predict*, using the fixed-effects components of the model, and averaged the predictions across the 500 model refits. For each grid point, I computed pointwise 95% confidence intervals as the 2.5^{th} and 97.5^{th} percentiles of the 500 predictions.

In order to predict diameter from the size-metric models, which included 'size metric' (height or diameter) and 'stem architecture', I generated response surfaces by holding these categorical explanatory variables constant at reference levels. Specifically, I set size metric to diameter (so the surface represents predicted diameter rather than height and diameter combined) and stem architecture to single-stemmed. The plotted surface therefore shows predicted diameter values for single-stemmed trees across the elevation × neighbour-density gradient. Because stem architecture entered the model as an additive main effect, surfaces for forked or shrublike trees have the same shape and differ only by a constant vertical offset. I did not repeat this procedure for *Larix decidua* height in later life stages because I had already generated the elevation × neighbour-density surfaces in the temporal model workflow. After confirming that the temporal and size-metric models produced comparable height predictions for *Larix decidua*, I used the temporal-model surfaces for the size-metric comparison.

To predict surfaces for each species separately, I generated response surfaces by holding the categorical explanatory variables 'species' and 'topography' constant at a specific level. Specifically, I set the species variable to either *Pinus cembra* or *Pinus mugo* when generating each elevation × neighbour-density surface. I held topography constant at 'north-facing', as this was the most common type. The resulting surfaces therefore show the predicted height for either *Pinus cembra* or *Pinus mugo* at a topography type of north-facing. As topography entered the model only as an additive main effect, surfaces for other topography types would have the same shape, differing by a constant vertical offset. I did not repeat this procedure for *Larix decidua* in early life stages because I had already generated the elevation × neighbour-density surfaces in the temporal model workflow. After confirming that temporal and species-specific models produced comparable predictions for *Larix decidua*, I used the temporal-model surfaces for the species comparison.

2.5.7.3 Predicted height at high and low neighbour densities

To visualise how predicted tree performance (height or diameter) varied at the extremes of the elevation and neighbour density gradients, and to test for differences between these extremes, I derived predictions at low and high elevation and neighbour density levels. Within each subsample and year, I defined 'low' and 'high' values as the 10^{th} and 90^{th} percentiles of elevation and total neighbour density. For each fitted model (500 refits per year), I used *emmeans* to predict the response at all combinations of low versus high elevation and low versus high neighbour density (Lenth 2025). Predictions were based on fixed effects only (random effects set to zero), and I back transformed predictions from the logarithmic to the original scale. For each subsample, I computed the contrast between high and low neighbour density at both low and high elevations. Across subsamples, I summarised these contrasts by their mean and empirical 95% uncertainty intervals (2.5^{th} and 97.5^{th} percentiles). I assessed significance using a two-sided sign-based *p*-value across subsamples: I computed the fraction of subsample estimates that were < 0 and the fraction that were > 0 and defined the *p*-value as twice the smaller of these two fractions. Thus, the *p*-value is small when most subsample estimates lie on the same side of zero.

I generated predicted responses from the fitted models by setting the categorical explanatory variable to the level of interest while holding other explanatory variables constant (at reference levels). For the size-metric models, I obtained predictions for diameter by setting the size-metric factor to 'diameter'. For the species models, I obtained predictions by setting the species factor to *Pinus cembra* or *Pinus mugo*. I did not repeat this procedure for *Larix decidua* height in earlier and later life stages for the same reasons described in section 2.5.7.2.

3 Results

3.1 Soil temperature

Across elevation levels, plot-level soil temperature differed slightly (Figure 7). The median of the plot-level soil temperatures was slightly larger at mid and high elevations compared to low elevations. The distributions overlapped strongly among groups, indicating no pronounced elevation gradient in plot-level soil temperature during the measurement period. As there were more loggers across different types of topography, the greatest variability was found at mid elevations, where the loggers spanned the widest range of plot-level soil temperatures.

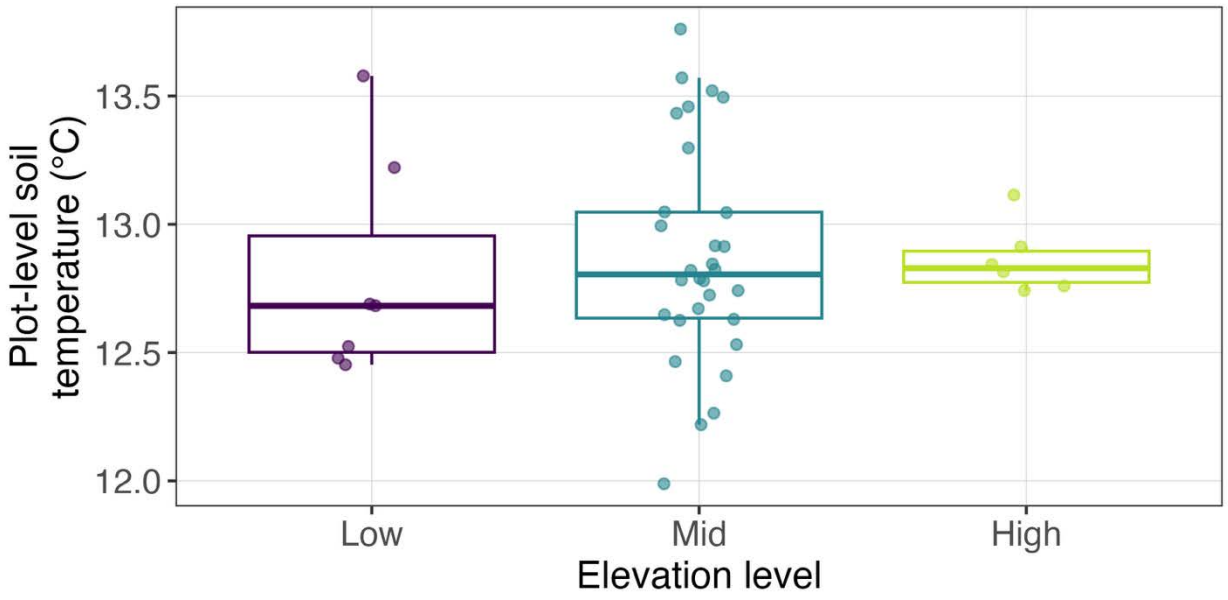

Figure 7: Plot-level soil temperature across elevation levels.
Boxplots show the distribution of plot-level soil temperature (°C) averaged across the 2025 growing season for loggers grouped into low, mid and high elevation levels. Mid elevation includes all loggers located in plots with different topography types (east-facing, north-facing, gully, ridge). Points represent individual loggers (plot-level means); boxes indicate the interquartile range (IQR) with the median (bold line), and whiskers extend to 1.5 × IQR.

Within the mid-elevation level, plot-level soil temperature varied among topography types (Figure 8). East-facing plots and plots located in gullies tended to have higher medians of plot-level soil temperatures than north-facing plots, while plots located on ridges were intermediate. However, overlap among the boxplots suggests that differences among topography types were small relative to within-topography-type variability.

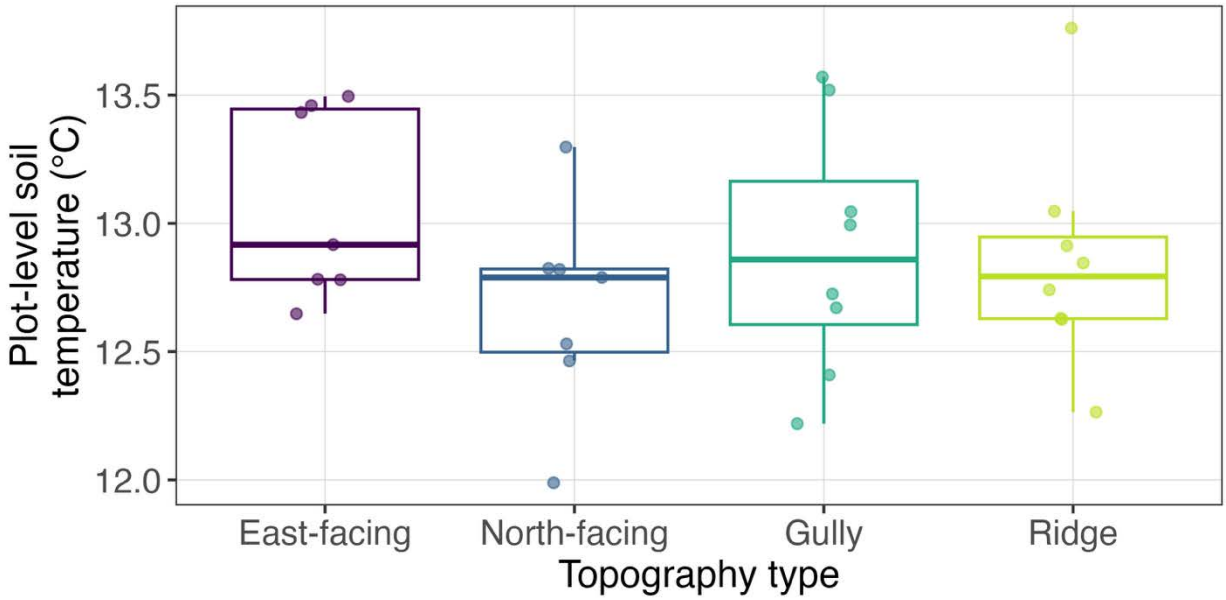

Figure 8: Plot-level soil temperature across topography types at mid elevation level.
Boxplots show the distribution of plot-level soil temperature (°C) averaged across the 2025 growing season among mid-elevation topography types (east-facing, north-facing, gully, ridge). Points represent individual loggers (plot-level means); boxes indicate the interquartile range (IQR) with the median (bold line), and whiskers extend to 1.5 × IQR.

3.2 Dimensions of the stress-gradient hypothesis

3.2.1 Temporal dimension

3.2.1.1 *Larix decidua* height for 1985–2015

Neighbour effects on height ratio tended to decline over time and shifted from clearly positive (ratio > 1) to neutral (ratio = 1), while differences among elevation levels became less distinct (Figure 9). In 1985, neighbour effects were significantly positive at all elevations, indicating facilitative interactions. In 1995, positive neighbour effects persisted at high elevations but were weaker at mid and low elevations. In 2005 and 2015, neighbour effects tended to be neutral to slightly negative (ratio < 1) across elevations. In 1985, neighbour effects differed significantly between mid and high elevations (Table 16). In both 1985 and 1995, neighbour effects differed significantly between low and high elevations.

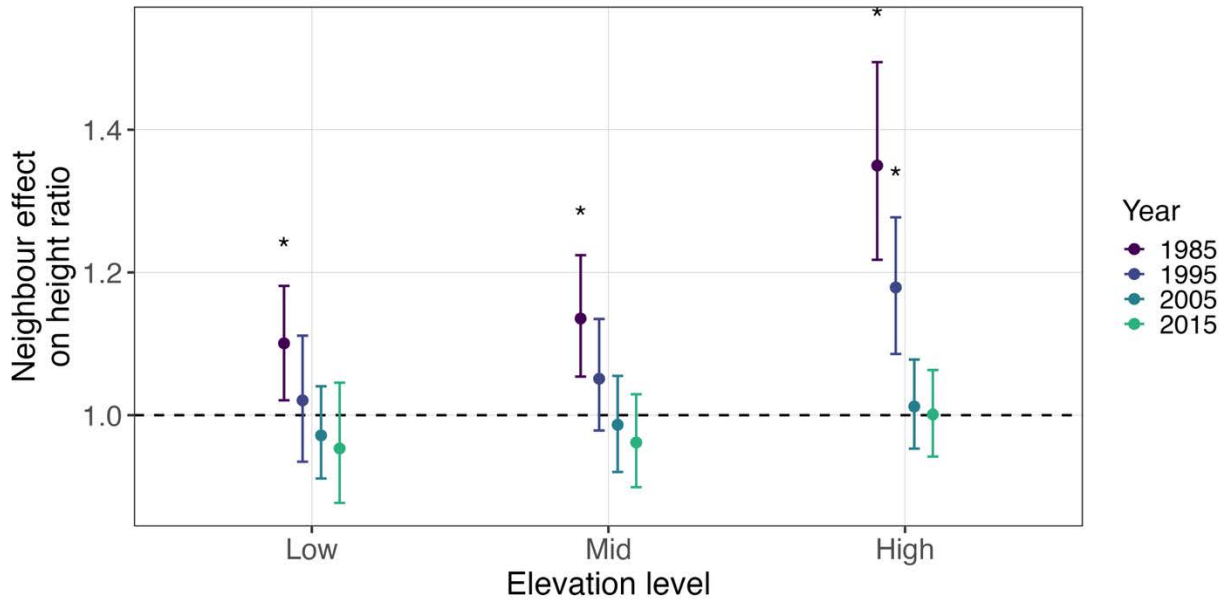

Figure 9: Neighbour effects on tree height across elevation levels and years 1985–2015 for Larix decidua*. Points show the mean predicted height ratio per one standard deviation increase in neighbour density from 500 model refits, and error bars indicate pointwise 95% confidence intervals. Colours distinguish survey years. Asterisks mark cases where the neighbour effect is significantly different from zero (confidence interval does not include one).*

Table 16: Pairwise contrasts in neighbour effect on tree height ratio among elevation levels for Larix decidua *from 1985–2015.*

For each year, the difference in the estimated neighbour effect on height ratio between two elevation levels (shown in 'Contrast') is reported. 'Mean difference' shows the mean difference in the neighbour effect between two elevation levels. Positive values indicate a more positive neighbour effect at the first listed elevation level. The '2.5th percentile' and '97.5th percentile' columns give 2.5% and 97.5% quantiles of the contrast distribution (pointwise 95% confidence interval). The 'p-value' is derived from these distributions, and asterisks mark contrasts whose 95% confidence interval excludes zero. Significance levels: $p < 0.05$ (*), $p < 0.01$ (**) *and* $p < 0.001$ (***).

Year	Contrast	Median difference	2.5th percentile	97.5th percentile	*p*-value
1985	Low vs High	-0.20	-0.32	-0.06	0.008 **
1985	Low vs Mid	-0.03	-0.13	0.08	0.59
1985	Mid vs High	-0.17	-0.30	-0.05	0.008 **
1995	Low vs High	-0.14	-0.26	-0.02	0.02 *
1995	Low vs Mid	-0.03	-0.16	0.09	0.62
1995	Mid vs High	-0.11	-0.23	0.0018	0.05
2005	Low vs High	-0.04	-0.13	0.05	0.42
2005	Low vs Mid	-0.02	-0.11	0.08	0.72
2005	Mid vs High	-0.03	-0.12	0.07	0.61
2015	Low vs High	-0.05	-0.15	0.06	0.37
2015	Low vs Mid	-0.0088	-0.12	0.10	0.89
2015	Mid vs High	-0.04	-0.14	0.05	0.48

In both 1985 and 2015, predicted tree height declined with increasing elevation (Figure 10). In 1985, trees tended to be taller at higher neighbour densities across the elevation gradient. By contrast, in 2015, predicted height at high elevations was largely independent of neighbour density, whereas at low elevations trees were generally taller at lower neighbour densities. Interaction surfaces for an early and a late life stage are shown as representative examples; corresponding height surfaces for other years, as well as confidence interval plots of the interaction surfaces, are provided in Appendix 8.5.1.1.

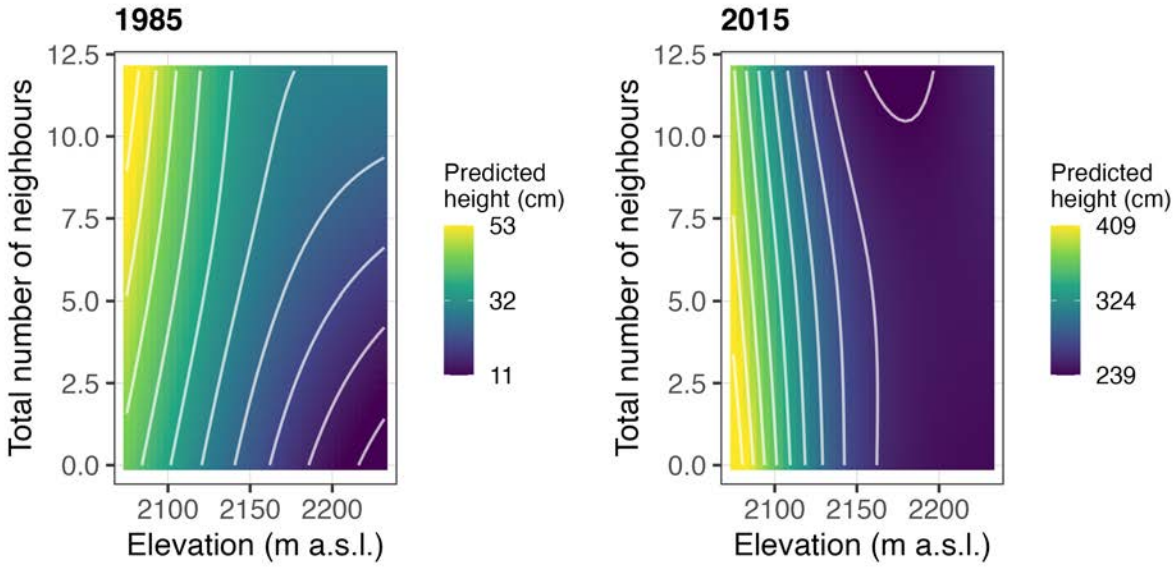

Figure 10: Predicted tree height surface for Larix decidua *for 1985 (left) and 2015 (right).*
Each surface is shown as a raster where each grid cell is coloured by the mean predicted tree height, with white contour lines indicating isolines of equal predicted height. Predictions are mapped across the observed gradients of elevation (m a.s.l.; x-axis) and neighbour density (y-axis). Values represent the average of model refits, using fixed effects only (random plot effects set to zero).

Predicted tree height differed between neighbour-density classes and the pattern depended on elevation and year (Figure 11). At high elevation, predicted height was significantly higher under high neighbour density than under low neighbour density in 1985 and 1995. The same was true at low elevations in 1985. In later years, estimates for the two neighbour-density classes largely overlapped at high elevations. At low elevations, the predicted height was higher under low neighbour density, but the difference was not significant.

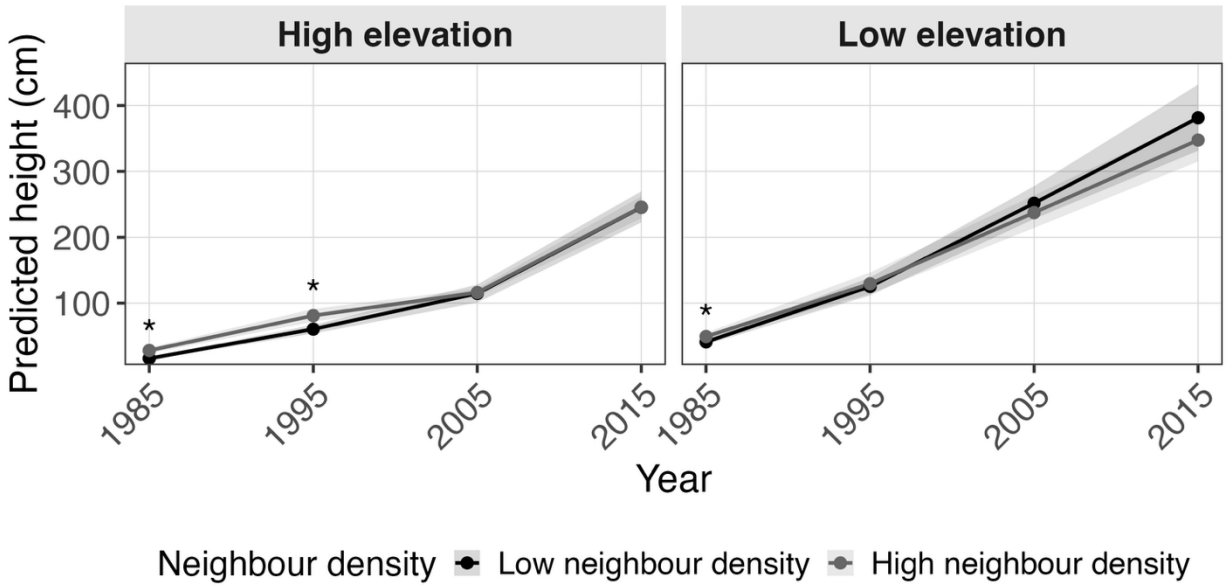

Figure 11: Predicted tree height over time at high (left) and low (right) elevations for Larix decidua *from 1985 to 2015. Lines show model-predicted mean height for low and high neighbour densities, with shaded bands indicating 95% uncertainty intervals. Asterisks denote years in which the contrast between neighbour-density classes was statistically supported (95% interval excluding zero).*

3.2.1.2 *Larix decidua* height for 1985–2025

When models were fitted to the subset dataset, the overall patterns were similar to those from the full-area dataset: neighbour effects on height ratio tended to decline over time and shifted from clearly positive to neutral or slightly negative effects, while differences among elevation levels became less distinct over time (Figure 12). Like the full-area results, in 1985 neighbour effects were significantly positive at mid and high elevations, and the positive effect persisted in 1995 at high elevations. In contrast to the full-area results, the neighbour effect was not significantly positive in 1985 for low elevations but significantly negative in 2005. Neighbour effects differed significantly for high compared to low elevations in 1995 and high compared to mid elevations in 2005 (Table 17).

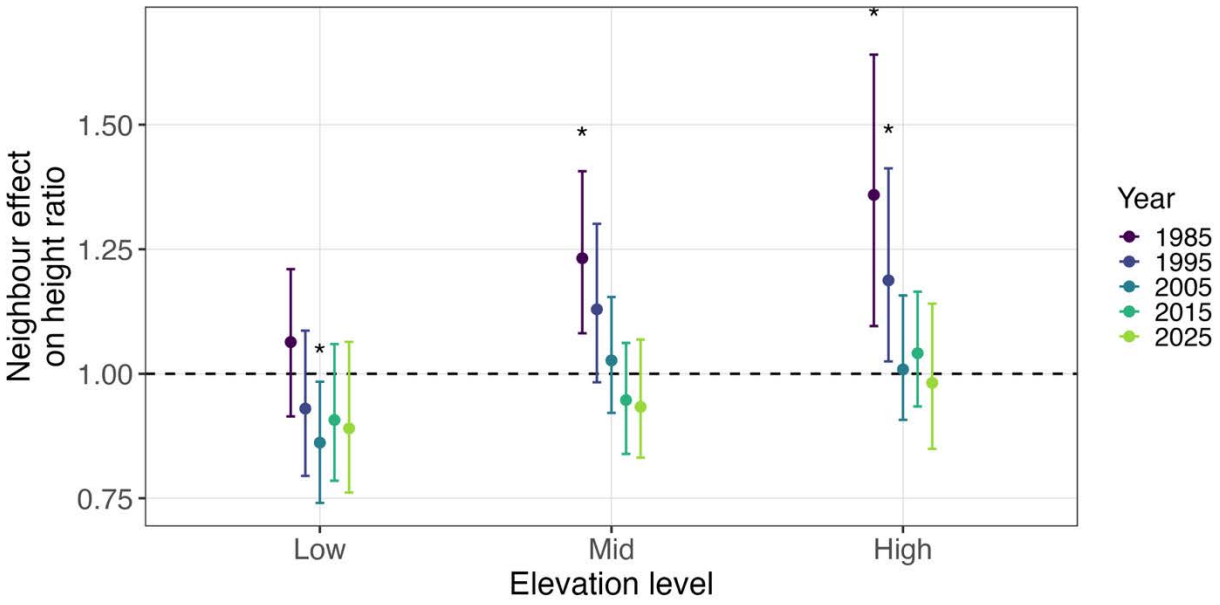

Figure 12: Neighbour effects on tree height across elevation levels and years 1985–2025 for Larix decidua*. Points show the mean predicted height ratio per one standard deviation increase in neighbour density from model refits, and error bars indicate pointwise 95% confidence intervals. Colours distinguish survey years. Asterisks mark cases where the neighbour effect is significantly different from zero (confidence interval does not include one).*

Table 17: Pairwise contrasts in neighbour effect on tree height ratio among elevation levels for Larix decidua *from 1985–2025.*

*For each year, the difference in the estimated neighbour effect on height ratio between two elevation levels (shown in 'Contrast') is reported. 'Mean difference' shows the mean difference in the neighbour effect between two elevation levels. Positive values indicate a more positive neighbour effect at the first listed elevation level. The '2.5th percentile' and '97.5th percentile' columns give 2.5% and 97.5% quantiles of the contrast distribution (pointwise 95% confidence interval). The '*p*-value' is derived from these distributions, and asterisks mark contrasts whose 95% confidence interval excludes zero. Significance levels:* $p < 0.05$ (*), $p < 0.01$ (**) *and* $p < 0.001$ (***).

Year	Contrast	Median difference	2.5th percentile	97.5th percentile	*p*-value
1985	Low vs High	-0.25	-0.48	0.02	0.08
1985	Low vs Mid	-0.14	-0.36	0.06	0.13
1985	Mid vs High	-0.09	-0.36	0.17	0.45
1995	Low vs High	-0.24	-0.46	-0.03	0.02 *
1995	Low vs Mid	-0.19	-0.42	0.03	0.09
1995	Mid vs High	-0.05	-0.26	0.16	0.63
2005	Low vs High	-0.15	-0.35	0.02	0.08
2005	Low vs Mid	-0.17	-0.37	-0.02	0.03 *
2005	Mid vs High	0.02	-0.17	0.18	0.80
2015	Low vs High	-0.14	-0.31	0.04	0.11
2015	Low vs Mid	-0.04	-0.24	0.18	0.65
2015	Mid vs High	-0.10	-0.27	0.09	0.29
2025	Low vs High	-0.10	-0.32	0.12	0.38
2025	Low vs Mid	-0.04	-0.25	0.16	0.63
2025	Mid vs High	-0.05	-0.26	0.16	0.63

In both, 1985 and 2025, the predicted height of trees declined with increasing elevation (Figure 13). In 1985, trees tended to be taller at medium neighbour density at low elevations, and at high neighbour density at high elevations. By contrast, in 2025, predicted height at high elevations was largely independent of neighbour density; at low elevations, however, trees were generally taller at lower neighbour densities. Representative examples of interaction surfaces for early and late life stages are shown;

corresponding height surfaces for other years, as well as confidence interval plots of the interaction surfaces, are provided in Appendix 8.5.1.2.

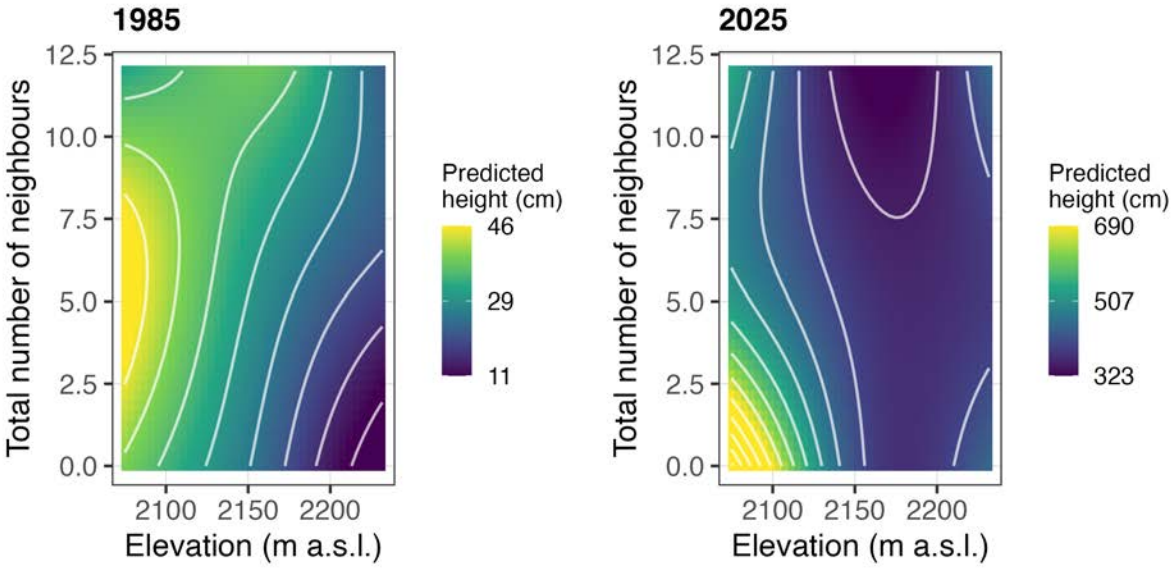

Figure 13: Predicted tree height surface for Larix decidua *for 1985 (left) and 2025 (right).*
The surface is shown as a raster where each grid cell is coloured by the mean predicted tree height, with white contour lines indicating isolines of equal predicted height. Predictions are mapped across the observed gradients of elevation (m a.s.l.; x-axis) and neighbour density as total number of neighbours (y-axis). Values represent the average of model refits, using fixed effects only (random plot effects set to zero).

Predicted tree height differed between neighbour-density classes and the pattern depended on elevation and year (Figure 14). At high elevation, predicted height was significantly larger under high neighbour density than under low neighbour density in 1985 and 1995. In later years, estimates for the two neighbour-density classes largely overlapped. At low elevation, predicted height was significantly larger under low neighbour density in 2005. The same trend was observed in 2015 and 2025 but was not significant.

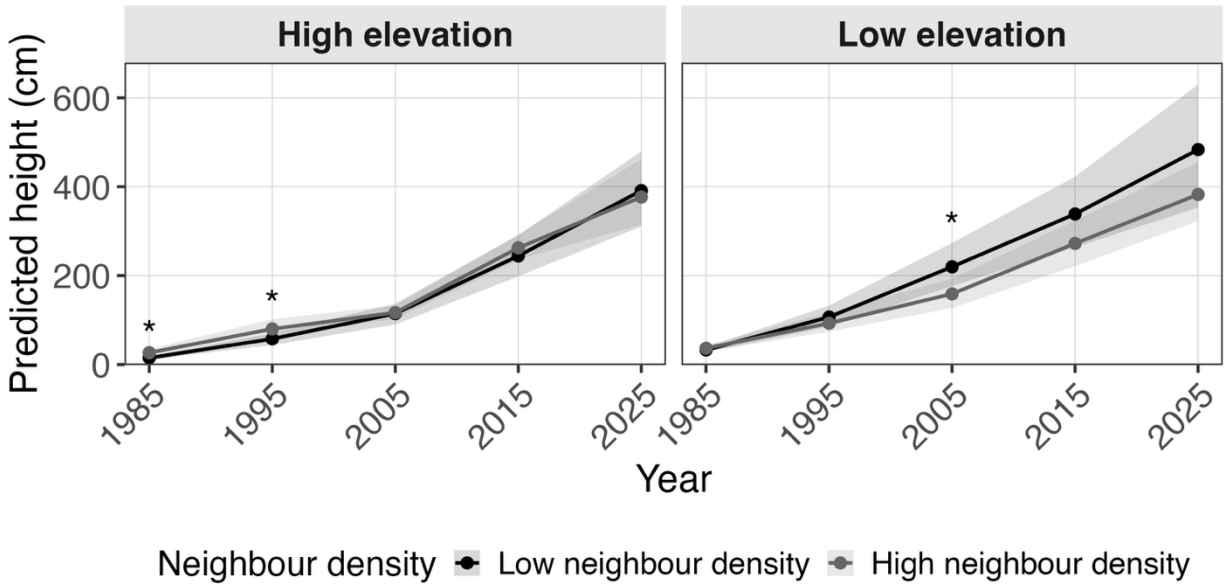

Figure 14: Predicted tree height over time at high (left) and low (right) elevations for Larix decidua from 1985 to 2025. Lines show model-predicted mean height for low and high neighbour densities, with shaded bands indicating 95% uncertainty intervals. Asterisks denote years in which the contrast between neighbour-density classes was statistically supported (95% interval excluding zero).

3.2.2 Size-metric dimension

3.2.2.1 *Larix decidua* diameter for 2015 and 2025

Neighbour effects on diameter ratio tended to decline over time, while differences among elevation levels became less distinct (Figure 15). Except for mid elevations in 2015, all neighbour effects were significantly negative, indicating competitive interactions. Neighbour effects on diameter ratio did not differ significantly among elevation levels in 2015 and 2025 (Table 18). Even though not significant, the neighbour effect tended to be more positive at mid compared to low and high elevations in both years.

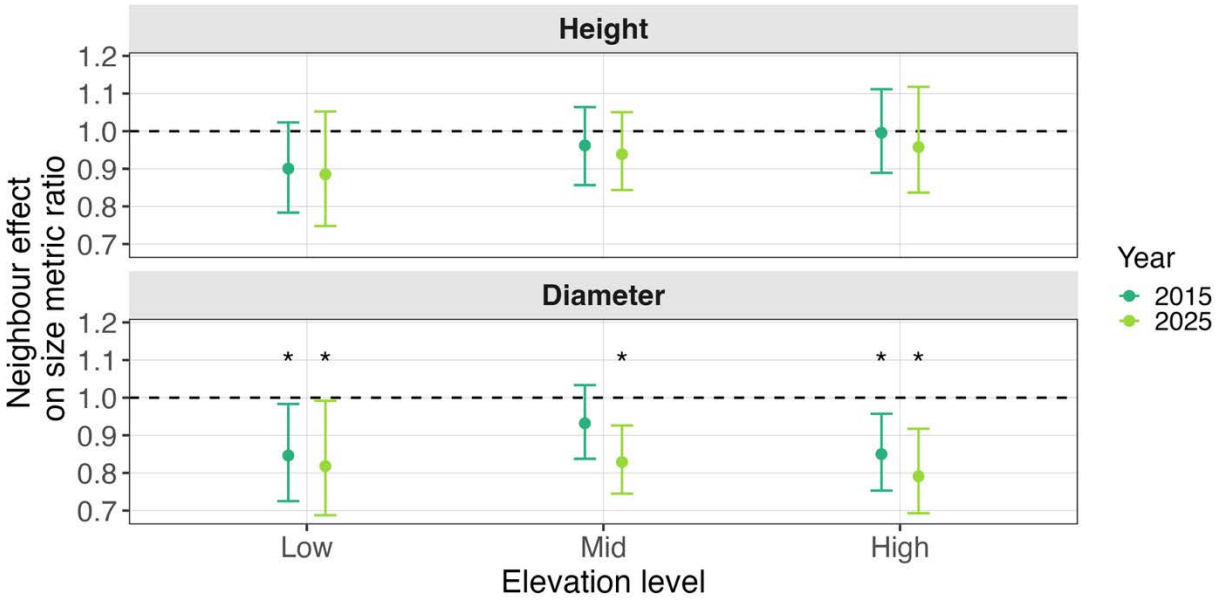

Figure 15: Neighbour effects on tree height (upper) and diameter (lower) across elevation levels and years 2015 and 2025 for Larix decidua*.*
Points show the mean predicted response variable ratio per one standard deviation increase in neighbour density from model refits, and error bars indicate pointwise 95% confidence intervals. Colours distinguish survey years. Asterisks mark cases where the neighbour effect is significantly different from zero (confidence interval does not include one).

Table 18: Pairwise contrasts in neighbour effect on tree diameter ratio among elevation levels for Larix decidua *for 2015 and 2025.*
*For each year, the difference in the estimated neighbour effect on diameter ratio between two elevation levels (shown in 'Contrast') is reported. 'Mean difference' shows the mean difference in the neighbour effect between two elevation levels. Positive values indicate a more positive neighbour effect at the first listed elevation level. The '2.5th percentile' and '97.5th percentile' columns give 2.5% and 97.5% quantiles of the contrast distribution (pointwise 95% confidence interval). The '*p*-value' is derived from these distributions, and asterisks mark contrasts whose 95% confidence interval excludes zero. Significance levels:* $p < 0.05$ *(*), *$p < 0.01$ *(**) and* $p < 0.001$ *(***).*

Year	Contrast	Median difference	2.5th percentile	97.5th percentile	*p*-value
2015	Low vs High	-0.02	-0.20	0.15	0.82
2015	Low vs Mid	-0.10	-0.27	0.09	0.34
2015	Mid vs High	0.08	-0.11	0.24	0.37
2025	Low vs High	0.02	-0.20	0.26	0.92
2025	Low vs Mid	-0.02	-0.23	0.20	0.87
2025	Mid vs High	0.04	-0.16	0.22	0.74

In both 2015 and 2025, predicted diameter decreased more strongly with increasing neighbour density than with increasing elevation (Figure 16). In 2015, trees were predicted to have the largest diameter at low elevations combined with low neighbour density. By 2025, this pattern was evident both at low and high elevations. At mid elevations, the negative effect of neighbour density on diameter was generally weaker in both years. Confidence-interval plots of the interaction surfaces are provided in Appendix 8.5.2.1.

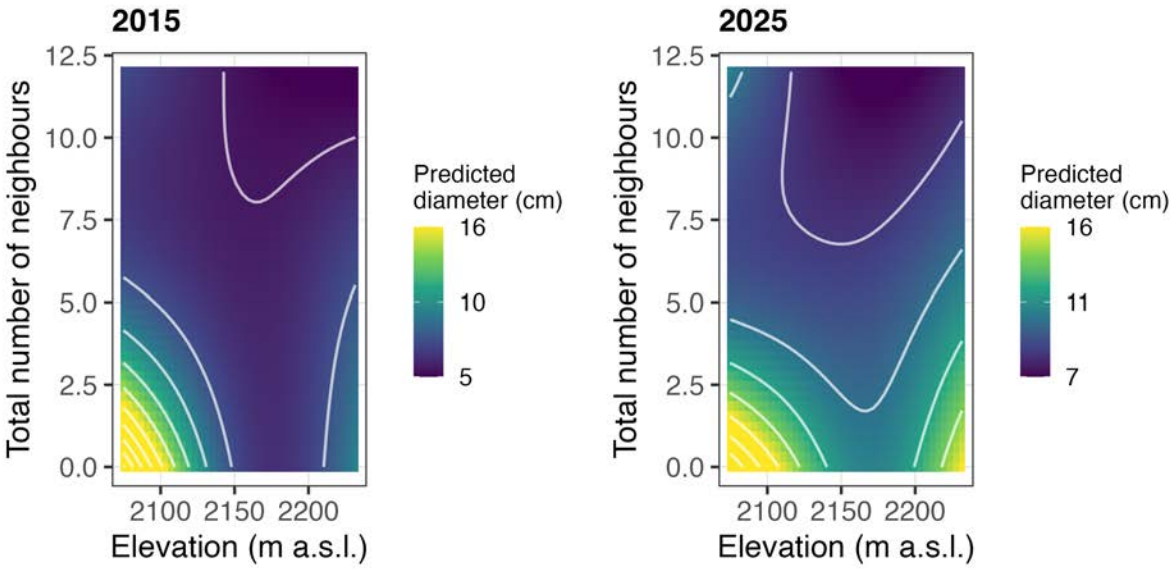

Figure 16: Predicted tree diameter surface for Larix decidua for 2015 (left) and 2025 (right).
The surface is shown as a raster where each grid cell is coloured by the mean predicted diameter, with white contour lines indicating isolines of equal predicted diameter. Predictions are mapped across the observed gradients of elevation (m a.s.l.; x-axis) and neighbour density as total number of neighbours (y-axis). Values represent the average of model refits, using fixed effects only (random plot effects set to zero).

Predicted tree diameter was significantly higher under low neighbour density than under high neighbour density at both high and low elevations in 2015 and 2025 (Figure 17).

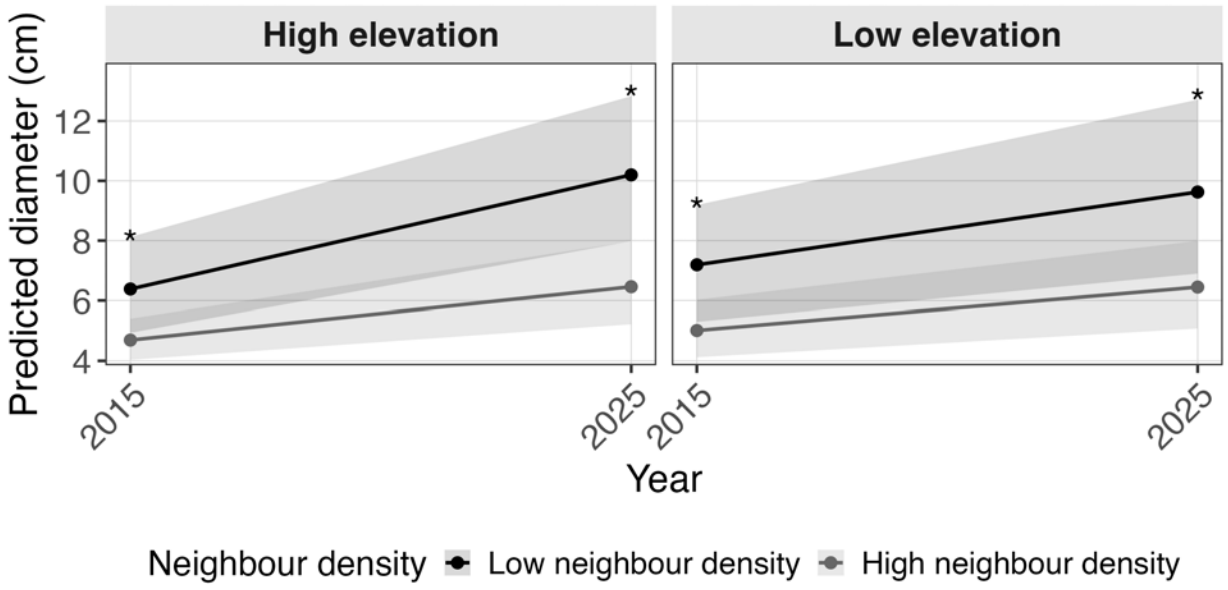

Figure 17: Predicted tree diameter over time at high (left) and low (right) elevations for Larix decidua for 2015 and 2025. Lines show model-predicted mean diameter for low and high neighbour densities, with shaded bands indicating 95% uncertainty intervals. Asterisks denote years in which the contrast between neighbour-density classes was statistically supported (95% interval excluding zero).

3.2.2.2 Size-metric comparison

Overall, neighbour effects on height ratios were more positive than on diameter ratios (Figure 15). Consistent with this, diameter showed significant negative neighbour effects for most elevation and year combinations, whereas height did not. Direct contrasts between neighbour effects on height and diameter ratios indicated that responses to neighbours differed significantly between size metrics at high elevations in 2015 and at both mid and high elevations in 2025 (Table 19).

Response surface comparisons further illustrate these size-metric-specific patterns. In 2025, tree height decreased with elevation, whereas diameter showed no consistent elevational trend (for height see Figure 13 and for diameter see Figure 16). For both size metrics, trees attained the largest predicted size at low neighbour density at low elevations. However, at high elevations this negative effect of neighbour density remained evident only for diameter. Moreover, within-size-metric contrasts revealed different patterns: height exhibited most positive neighbour effects at high elevations, whereas diameter showed most positive neighbour effects at mid elevations (for height see Table 17 and for diameter see Table 18).

Table 19: Difference in neighbour effects on tree height vs diameter ratios among elevation levels for Larix decidua *for 2015 and 2025.*
'Mean difference' gives the mean difference in neighbour effects (height minus diameter) for a given elevation level and year. Positive values indicate that the neighbour effect on height ratio was more positive than the neighbour effect on diameter ratio. The columns '2.5th percentile' and '97.5th percentile' report the 2.5% and 97.5% quantiles of the contrast distribution, corresponding to an empirical 95% uncertainty interval. The p*-values are based on a two-sided sign test across subsamples; values marked with asterisks indicate contrasts for which the 95% interval excludes zero. Significance levels:* p < *0.05 (*),* p < *0.01 (**) and* p < *0.001 (***).*

Year	Elevation level	Mean difference	2.5th percentile	97.5th percentile	*p*-value
2015	Low	0.06	-0.0071	0.13	0.07
2015	Mid	0.03	-0.03	0.09	0.29
2015	High	0.16	0.11	0.21	< 0.001 ***
2025	Low	0.08	-0.02	0.18	0.11
2025	Mid	0.12	0.05	0.20	< 0.001 ***
2025	High	0.19	0.11	0.27	< 0.001 ***

3.2.3 Species dimension

3.2.3.1 *Pinus cembra* height for 1985 and 1995

For *Pinus cembra*, the neighbour effect on height ratio was significantly positive at low elevations in 1985, but this weakened by 1995, shifting to a neutral neighbour effect (Figure 18). At mid elevations, neighbour effect remained positive in both years. At high elevations, neighbour effects were close to neutral in both years. There was no significant difference in neighbour effect on height ratio among elevation levels in 1985 and 1995 (Table 20). Although non-significant, neighbour effects tended to be more positive at mid than at high elevations in both years.

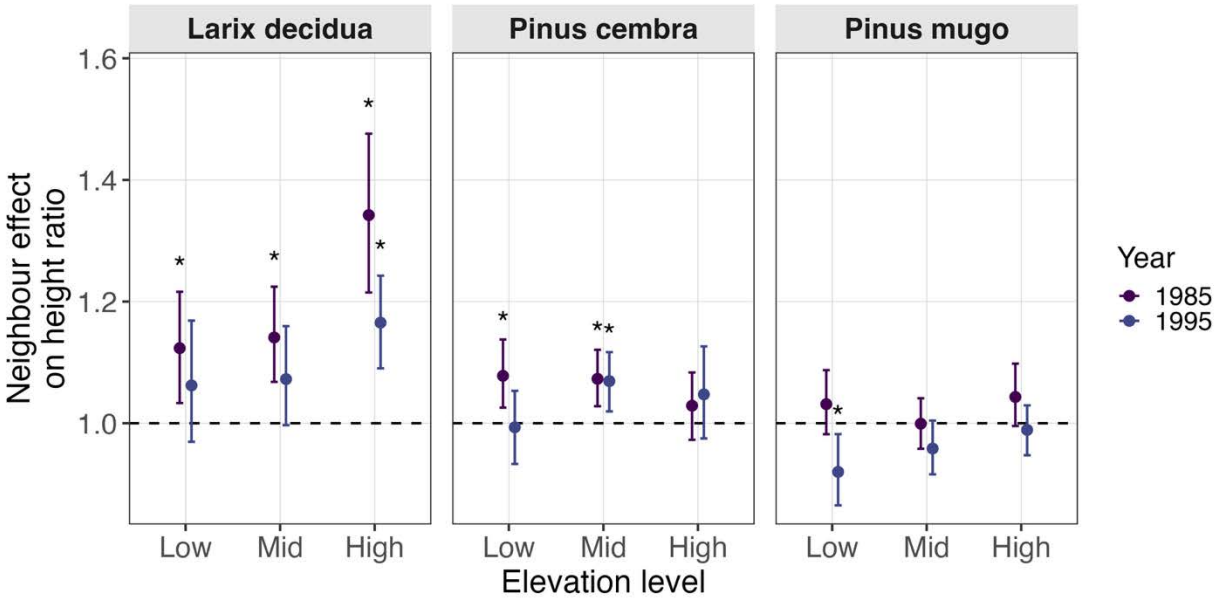

Figure 18: Neighbour effects on tree height for all focal species across elevation levels and years 1985 and 1995. Points show the mean predicted response variable ratio per one standard deviation increase in neighbour density from model refits, and error bars indicate pointwise 95% confidence intervals. Colours distinguish survey years. Asterisks mark cases where the neighbour effect is significantly different from zero (confidence interval does not include one).

Table 20: Pairwise contrasts in the neighbour effect on tree height ratio among elevation levels for Pinus cembra for 1985 and 1995.
For each year, the difference in the estimated neighbour effect on height ratio between two elevation levels (shown in 'Contrast') is reported. 'Mean difference' shows the mean difference in the neighbour effect between two elevation levels. Positive values indicate a more positive neighbour effect at the first listed elevation level. The '2.5th percentile' and '97.5th percentile' columns give 2.5% and 97.5% quantiles of the contrast distribution (pointwise 95% confidence interval). The 'p-value' is derived from these distributions and asterisks mark contrasts whose 95% confidence interval excludes zero. Significance levels: p < *0.05 (*),* p < *0.01 (**) and* p < *0.001 (***).*

Year	Contrast	Mean difference	2.5th percentile	97.5th percentile	*p*-value
1985	Low vs High	0.05	-0.02	0.12	0.18
1985	Low vs Mid	0.0046	-0.06	0.08	0.92
1985	Mid vs High	0.04	-0.03	0.12	0.28
1995	Low vs High	-0.05	-0.14	0.04	0.28
1995	Low vs Mid	-0.07	-0.15	0.0012	0.06
1995	Mid vs High	0.02	-0.07	0.12	0.70

In both 1985 and 1995, the predicted height decreased more strongly along the elevation axis than along the neighbour density axis (Figure 19). In both years, the largest trees

were predicted at low elevations, with slightly larger predicted height at higher neighbour densities. Confidence-interval plots of the interaction surfaces are provided in Appendix 8.5.3.1.

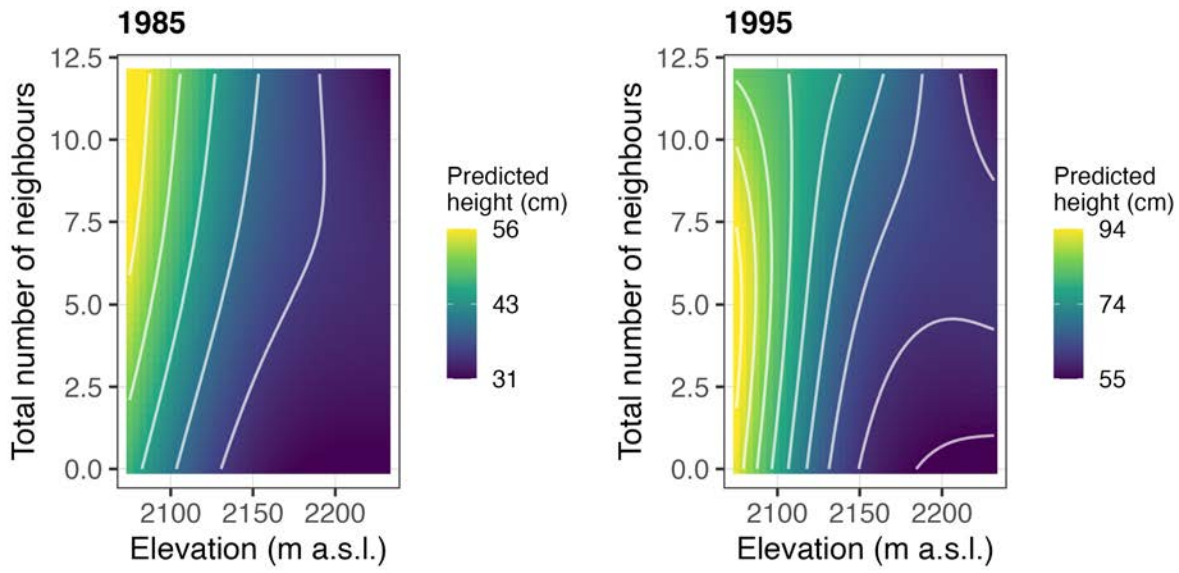

Figure 19: Predicted tree height surface for Pinus cembra *for 1985 (left) and 1995 (right).*
The surface is shown as a raster where each grid cell is coloured by the mean predicted tree height, with white contour lines indicating isolines of equal predicted height. Predictions are mapped across the observed gradients of elevation (m a.s.l.; x-axis) and neighbour density as total number of neighbours (y-axis). Values represent the average of model refits, using fixed effects only (random plot effects set to zero).

In 1985, predicted tree height differed significantly between neighbour density classes at low elevations, where trees were taller at high neighbour density (Figure 20). At other elevation-year combinations, however, predicted height did not differ between neighbour density classes.

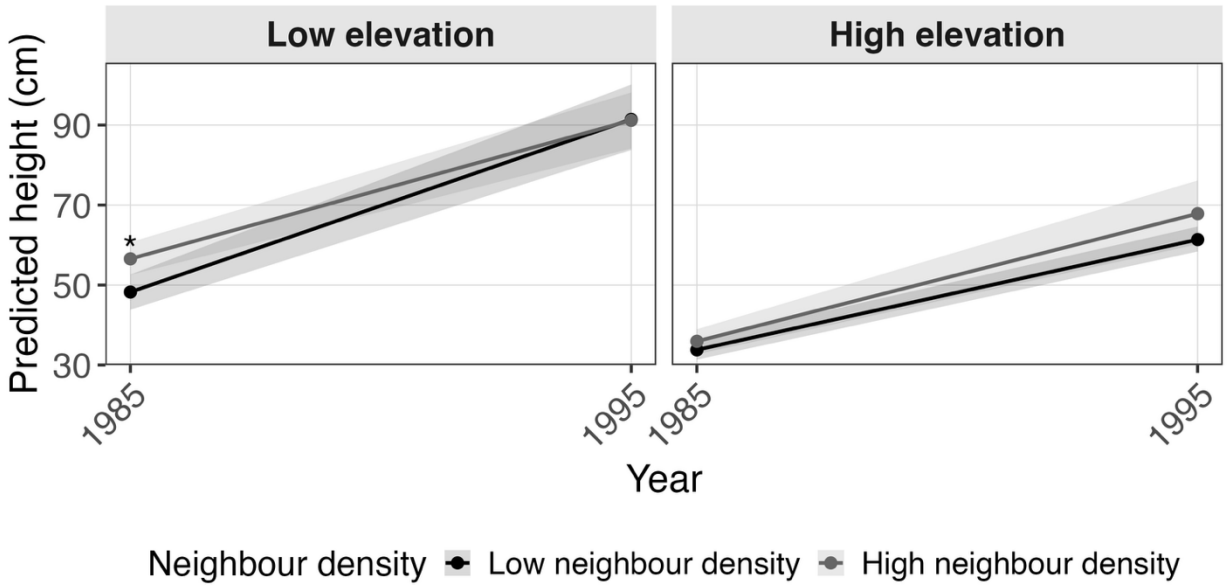

Figure 20: Predicted tree height over time at high (left) and low (right) elevations for Pinus cembra *for 1985 and 1995. Lines show model-predicted mean height for low and high neighbour densities, with shaded bands indicating 95% uncertainty intervals. Asterisks denote years in which the contrast between neighbour-density classes was statistically supported (95% interval excluding zero).*

3.2.3.2 *Pinus mugo* height for 1985 and 1995

For *Pinus mugo*, the neighbour effect on the height ratio was neutral to slightly positive across elevation levels in 1985, but this was not significant (Figure 18). In 1995, the height ratio was neutral to slightly negative overall, and significantly negative at low elevations. There were no significant differences in neighbour effects on height ratio among elevation levels in 1985 and 1995 (Table 21).

Table 21: Pairwise contrasts in the neighbour effect on tree height ratio among elevation levels for Pinus mugo *for 1985 and 1995.*

*For each year, the difference in the estimated neighbour effect on height ratio between two elevation levels (shown in 'Contrast') is reported. 'Mean difference' shows the mean difference in the neighbour effect between two elevation levels. Positive values indicate a more positive neighbour effect at the first listed elevation level. The '2.5th percentile' and '97.5th percentile' columns give 2.5% and 97.5% quantiles of the contrast distribution (pointwise 95% confidence interval). The '*p*-value' is derived from these distributions, and asterisks mark contrasts whose 95% confidence interval excludes zero. Significance levels:* $p < 0.05$ (*), $p < 0.01$ (**) *and* $p < 0.001$ (***).

Year	Contrast	Mean difference	2.5th percentile	97.5th percentile	*p*-value
1985	Low vs High	-0.01	-0.08	0.06	0.75
1985	Low vs Mid	0.03	-0.03	0.10	0.32
1985	Mid vs High	-0.04	-0.11	0.02	0.22
1995	Low vs High	-0.07	-0.14	0.0051	0.06
1995	Low vs Mid	-0.04	-0.12	0.03	0.32
1995	Mid vs High	-0.03	-0.10	0.04	0.35

In both 1985 and 1995, the predicted height decreased more strongly along the elevation axis than along the neighbour density axis (Figure 21). In 1985, trees were tallest at low elevations in areas with higher neighbour densities. However, by 1995, this pattern changed slightly, with trees being tallest in areas with a lower neighbour density. Confidence-interval plots of the interaction surfaces are provided in Appendix 8.5.3.2.

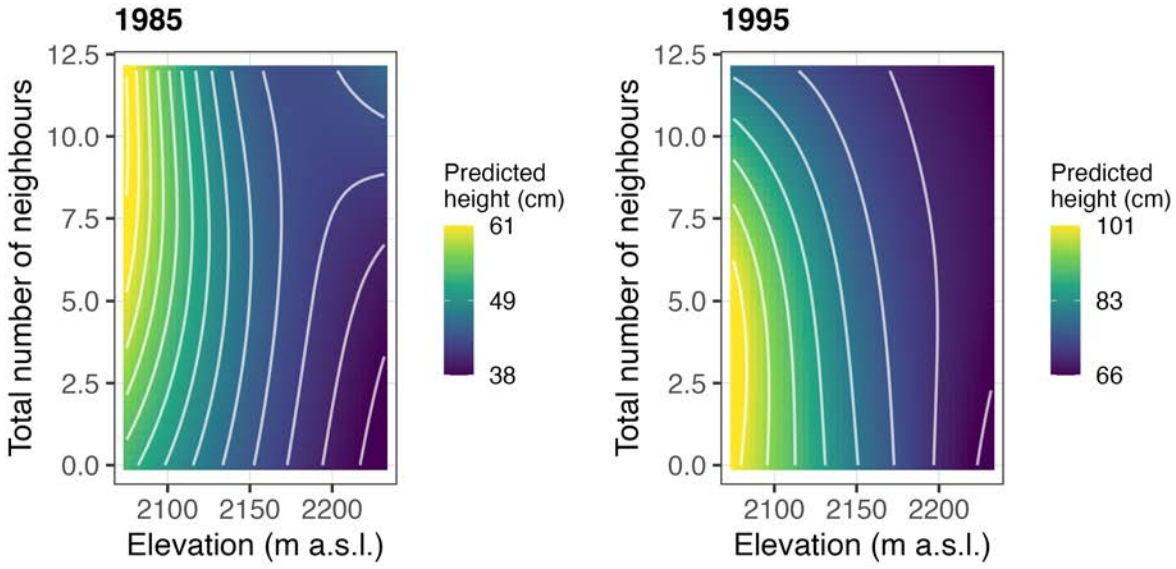

Figure 21: Predicted tree height surface for Pinus mugo *for 1985 (left) and 1995 (right).*
The surface is shown as a raster where each grid cell is coloured by the mean predicted tree height, with white contour lines indicating isolines of equal predicted height. Predictions are mapped across the observed gradients of elevation (m a.s.l.; x-axis) and neighbour density as total number of neighbours (y-axis). Values represent the average of model refits, using fixed effects only (random plot effects set to zero).

In 1985, there was no significant difference in predicted tree height between the two neighbour density classes and two elevation levels (Figure 22). By 1995, the pattern did not change, except that the predicted tree height was significantly larger at low elevations and low neighbour densities.

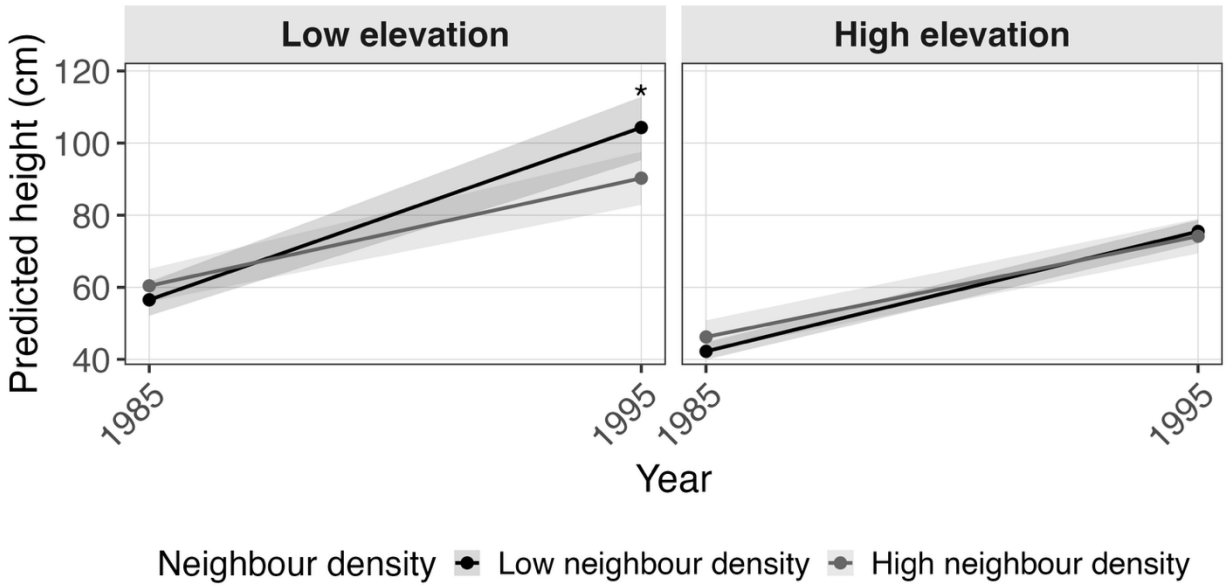

Figure 22: Predicted tree height over time at high (left) and low (right) elevations for Pinus mugo *for 1985 and 1995. Lines show model-predicted mean height for low and high neighbour densities, with shaded bands indicating 95% uncertainty intervals. Asterisks denote years in which the contrast between neighbour-density classes was statistically supported (95% interval excluding zero).*

3.2.3.3 Species comparison

Overall, neighbour effects on height ratios were most pronounced for *Larix decidua*, followed by *Pinus cembra* and *Pinus mugo* (Figure 18). In line with this, the direct contrasts between neighbour effects on height among species indicated that at mid elevations the neighbour effect was significantly more positive for *Larix decidua* and *Pinus cembra* compared with *Pinus mugo* in both years (Table 22). At high elevations, neighbour effects for *Larix decidua* were significantly more positive compared with the other two species in both years. Additionally, in 1995 at low elevations, *Larix decidua* had a significantly more positive neighbour effect compared with *Pinus mugo.*

Response-surface figures highlight these species-specific patterns. Predicted height declined with elevation for all three species. For *Larix decidua* the relationship between elevation and height did vary with neighbour density (i.e. a density × elevation interaction; Figure 16), whereas surfaces for *Pinus cembra* and *Pinus mugo* were largely consistent across neighbour density (for *Pinus cembra* see Figure 19 and for *Pinus mugo* see Figure 21).

In the predicted-height figures, the patterns were consistent with the neighbour-effect results for the early years. *Larix decidua* and *Pinus cembra* either showed height independent of neighbour density, or height increasing with neighbour density (for *Larix decidua* see Figure 14 and for *Pinus cembra* see Figure 20). In contrast, *Pinus mugo* showed a neutral effect or tended to be taller at lower neighbour density in the early years (Figure 22). *Larix decidua* was the only species that exhibited significant differences in height among elevations in 1985 when within-species differences were compared (for *Larix decidua* see Table 17, for *Pinus cembra* see Table 19 and for *Pinus mugo* see Table 20).

Table 22: Difference in neighbour effects on tree height ratios among species for 1985 and 1995.
'Mean difference' gives the mean difference in neighbour effects for a given elevation level and year. Positive values indicate that the neighbour effect on height ratio was more positive for the first species listed in the 'Species contrast' column. The columns '2.5th percentile' and '97.5th percentile' report the 2.5% and 97.5% quantiles of the contrast distribution, corresponding to an empirical 95% uncertainty interval. The p*-values are based on a two-sided sign test across subsamples; values marked with asterisks indicate contrasts for which the 95% interval excludes zero. Significance levels:* p < *0.05 (*),* p < *0.01 (**) and* p < *0.001 (***).*

Year	Elevation level	Species contrast	Mean difference	2.5th percentile	97.5th percentile	*p*-value
1985	Low	*Larix decidua* vs *Pinus cembra*	0.04	-0.04	0.14	0.38
1985	Low	*Larix decidua* vs *Pinus mugo*	0.09	-0.0085	0.17	0.07
1985	Low	*Pinus cembra* vs *Pinus mugo*	0.04	-0.02	0.11	0.21
1985	Mid	*Larix decidua* vs *Pinus cembra*	0.06	-0.03	0.14	0.17
1985	Mid	*Larix decidua* vs *Pinus mugo*	0.13	0.05	0.21	< 0.001 ***
1985	Mid	*Pinus cembra* vs *Pinus mugo*	0.07	0.0076	0.13	0.008 **
1985	High	*Larix decidua* vs *Pinus cembra*	0.27	0.15	0.37	< 0.001 ***
1985	High	*Larix decidua* vs *Pinus mugo*	0.25	0.15	0.35	< 0.001 ***
1985	High	*Pinus cembra* vs *Pinus mugo*	-0.01	-0.09	0.06	0.71
1995	Low	*Larix decidua* vs *Pinus cembra*	0.07	-0.04	0.18	0.25
1995	Low	*Larix decidua* vs *Pinus mugo*	0.14	0.04	0.26	0.004 **
1995	Low	*Pinus cembra* vs *Pinus mugo*	0.08	-0.0072	0.16	0.08
1995	Mid	*Larix decidua* vs *Pinus cembra*	0.0031	-0.09	0.09	0.94
1995	Mid	*Larix decidua* vs *Pinus mugo*	0.11	0.03	0.20	0.01 **
1995	Mid	*Pinus cembra* vs *Pinus mugo*	0.11	0.05	0.17	< 0.001 ***
1995	High	*Larix decidua* vs *Pinus cembra*	0.11	0.0041	0.21	0.04 *
1995	High	*Larix decidua* vs *Pinus mugo*	0.16	0.09	0.24	< 0.001 ***
1995	High	*Pinus cembra* vs *Pinus mugo*	0.06	-0.03	0.14	0.20

4 Discussion

4.1 Temporal dimension and the role of life stage

Overall, hypothesis 1 was partially supported. As expected, neighbour effects on *Larix decidua* height followed an SGH-like elevation pattern, with stronger competition at low elevations and weaker competition or even facilitation at high elevations. My results therefore confirm the results of another preliminary study where neighbour interactions were examined along the elevation gradient at Stillberg (Barbeito 2013). They are also consistent with previous evidence for SGH-like patterns along elevation gradients. (Callaway 1998; Eränen & Kozlov 2008; LaManna *et al.* 2022).

Throughout the monitoring period, interaction outcomes were not static but shifted. The SGH-like elevation differences were most evident early on. Competitive neighbour effects intensified over time (1985–2025), while elevation differences became less distinct as the stand developed. This observed shift confirms the findings of previous studies that the magnitude and direction of the SGH-like pattern can vary throughout tree life stages (Barbeito 2013; Callaway 1998; LaManna *et al.* 2022). In my study system, three non-exclusive mechanisms could explain this shift: reduction in temperature limitation under climatic warming, stand development processes that increase competition, and seasonal or interannual variation in interaction outcomes.

Warming-driven changes in temperature limitation could help explain why elevation differences became less distinct over time. In the Swiss Alps, temperature isotherms have shifted upwards, meaning that trees at the treeline may grow well below their potential climatic limit (Jochner *et al.* 2018; Körner & Hiltbrunner 2024). This is because warming has reduced temperature limitations. This warming trend is supported by meteorological measurements at Stillberg, which indicate that mean annual air temperature increased by 1.4 °C from 1975 to 2022 (Lechler *et al.* 2024). Similar temporal shifts in the apparent stress gradient have been associated with warming in other treeline contexts (Wang *et al.* 2016). In that study, warming-driven stand densification was suggested to increase neighbour competition over time.

The increase in competition with life stage is consistent with stand development processes and with the fact that *Larix decidua* is a fast-growing and light-demanding species (Brzeziecki & Kienast 1994; Risch *et al.* 2003). Stillberg is an even-aged afforestation. Over the 50-year study period, neighbourhoods were increasingly made up

of *Larix decidua* trees that had survived. This implies that rising intraspecific competition and self-thinning play a greater role in shaping tree performance (Westoby 1984). In line with this are the general expectations that competitive effects intensify as size asymmetry increases and dense stands develop (Ford *et al.* 2017). In particular, size-asymmetric light competition tends to disproportionately affect less shade-tolerant (i.e. more light-demanding) species (Ford *et al.* 2017), which is consistent with the pattern observed in my study.

Finally, interaction outcomes may vary seasonally or among years, particularly in the treeline ecotone. Facilitation can be most pronounced during episodically stressful conditions (e.g. winters with irregular snowpack), and net interaction effects can switch as the abiotic context changes (Batllori *et al.* 2009; Loranger *et al.* 2017). This may help explain departures from the overall temporal trend, such as the comparatively negative neighbour effects observed in 2005 at low elevations. Higher-frequency measurements (e.g. derived from dendrometers) could further resolve seasonal and interannual stress responses, including drought-related effects (Ziegler *et al.* 2024) or freezing events, which were found to be especially damaging for *Larix decidua* (Rixen *et al.* 2012). Moreover, facilitation can be difficult to distinguish from shared favourable microsites, which may be misinterpreted as positive interactions in neighbourhood analyses (Steinbauer *et al.* 2016).

Overall, neighbour effects on *Larix decidua* height broadly followed an SGH-like elevation pattern, but this pattern weakened over the study period and competition intensified. Reduced temperature limitation under climatic warming and increasing intraspecific competition most likely acted concurrently in shaping these temporal patterns and cannot be disentangled in this system. While interannual deviations occurred, they were limited to a few years and modulated rather than altered the long-term trajectory. Sensitivity to neighbourhood composition and sampling design (as illustrated by differences between the full-area and subset analyses) further indicates that robust inference of SGH-like patterns requires sufficient replication and careful definition of the abiotic stress gradient. Ongoing climatic warming may therefore shift tree–tree interactions in treeline ecotones towards stronger competition, potentially offsetting growth gains expected from reduced temperature stress (Wang *et al.* 2016). My results highlight the continued importance of long-term, well-replicated studies across multiple life stages, that explicitly characterise neighbourhood context along a stress gradient.

4.2 Importance of size-metric dimension

My results largely support hypothesis 2 by showing that neighbour effects differ between height and diameter for *Larix decidua* and are generally more negative for diameter. This is consistent with evidence that performance metrics can respond differently along elevation gradients (Eränen & Kozlov 2008). Height showed a SGH-like response to elevation, whereas diameter was less strongly structured by elevation and more strongly influenced by neighbourhood density.

The stronger competitive signal in diameter is consistent with evidence that reducing competition through thinning in *Larix decidua* stands lowers the height-to-diameter ratio, indicating that dense neighbourhoods promote more slender growth forms (Novák & Slodičák 2006). Similar density-dependent increases in height-to-diameter ratios have also been reported for other conifer species (Vospernik *et al.* 2010). This supports the general interpretation that diameter is particularly sensitive to local competitive pressure.

Unexpectedly, diameter exhibited a weak hump-shaped SGH pattern, a response that has also been reported for diameter growth along elevation gradients in other systems (He *et al.* 2023). This divergence from the monotonic SGH response observed for height suggests that height and diameter differ in their sensitivity to abiotic conditions, particularly air versus soil temperature. One plausible explanation is that diameter growth is less sensitive to air temperature than height (Bernoulli & Körner 1999; Körner & Hiltbrunner 2024), and responds more strongly to soil temperature (Cui *et al.* 2025). At Stillberg, the effective stress gradient for soil temperature at 10 cm depth did not vary monotonically with elevation and has been reported to be lowest at mid elevations (Hilman *et al.* 2024). Such a pattern could generate a hump-shaped response in diameter meaning that mid-elevation conditions impose stronger temperature constraints on diameter growth. In my study, soil temperature measurements did not show a clear mid-elevation minimum, potentially because loggers were installed at a shallower depth (5 cm) than in Hilman *et al.* (2024). It may also be due to differences in the number of replicates. Uneven replication across topography types and elevations may have reduced my ability to resolve fine-scale temperature patterns, as mid elevations were better represented than lower and higher elevations.

The differences in soil temperature among topography types observed in my study, though not tested for significance, could suggest that diameter is linked to fine-scale microsite conditions. The relatively high variability at mid elevations likely reflects a

broader representation of topography types at this elevation level. Similar, microsite-driven variability may occur at other elevation levels but was less well represented in the available data. Other microsite features, such as slope and aspect, have been shown to influence height–diameter relationships (Long *et al.* 2020) and may have contributed to the partial decoupling of height and diameter responses along the elevation gradient.

In conclusion, I have shown that abiotic stress along an elevation gradient can be expressed differently across performance metrics, with important consequences for detecting and interpreting SGH patterns (Eränen & Kozlov 2008). These size-metric-specific responses should be considered when testing the SGH and when predicting forest dynamics under ongoing climatic warming. Future work linking performance metrics to life stage and microsite heterogeneity may further improve abiotic stress assessments and the understanding of competition–facilitation dynamics in the treeline ecotone (Barbeito 2013; Barbeito *et al.* 2012; LaManna *et al.* 2022).

4.3 Species dimension and life-history strategy

Overall, hypothesis 3 was partially supported. Neighbour effects on height during early life stages differed among *Larix decidua*, *Pinus cembra* and *Pinus mugo*. Specifically, an SGH-like pattern, with stronger competition at low elevations and weaker competition or even facilitation at high elevations, was evident for *Larix decidua* and *Pinus mugo*, but not clearly for *Pinus cembra*. This pattern is consistent with evidence that SGH outcomes vary among tree species along temperature gradients (Beauchamp *et al.* 2025) and supports the view that responses to neighbouring trees in treeline ecotones are species-specific. Moreover, the magnitude of neighbour effects varied among species in a manner consistent with refinements of the SGH based on life-history strategy (Maestre *et al.* 2009). Notably, *Larix decidua* showed the strongest facilitation at high elevations, *Pinus cembra* exhibited weaker positive neighbour effects and *Pinus mugo* was largely neutral to slightly negative. This suggests that stress-tolerant species may experience weaker net interaction benefits from neighbour-mediated stress amelioration.

These species-specific differences in neighbour effects were broadly consistent with contrasts in life-history strategy but highlight limits to applying CSR classifications to predict SGH responses in treeline trees. Because the neighbourhood metric I applied pooled conspecific and heterospecific neighbours, focal trees experienced a mixture of life-history strategies rather than a single benefactor type. Neighbourhood composition

was more or less balanced between competitive and stress-tolerant life-history strategies in 1985 and 1995 as survival proportion of *Larix decidua* alone was comparable to the combined survival of the pine species. Within the strategy-based framework of Maestre *et al.* (2009), this mixed neighbourhood context implies that net interaction effects reflect combined contributions of competitive and stress-tolerant life-history strategies. This is consistent with the stronger shift towards facilitation observed for *Larix decidua* at high elevations. This pattern supports the expectation that species with a competitive life-history strategy can gain more from neighbour-mediated stress amelioration under non-resource stress, whereas stress-tolerant species tend to show weaker net interaction benefits. However, because Maestre *et al.* (2009) did not explicitly incorporate ruderal strategies or successional dynamics, and because neighbour identity was not resolved in my study, life-history strategy alone cannot fully explain the weak or inconsistent SGH responses observed for the pine species. To place these patterns into a broader ecological context, I next compare the Stillberg results for each species with evidence from natural systems, focusing on whether spatial clustering and inferred neighbour associations align with the species-specific responses observed.

Larix decidua often exhibits a clustered spatial structure in natural treeline ecotones (Didier 2001; Lingua *et al.* 2008), consistent with the facilitation observed during early life stages at Stillberg. Clustering becomes more pronounced towards the treeline (Lingua *et al.* 2008), suggesting that close neighbouring trees may be beneficial under more stressful abiotic conditions. One plausible mechanism is buffering against freezing: *Larix decidua* shoots are more susceptible to freezing damage than those of *Pinus mugo* (Rixen *et al.* 2012). Summer freezing events occur regularly at Stillberg and can substantially reduce *Larix decidua* productivity within the same growing season (Rixen *et al.* 2012). Higher neighbour density may therefore mitigate microclimatic extremes, potentially reducing exposure to freezing, contributing to more positive neighbour effects at higher elevations.

In naturally regenerated treeline systems, seed dispersal of *Pinus cembra* is largely mediated by *Nucifraga caryocatactes* (spotted nutcracker; Gugerli *et al.* 2022). The caching behaviour of *Nucifraga caryocatactes* often results in spatially clustered seed deposits, such that *Pinus cembra* seedlings often establish in aggregated clusters (Didier 2001; Gugerli *et al.* 2022; Tomback *et al.* 1993). However, typically just one individual survives beyond early life stages (Gugerli *et al.* 2022), indicating CNDD after establishment. These patterns align with the weak but positive neighbour effects on early height observed for *Pinus cembra* at Stillberg and with evidence that *Pinus cembra* can

associate positively with *Larix decidua* in natural treeline ecotones (Lingua *et al.* 2008). In addition, *Larix decidua* and *Pinus cembra* have been reported to co-occur in stable forest stages (Risch *et al.* 2003). Lingua *et al.* (2008) further reported positive associations for *Pinus cembra* with *Pinus mugo* at high elevations. Together, these studies support the occurrence of early facilitation in *Pinus cembra* but do not explain why no SGH-like pattern was found.

In natural treeline ecotones, *Pinus mugo* often shows weak or no interspecific spatial clustering at small scales (<10 m) and random spatial associations with *Larix decidua* (Lingua *et al.* 2008), consistent with the largely neutral neighbour effects observed in my study. The negative neighbour effect detected at low elevation in 1995 could reflect either intraspecific self-thinning, which has been reported for *Pinus mugo* stands (Risch et al. 2003; Westoby 1984), or interspecific competition. Lingua *et al.* (2008) documented an SGH-like shift in *Pinus mugo–Pinus cembra* associations along an elevation gradient, suggesting competition at low elevations and facilitation at higher elevations. At Stillberg, however, the more plausible driver is competition with the faster-growing *Larix decidua*, which can competitively replace *Pinus mugo* during succession (Risch *et al.* 2003). The interpretation of the SGH-like pattern for this species is further complicated by the growth form. Height may be an inappropriate performance metric for *Pinus mugo*, as individuals more often exhibit shrub-like stem architecture than the other species. Growth is expressed more through branching and lateral expansion than through vertical height.

Beyond species life-history strategy, the choice of stress gradient and pathogen pressure may further obscure SGH patterns at Stillberg, particularly for the pine species. At Stillberg, elevation may not capture the most relevant stress gradient because early-life mortality is strongly influenced by snow-related fungal infections linked to snowmelt timing (Barbeito *et al.* 2013; Senn 1999). Snowmelt timing does not correlate perfectly with elevation due to strong microhabitat variation (Barbeito *et al.* 2012), so elevation alone may be a poor proxy for pathogen-related stress. In case that disease pressure is primarily controlled by snowmelt timing rather than elevation per se, elevational differences in neighbour effects on tree height may appear weak or inconsistent because pathogen-driven mortality filters individuals before height responses can be expressed. This mechanism may help explain why SGH-like elevational patterns were difficult to detect for the pine species when using elevation alone and why neighbour effects were predominantly neutral during early life stages.

Additionally, interactions with the surrounding alpine grassland may obscure SGH patterns at Stillberg, particularly the early neighbour effects that occur during establishment. These treeline species have been shown to differ in their response to vegetation cover during establishment. Specifically, a study near treeline in the French Alps indicated that *Larix decidua* and *Pinus mugo* survival was particularly sensitive to vegetation cover, whereas *Pinus cembra* maintained high survival but exhibited reduced growth even under low levels of shade (Loranger *et al.* 2017). Further, a study looking at the structure and long-term development of mountain forests in the Swiss Central Alps, suggested that *Pinus mugo* can establish even in small soil openings, while *Larix decidua* needs larger patches of bare soil (Risch *et al.* 2003). If similar mechanisms apply at Stillberg, low-stature-vegetation-mediated effects could confound tree neighbour effects and potentially lead to species differences in early performance. *Larix decidua* was probably even more sensitive to such effects because it was smaller than the other species at the time of planting (2 cm on average, compared with 14 cm for *Pinus cembra* and 10 cm for *Pinus mugo*; Schönenberger & Frey 1988).

Together, these results show that neighbour interactions in the treeline ecotone are species-specific and are clearly expressed during early establishment. Patterns were broadly consistent with strategy-based refinements of the SGH and suggest that incorporating life-history strategy provides a simple yet promising step toward improving interpretation and prediction of forest dynamics in the treeline ecotone. This approach is practical because CSR strategies can be quantified using standardised trait-based tools such as the StrateFy spreadsheet (Pierce *et al.* 2017), which uses leaf area, specific leaf area and leaf dry matter content to derive continuous C, S and R scores. At the same time, because the neighbourhood metric used here pooled conspecific and heterospecific neighbours, future work on SGH in treeline settings could refine inferences by explicitly accounting for neighbour identity to disentangle inter- and intraspecific species interactions. More broadly, these findings imply that future treeline dynamics under climate change will depend not only on shifting temperature regimes but also on species-specific sensitivities to abiotic stress and life-history strategy.

4.4 Facilitation in early life stages and management implications

Neighbour effects were not detectably competitive in the earliest life stages assessed for 1985 and 1995, contrary to the expectations of hypotheses 1 and 3. In this section I

examine this result in the context of early-stage competition versus facilitation and its practical implications. The expectation of early competition was motivated by Eränen & Kozlov (2008), who showed that competition was apparent in seedling–seedling interactions.

The absence of detectable competition in the earliest years can be interpreted in light of life stage and experimental spacing. Eränen & Kozlov (2008) reported predominantly competitive effects in *Betula pubescens* seedlings along an elevation gradient, but the trees in their study were very young (1–5 years) and planted extremely close together (~10 cm), conditions that increase the likelihood and detectability of resource competition. In contrast, my Stillberg 'early' analysis (1985) concerned juveniles (13–14 years) planted as seedlings with a wider spacing (~70 cm), which most likely reduced competition intensity and may have favoured early facilitation or neutral effects. Moreover, Eränen & Kozlov (2008) noted that competitive signals can be weak and masked by genetic and environmental heterogeneity. Thus, while competition may not be detectable in the earliest years, it may emerge later as trees grow. Accordingly, neighbour effects became more negative over time in my study, particularly for *Larix decidua* and *Pinus mugo*.

These findings may inform afforestation strategies near treeline, particularly cluster afforestation. Cluster afforestation is a planting approach where trees are established in clusters and within each cluster in small collectives containing multiple seedlings, typically spaced about 50–100 cm apart, but planted in favourable microsites while leaving unfavourable microsites unplanted (Schönenberger 2001). Although the Stillberg area was not planted using a cluster design, the initial spacing (~70 cm) falls within the recommended range for collectives (Schönenberger 2001). In this context, the early-life-stage results (neutral to positive neighbour effects on height, especially for *Pinus cembra* and *Larix decidua*) are consistent with the idea that close tree neighbourhoods can be beneficial near treeline. In line with this, a study examining the spatial distribution of trees in the Italian Central Alps indicated clumped distributions of trees in naturally regenerated areas near the treeline, as well as a significant positive spatial association between young trees (< 100 years old) up to 14 m (Lingua *et al.* 2008). These findings suggest that clustering may be associated with facilitative neighbourhood effects near treeline.

At the same time, Schönenberger (2001) emphasised, based on the cluster afforestation trial at Müstair, Switzerland, that cluster design requires species-specific fine-tuning, aligning with the species-specific SGH patterns observed in my study. Importantly, the neighbourhood effects estimated at Stillberg are averaged across microsites and do not

distinguish conspecific from heterospecific neighbours, whereas cluster afforestation targets favourable microsites and often involves planting conspecific collectives (Schönenberger 2001). Together, this suggests that dense planting in the treeline ecotone can support early performance of some tree species, but outcomes may depend on microsite selection, neighbour identity and species-specific responses.

Early neighbour effects at Stillberg were not competitive for any of the species studied. However, the direction of the SGH pattern may be species-specific, and competition can emerge within a decade in particular species-elevation combination. From a forest management perspective, these early neutral-to-positive neighbour effects are consistent with the rationale of cluster afforestation and dense planting in favourable microsites.

5 Conclusions

Across life stages, performance metrics and species, this thesis shows that support for the stress-gradient hypothesis (SGH) in a treeline ecotone is conditional rather than universal. An SGH-like pattern in neighbour effects on height for *Larix decidua* weakened over time and became increasingly competitive, consistent with concurrent reductions in temperature limitation under climatic warming and increasing intraspecific competition as the even-aged stand developed. With ongoing climatic warming, reduced temperature limitation may further shift tree–tree interactions towards stronger competition, highlighting the sensitivity of treeline dynamics to climate change (Wang *et al.* 2016). Size-metric-specific responses further demonstrate that elevation-related stress can be expressed differently in height and diameter growth, indicating that performance metric choice can strongly influence inferred SGH pattern. Species-specific differences in the magnitude and direction of neighbour effects broadly aligned with life-history-based refinements of the SGH (Maestre *et al.* 2009), with more positive neighbour effects for *Larix decidua* (more competitive strategy) and weaker net interaction benefits for the pine species (more stress-tolerant strategies). In contrast, SGH-like elevation trends were clearer for some species than others. They were more pronounced for *Larix decidua* and *Pinus mugo* than for *Pinus cembra*, reinforcing the context dependence of neighbour effects. These results emphasise the importance of considering several abiotic stress gradients within a single system, when planning a study design. The prevalence of early neutral-to-positive neighbour effects underscores the importance of facilitation during the establishment. This supports specific forest management approaches such as cluster afforestation. Incorporating life-history strategy (including ruderal traits), life stage and performance metrics into the SGH alongside the full stress gradient is critical for predicting treeline forest dynamics and forest management approaches in the context of continued climatic warming.

Acknowledgements

I would like to thank my supervisor Peter Bebi, from the Mountain Ecosystems group at SLF, for sharing his expertise on the Stillberg research area and for guiding me throughout my Master's thesis. I also thank my co-supervisors, Melissa Dawes and Wouter Hantson from the Mountain Ecosystems group at SLF. I am grateful to Melissa Dawes for carefully reading and providing valuable suggestions and comments on the manuscript and for many scientific discussions and guidance through statistical difficulties. I would like to thank Wouter Hantson for providing valuable suggestions and comments on the manuscript and for supporting the fieldwork.

I am grateful to Mauro Marty for support with data cleaning, loading of the data into the Stillberg database and database maintenance. I thank Christian Rixen for providing the iButton soil temperature loggers and for statistical support. I am especially grateful to Anne Kempel for patience and guidance in selecting appropriate statistical methods, especially when I encountered difficulties. I would also like to thank the statistical consulting service at ETH for helping me with my analysis by providing useful tips.

Many thanks to the Stillberg field team for their persistence despite challenging conditions. In particular, I thank the core team, Alyssa Ringgenberg, Michelle Kobler and Viktoria Frank, as well as the additional helpers Loic Amrein, Noël Schneuwly, Ruber Zeitler, Xenia Davide and Zora van der Bie. I thank Heidi and Peter Sutter for hosting me during my time in Davos and Stella Hauff for hosting me during my visits. I am grateful to all the people I met during my time in Davos and at the SLF. I extend special thanks to the people of the Mountain Ecosystems group for insightful discussions and scientific exchange. Finally, I thank my family and friends for their continued support throughout my studies and during the completion of this thesis.

6 References

Bader, M.Y., Llambí, L.D., Case, B.S., Buckley, H.L., Toivonen, J.M., Camarero, J.J., Cairns, D.M., Brown, C.D., Wiegand, T. & Resler, L.M. (2021). A global framework for linking alpine-treeline ecotone patterns to underlying processes. *Ecography*, 44, 265–292.

Barbeito, I. (2013). *When I'm high I don't care about my neighbors: a story of treeline neighbor interactions*. 11th INTECOL Congress, Ecology, London.

Barbeito, I., Brücker, R.L., Rixen, C. & Bebi, P. (2013). Snow fungi—induced mortality of *Pinus cembra* at the alpine treeline: evidence from plantations. *Arctic, Antarctic, and Alpine Research*, 45, 455–470.

Barbeito, I., Dawes, M.A., Rixen, C., Senn, J. & Bebi, P. (2012). Factors driving mortality and growth at treeline: a 30-year experiment of 92 000 conifers. *Ecology*, 93, 389–401.

Bates, D., Mächler, M., Bolker, B. & Walker, S. (2015). Fitting linear mixed-effects models using lme4. *Journal of Statistical Software*, 67, 1–48.

Batllori, E., Camarero, J.J., Ninot, J.M. & Gutiérrez, E. (2009). Seedling recruitment, survival and facilitation in alpine *Pinus uncinata* tree line ecotones. Implications and potential responses to climate warming. *Global Ecology and Biogeography*, 18, 460–472.

Beauchamp, N., Kunstler, G., Touzot, L., Ruiz-Benito, P., Cienciala, E., Dahlgren, J., Hawryło, P., Klopčič, M., Lehtonen, A., Šebeň, V., Socha, J., Zavala, M.A. & Courbaud, B. (2025). Light competition affects how tree growth and survival respond to climate. *Journal of Ecology*, 113, 672–688.

Bernoulli, M. & Körner, C. (1999). Dry matter allocation in treeline trees. *Phyton (Austria) Special issue: "Eurosilva,"* 39, (7)-(12).

Bertness, M.D. & Callaway, R. (1994). Positive interactions in communities. *Trends in Ecology & Evolution*, 9, 191–193.

Broekman, M.J.E., Muller-Landau, H.C., Visser, M.D., Jongejans, E., Wright, S.J. & de Kroon, H. (2019). Signs of stabilisation and stable coexistence. *Ecology Letters*, 22, 1957–1975.

Brzeziecki, B. & Kienast, F. (1994). Classifying the life-history strategies of trees on the basis of the Grimian model. *Forest Ecology and Management*, 69, 167–187.

Callaway, R.M. (1998). Competition and facilitation on elevation gradients in subalpine forests of the northern Rocky Mountains, USA. *Oikos*, 82, 561–573.

Callaway, R.M., Brooker, R.W., Choler, P., Kikvidze, Z., Lortie, C.J., Michalet, R., Paolini, L., Pugnaire, F.I., Newingham, B., Aschehoug, E.T., Armas, C., Kikodze, D. & Cook, B.J. (2002). Positive interactions among alpine plants increase with stress. *Nature*, 417, 844–848.

Coomes, D.A. & Allen, R.B. (2007). Effects of size, competition and altitude on tree growth. *Journal of Ecology*, 95, 1084–1097.

Cui, M., Jiang, Y., Xue, F., Cao, P. & Kang, M. (2025). Soil temperature explains radial growth of coniferous trees more effectively than air temperature in mountainous cold temperate habitat. *Ecological Indicators*, 176, 113667.

Didier, L. (2001). Invasion patterns of European larch and Swiss stone pine in subalpine pastures in the French Alps. *Forest Ecology and Management*, 145, 67–77.

Dullinger, S., Dirnböck, T., Köck, R., Hochbichler, E., Englisch, T., Sauberer, N. & Grabherr, G. (2005). Interactions among tree-line conifers: differential effects of pine on spruce and larch. *Journal of Ecology*, 93, 948–957.

Eränen, J.K. & Kozlov, M.V. (2008). Increasing intraspecific facilitation in exposed environments: consistent results from mountain birch populations in two subarctic stress gradients. *Oikos*, 117, 1569–1577.

Ettinger, A.K. & HilleRisLambers, J. (2013). Climate isn't everything: competitive interactions and variation by life stage will also affect range shifts in a warming world. *American Journal of Botany*, 100, 1344–1355.

Ford, K.R., Breckheimer, I.K., Franklin, J.F., Freund, J.A., Kroiss, S.J., Larson, A.J., Theobald, E.J. & HilleRisLambers, J. (2017). Competition alters tree growth responses to climate at individual and stand scales. *Can. J. For. Res.*, 47, 53–62.

Germino, M.J., Smith, W.K. & Resor, A.C. (2002). Conifer seedling distribution and survival in an alpine-treeline ecotone. *Plant Ecology*, 162, 157–168.

Grime, J.P. (1977). Evidence for the existence of three primary strategies in plants and its relevance to ecological and evolutionary theory. *The American Naturalist*, 111, 1169–1194.

Gugerli, F., Brodbeck, S., Bebi, P., Bollmann, K., Dauphin, B., Gossner, M., Krumm, F., Peter, M., Queloz, V., Reiss, G., Rellstab, C., Stofer, S., Von Arx, G., Wasem, U. & Zweifel, R. (2022). *Die Arve - Portrait eines Gebirgswaldbaums*. Merkblatt für die Praxis. Swiss Federal Institute for Forest, Snow and Landscape Research, WSL.

Hansson, A., Dargusch, P. & Shulmeister, J. (2021). A review of modern treeline migration, the factors controlling it and the implications for carbon storage. *J. Mt. Sci.*, 18, 291–306.

Harsch, M.A., Hulme, P.E., McGlone, M.S. & Duncan, R.P. (2009). Are treelines advancing? A global meta-analysis of treeline response to climate warming. *Ecology Letters*, 12, 1040–1049.

Hartig, F. (2024). DHARMa: residual diagnostics for hierarchical (multi-level / mixed) regression models. doi:10.32614/CRAN.package.DHARMa, <https://doi.org/10.32614/CRAN.package.DHARMa>, R package version 0.4.7, <https://CRAN.R-project.org/package=DHARMa>.

He, J., Ning, C., Zhang, W., Halik, Ü. & Shen, Z. (2023). The effect of elevation on the population structure, spatial patterning and intraspecific interactions of *Picea schrenkiana* in the eastern tianshan mountains: a test of the stress gradient hypothesis. *Forests*, 14, 2092.

He, Q., Bertness, M.D. & Altieri, A.H. (2013). Global shifts towards positive species interactions with increasing environmental stress. *Ecology Letters*, 16, 695–706.

Hilman, B., Solly, E.F., Kuhlmann, I., Brunner, I. & Hagedorn, F. (2024). Species-specific reliance of trees on ectomycorrhizal fungi for nitrogen supply at an alpine treeline. *Fungal Ecology*, 71, 101361.

Jefferis, G., Kemp, S.E., Arya, S. & Mount, D. (2024). RANN: fast nearest neighbour search (wraps ANN library) using L2 metric. doi:10.32614/CRAN.package.RANN, <https://doi.org/10.32614/CRAN.package.RANN>, R package version 2.6.2, <https://CRAN.R-project.org/package=RANN>.

Jochner, M., Bugmann, H., Nötzli, M. & Bigler, C. (2018). Tree growth responses to changing temperatures across space and time: a fine-scale analysis at the treeline in the Swiss Alps. *Trees*, 32, 645–660.

Jourdan, M., Piedallu, C., Baudry, J., Defossez, E. & Morin, X. (2021). Tree diversity and the temporal stability of mountain forest productivity: testing the effect of species composition, through asynchrony and overyielding. *Eur J Forest Res*, 140, 273–286.

Körner, C. (1998). A re-assessment of high elevation treeline positions and their explanation. *Oecologia*, 115, 445–459.

Körner, C. (2012). *Alpine treelines*. Springer Basel, Basel.

Körner, C. (2021). *Alpine Plant Life: Functional Plant Ecology of High Mountain Ecosystems*. Springer International Publishing, Cham.

Körner, C. & Hiltbrunner, E. (2024). Rapid advance of climatic tree limits in the Eastern Alps explained by on-site temperatures. *Reg Environ Change*, 24, 98.

Körner, C. & Paulsen, J. (2004). A world-wide study of high altitude treeline temperatures. *Journal of Biogeography*, 31, 713–732.

Kulha, N., Honkaniemi, J., Barrere, J., Brandl, S., Cordonnier, T., Korhonen, K.T., Kunstler, G., Paul, C., Reineking, B. & Peltoniemi, M. (2023). Competition-induced tree mortality across Europe is driven by shade tolerance, proportion of conspecifics and drought. *Journal of Ecology*, 111, 2310–2323.

LaManna, J.A., Jones, F.A., Bell, D.M., Pabst, R.J. & Shaw, D.C. (2022). Tree species diversity increases with conspecific negative density dependence across an elevation gradient. *Ecology Letters*, 25, 1237–1249.

Lechler, L., Rixen, C., Bebi, P., Bavay, M., Marty, M., Barbeito, I., Dawes, M.A., Hagedorn, F., Krumm, F., Möhl, P., Schaub, M. & Frei, E.R. (2024). Five decades of ecological and meteorological data enhance the mechanistic understanding of global change impacts on the treeline ecotone in the European Alps. *Agricultural and Forest Meteorology*, 355, 110126.

Lenth, R.V. (2025). emmeans: estimated marginal means, aka least-squares means. doi:10.32614/CRAN.package.emmeans <https://doi.org/10.32614/CRAN.package.emmeans>, R package version 2.0.1, <https://CRAN.R-project.org/package=emmeans>.

Li, L., Girguis, M., Lurmann, F., Wu, J., Urman, R., Rappaport, E., Ritz, B., Franklin, M., Breton, C., Gilliland, F. & Habre, R. (2019). Cluster-based bagging of constrained mixed-effects models for high spatio-temporal resolution nitrogen oxides prediction over large regions. *Environment International*, 128, 310–323.

Lingua, E., Cherubini, P., Motta, R. & Nola, P. (2008). Spatial structure along an altitudinal gradient in the Italian Central Alps suggests competition and facilitation among coniferous species. *Journal of Vegetation Science*, 19, 425–436.

Liu, P., Wang, W., Bai, Z., Guo, Z., Ren, W., Huang, J., Xu, Y., Yao, J., Ding, Y. & Zang, R. (2020). Competition and facilitation co-regulate the spatial patterns of boreal tree species in Kanas of Xinjiang, northwest China. *Forest Ecology and Management*, 467, 118167.

Long, S., Zeng, S., Liu, F. & Wang, G. (2020). Influence of slope, aspect and competition index on the height-diameter relationship of *Cyclobalanopsis glauca* trees for improving prediction of height in mixed forests. *Silva Fenn.*, 54, 10242.

Loranger, H., Zotz, G. & Bader, M.Y. (2017). Competitor or facilitator? The ambiguous role of alpine grassland for the early establishment of tree seedlings at treeline. *Oikos*, 126, 1625–1636.

Lyu, L., Büntgen, U., Li, M.-H., Yu, K., Palosse, A., Zhang, Q.-B. & Cherubini, P. (2025). Intensifying neighbouring tree competition suppresses tree growth at the eastern Tibetan tree line. *Functional Ecology*, 39, 1234–1246.

Maestre, F.T., Callaway, R.M., Valladares, F. & Lortie, C.J. (2009). Refining the stress-gradient hypothesis for competition and facilitation in plant communities. *Journal of Ecology*, 97, 199–205.

Michalet, R., Brooker, R.W., Cavieres, L.A., Kikvidze, Z., Lortie, C.J., Pugnaire, F.I., Valiente-Banuet, A. & Callaway, R.M. (2006). Do biotic interactions shape both sides of the humped-back model of species richness in plant communities? *Ecology Letters*, 9, 767–773.

Müller, K. & Wickham, H. (2025). tibble: simple data frames. doi:10.32614/CRAN.package.tibble, <https://doi.org/10.32614/CRAN.package.tibble>, R package version 3.3.0, <https://CRAN.R-project.org/package=tibble>.

Novák, J. & Slodičák, M. (2006). Development of young substitute larch (*Larix decidua* Mill.) stands after first thinning. *Journal of Forest Science*, 52, 147–157.

Okano, K., Bret-Harte, M.S., Mulder, C.P.H. & Juday, G.P. (2021). Resource availability drives plant–plant interactions of conifer seedlings across elevations under warming in Alaska. *Ecosphere*, 12, e03508.

Pedersen, T.L. (2025). patchwork: the composer of plots. doi:10.32614/CRAN.package.patchwork, <https://doi.org/10.32614/CRAN.package.patchwork>, R package version 1.3.2, <https://CRAN.R-project.org/package=patchwork>.

Pepin, N.C., Arnone, E., Gobiet, A., Haslinger, K., Kotlarski, S., Notarnicola, C., Palazzi, E., Seibert, P., Serafin, S., Schöner, W., Terzago, S., Thornton, J.M., Vuille, M. & Adler, C. (2022). Climate changes and their elevational patterns in the mountains of the world. *Reviews of Geophysics*, 60, e2020RG000730.

Pierce, S., Negreiros, D., Cerabolini, B.E.L., Kattge, J., Díaz, S., Kleyer, M., Shipley, B., Wright, S.J., Soudzilovskaia, N.A., Onipchenko, V.G., van Bodegom, P.M., Frenette-Dussault, C., Weiher, E., Pinho, B.X., Cornelissen, J.H.C., Grime, J.P., Thompson, K., Hunt, R., Wilson, P.J., Buffa, G., Nyakunga, O.C., Reich, P.B., Caccianiga, M., Mangili, F., Ceriani, R.M., Luzzaro, A., Brusa, G., Siefert, A., Barbosa, N.P.U., Chapin III, F.S., Cornwell, W.K., Fang, J., Fernandes, G.W., Garnier, E., Le Stradic, S., Peñuelas, J., Melo, F.P.L., Slaviero, A., Tabarelli, M. & Tampucci, D. (2017). A global method for calculating plant CSR ecological strategies applied across biomes world-wide. *Functional Ecology*, 31, 444–457.

R Core Team. (2025). *R: a language and environment for statistical computing*. R Foundation for Statistical Computing, Vienna, Austria.

Risch, A.C., Nagel, L.M., Schutz, M., Krusi, B.O., Kienast, F. & Bugmann, H. (2003). Struktur und Langzeitentwicklung von subalpinen *Pinus montana* Miller und *Pinus cembra* L. Waldern in den zentraleuropaischen Alpen. *Forstwissen Centr*, 122, 219–230.

Rixen, C., Dawes, M.A., Wipf, S. & Hagedorn, F. (2012). Evidence of enhanced freezing damage in treeline plants during six years of CO2 enrichment and soil warming. *Oikos*, 121, 1532–1543.

Schloerke, B., Cook, D., Larmarange, J., Briatte, F., Marbach, M., Thoen, E., Elberg, A. & Crowley, J. (2025). GGally: extension to “ggplot2”. doi:10.32614/CRAN.package.GGally, <https://doi.org/10.32614/CRAN.package.GGally>, R package version 2.4.0, <https://CRAN.R-project.org/package=GGally>.

Schönenberger, W. (2001). Cluster afforestation for creating diverse mountain forest structures — a review. *Forest Ecology and Management*, Structure of Mountain Forests-Assessment, Impacts, Managements, Modelling, 145, 121–128.

Schönenberger, W. & Frey, W. (1988). Untersuchungen zur Ökologie und Technik der Hochlagenaufforstung : Forschungsergebnisse aus dem Lawinenanrissgebiet Stillberg. *Swiss forestry journal*, 139, 735–820.

Senn, J. (1999). Tree mortality caused by *Gremmeniella abietina* in a subalpine afforestation in the central Alps and its relationship with duration of snow cover. *European Journal of Forest Pathology*, 29, 65–74.

Smith, A.N.H., Anderson, M.J. & Pawley, M.D.M. (2017). Could ecologists be more random? Straightforward alternatives to haphazard spatial sampling. *Ecography*, 40, 1251–1255.

Song, X. & Corlett, R.T. (2022). Do natural enemies mediate conspecific negative distance- and density-dependence of trees? A meta-analysis of exclusion experiments. *Oikos*, 2022, e08509.

Steinbauer, M.J., Beierkuhnlein, C., Arfin Khan, M.A.S., Harter, D.E.V., Irl, S.D.H., Jentsch, A., Schweiger, A.H., Svenning, J.-C. & Dengler, J. (2016). How to differentiate facilitation and environmentally driven co-existence. *Journal of Vegetation Science*, 27, 1071–1079.

Tomback, D.F., Holtmeier, F.-K., Mattes, H., Carsey, K.S. & Powell, M.L. (1993). Tree clusters and growth form distribution in *Pinus cembra*, a bird-dispersed pine. *Arctic and Alpine Research*, 25, 374.

Vospernik, S., Monserud, R.A. & Sterba, H. (2010). Do individual-tree growth models correctly represent height:diameter ratios of Norway spruce and Scots pine? *Forest Ecology and Management*, 260, 1735–1753.

Wang, H., Peng, H., Hui, G., Hu, Y. & Zhao, Z. (2018). Large trees are surrounded by more heterospecific neighboring trees in Korean pine broad-leaved natural forests. *Sci Rep*, 8, 9149.

Wang, Y., Mao, Q., Ren, P. & Sigdel, S.R. (2021). Opposite Tree-Tree Interactions Jointly Drive the Natural Fir Treeline Population on the Southeastern Tibetan Plateau. *Forests*, 12, 1417.

Wang, Y., Pederson, N., Ellison, A.M., Buckley, H.L., Case, B.S., Liang, E. & Julio Camarero, J. (2016). Increased stem density and competition may diminish the positive effects of warming at alpine treeline. *Ecology*, 97, 1668–1679.

Westoby, M. (1984). *The self-thinning rule*. Advances in ecological research. Academic Press, Londres.

Wickham, H. (2016). *ggplot2: elegant graphics for data analysis*. Springer-Verlag New York.

Wickham, H., François, R., Henry, L., Müller, K. & Vaughan, D. (2023). dplyr: a grammar of data manipulation. doi:10.32614/CRAN.package.dplyr, <https://doi.org/10.32614/CRAN.package.dplyr>, R package version 1.1.4, <https://CRAN.R-project.org/package=dplyr>.

Wickham, H., Vaughan, D. & Girlich, M. (2024). tidyr: tidy messy data. doi:10.32614/CRAN.package.tidyr, <https://doi.org/10.32614/CRAN.package.tidyr>, R package version 1.3.1, <https://CRAN.R-project.org/package=tidyr>.

Xu, M. & Yu, S. (2014). Elevational variation in density dependence in a subtropical forest. *Ecology and Evolution*, 4, 2823–2833.

Zheng, X., Babst, F., Camarero, J.J., Li, X., Lu, X., Gao, S., Sigdel, S.R., Wang, Y., Zhu, H. & Liang, E. (2024). Density-dependent species interactions modulate alpine treeline shifts. *Ecology Letters*, 27, e14403.

Ziegler, Y., Grote, R., Alongi, F., Knüver, T. & Ruehr, N.K. (2024). Capturing drought stress signals: the potential of dendrometers for monitoring tree water status. *Tree Physiology*, 44, tpae140.

Zuur, A.F., Ieno, E.N., Walker, N., Saveliev, A.A. & Smith, G.M. (2009). *Mixed effects models and extensions in ecology with R*. Statistics for Biology and Health. Springer New York, New York, NY.

7 Use of AI

I used ChatGPT (version GPT-5.2) by OpenAI for programming, brainstorming ideas and improving paragraph structure (last accessed 17.01.2026, https://chatgpt.com). After writing, I used DeepL Write for spellchecking and grammar improvements (last accessed 17.01.2026, https://www.deepl.com/en/write).

8 Appendix

8.1 Tree selection

1	5	6	7	2
16	17	18	19	8
15	24	25	20	9
14	23	22	21	10
4	13	12	11	3

Tree 1:
Close to corners if possible

16	18	20	22	24
12	4	6	8	14
10	2	1	3	11
13	5	7	9	15
17	19	21	23	25

Tree 2:
Close to the centre

25	10	9	8	24
11	19	18	17	7
12	20	21	16	6
1	13	14	15	5
22	2	3	4	23

Tree 3:
Tree along plot edge

Figure 23: Tree selection scheme used during field surveys for odd-numbered plots.
Each panel shows a 5 × 5 schematic of potential tree positions within a plot. Numbers indicate the priority order for tree selection (1 = highest priority, 25 = lowest priority) and do not correspond to tree IDs. In odd-numbered plots, priority ordering starts at the upper-left cell of the schematic. Tree 1 was selected preferentially at plot corners, Tree 2 near the plot centre and Tree 3 along plot edges while avoiding corners.

2	7	6	5	1
8	19	18	17	16
9	20	25	24	15
10	21	22	23	14
3	11	12	13	4

Tree 1:
Close to corners if possible

25	23	21	19	17
15	9	7	5	13
11	3	1	2	10
14	8	6	4	12
24	22	20	18	16

Tree 2:
Close to the centre

24	8	9	10	25
7	17	18	19	11
6	16	21	20	12
5	15	14	13	1
23	4	3	2	22

Tree 3:
Tree along plot edge

Figure 24: Tree selection scheme used during field surveys for even-numbered plots.
Each panel shows a 5 × 5 schematic of potential tree positions within a plot. Numbers indicate the priority order for tree selection (1 = highest priority, 25 = lowest priority) and do not correspond to tree IDs. In even-numbered plots, priority ordering starts at the upper-right cell of the schematic. Tree 1 was selected preferentially at plot corners, Tree 2 near the plot centre and Tree 3 along plot edges while avoiding corners.

8.2 Subsampling

Table 23: Number of observations per subsampling stratum in the subset dataset.
Counts are shown for each year across the nine strata defined by elevation bin (low, mid, high) and neighbour-density bin (low, mid, high). Strata with limited sample sizes are highlighted in light blue.

Year	Elevation bin	Neighbour density bin	Nr. of observations per stratum
1985	low	low	112
1985	low	mid	927
1985	low	high	2112
1985	mid	low	306
1985	mid	mid	1210
1985	mid	high	1380
1985	high	low	654
1985	high	mid	1477
1985	high	high	780
1995	low	low	227
1995	low	mid	1395
1995	low	high	1398
1995	mid	low	444
1995	mid	mid	1325
1995	mid	high	899
1995	high	low	876
1995	high	mid	1266
1995	high	high	349
2005	low	low	104
2005	low	mid	245
2005	low	high	136
2005	mid	low	194
2005	mid	mid	243
2005	mid	high	76
2005	high	low	341
2005	high	mid	189
2005	high	high	36
2015	low	low	153
2015	low	mid	302
2015	low	high	108
2015	mid	low	227
2015	mid	mid	308
2015	mid	high	84
2015	high	low	421
2015	high	mid	209
2015	high	high	32
2025	low	low	198
2025	low	mid	216
2025	low	high	75
2025	mid	low	276
2025	mid	mid	205
2025	mid	high	33
2025	high	low	448
2025	high	mid	160
2025	high	high	13

8.3 Collinearity analyses

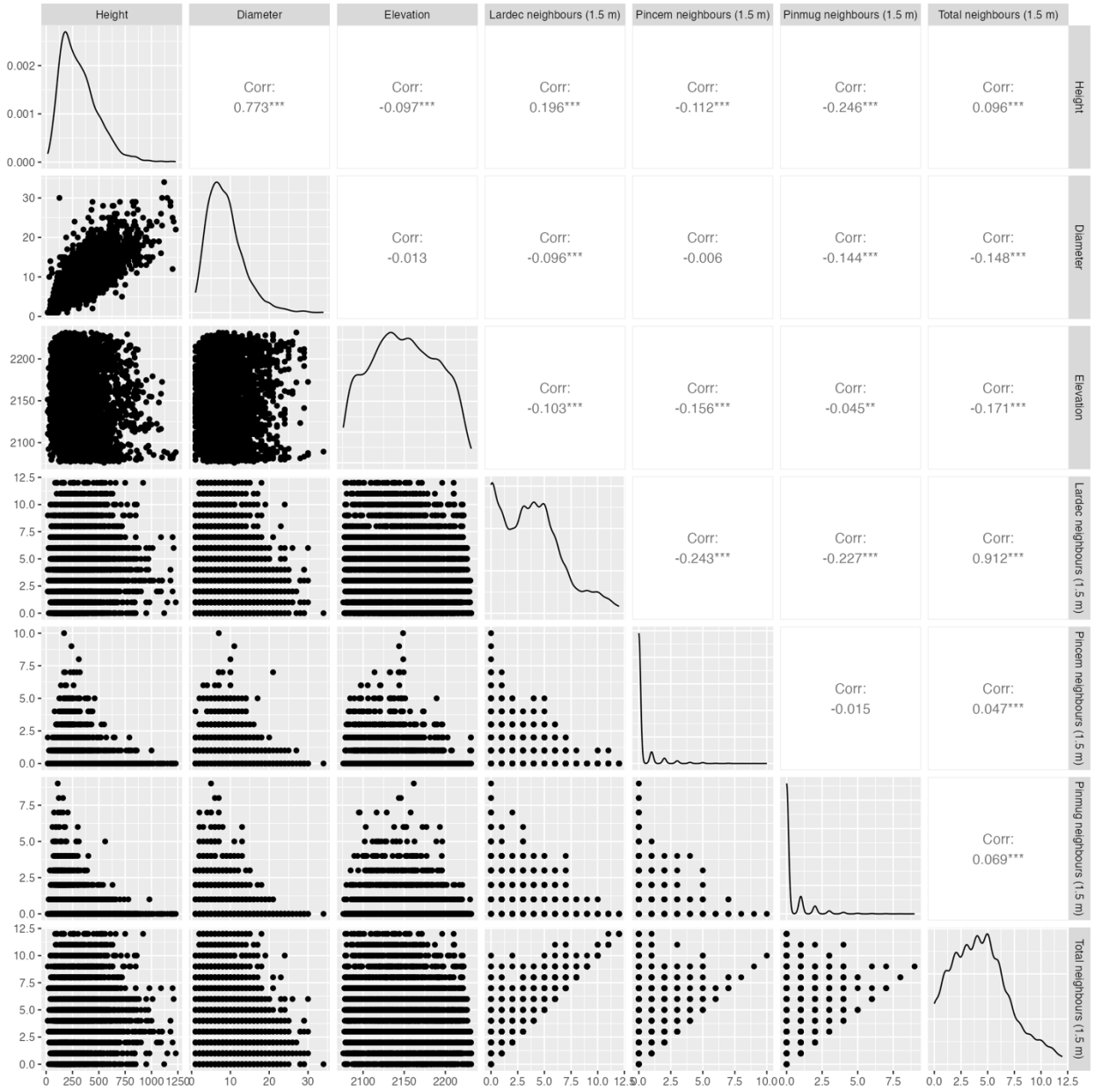

Figure 25: Pairwise scatterplot matrix of height, diameter, elevation and neighbour density within a 1.5 m radius. Diagonal panels show the probability distribution of each variable, panels in the lower left show pairwise scatterplots and panels in the upper right report Pearson correlation coefficients with significance level indicated by asterisks: p < *0.05 (*),* p < *0.01 (**) and* p < *0.001 (***). Abbreviations: Lardec* = Larix decidua*, Pincem* = Pinus cembra*, Pinmug* = Pinus mugo*.*

Table 24: Variance inflation factors (VIFs) for the explanatory variables (neighbour densities by species and elevation), used to assess multicollinearity.
All VIF values are close to 1, indicating negligible collinearity among explanatory variables.

Variable name	VIF
Total *Larix decidua* as neighbours	1.079
Total *Pinus cembra* as neighbours	1.056
Total *Pinus mugo* as neighbours	1.069
Elevation	1.058

8.4 Model selection

8.4.1 Temporal models for *Larix decidua* 1985–2015

Table 25: Extended summary of model fits (AIC and BIC) for the temporal models for 1985 and 2015.
For each model type and year, the median and the 2.5th and 97.5th percentiles of AIC and BIC across all model refits are reported.

Model type	Year	Median AIC	2.5th percentile AIC	97.5th percentile AIC	Median BIC	2.5th percentile BIC	97.5th percentile BIC
1.1	1985	1496.28	1409.85	1597.05	1525.10	1438.66	1625.87
1.1	2015	1433.16	1318.56	1546.29	1461.67	1347.06	1574.80
2.1	1985	1500.12	1409.36	1599.10	1524.13	1433.37	1623.11
2.1	2015	1426.82	1311.77	1539.41	1450.57	1335.53	1563.17
3.1	1985	1489.37	1400.46	1590.24	1542.19	1453.28	1643.07
3.1	2015	1425.11	1309.37	1534.88	1477.37	1361.63	1587.14
4.1	1985	1490.70	1402.02	1589.10	1548.33	1459.65	1646.73
4.1	2015	1424.88	1312.08	1537.39	1481.89	1369.09	1594.40
5.1	1985	1477.99	1391.61	1579.42	1574.04	1487.66	1675.46
5.1	2015	1399.27	1287.80	1515.32	1494.29	1382.82	1610.34

Table 26: Extended results of likelihood-ratio tests for the temporal models for 1985 and 2015.
For each model comparison, the rows 'Comparison' and 'Year' identify the contrasted model types and year. The rows 'Median Chi-squared' and 'Median p*-value' report the median chi-squared statistic and median* p*-value, together with the 2.5th and 97.5th percentiles across model refits. Significance levels are indicated using asterisks:* p < *0.05 (*),* p < *0.01 (**) and* p < *0.001 (***). The rows 'Median ΔAIC' and 'Median ΔBIC' give the median differences in AIC and BIC between the more complex model and the simpler model. Negative values in 'Median ΔAIC' or 'Median ΔBIC' indicate improved fit with the more complex model. The rows '2.5th percentile ΔAIC/ΔBIC' and '97.5th percentile ΔAIC/ΔBIC' report the 2.5th and 97.5th percentiles of these differences across model refits, summarising uncertainty in the relative model support.*

Comparison	2.1 vs 3.1	2.1 vs 3.1	2.1 vs 3.1	3.1 vs 4.1	3.1 vs 4.1	4.1 vs 5.1	4.1 vs 5.1
Year	1985	1985	2015	1985	2015	1985	2015
Median Chi-squared	19.07	19.07	10.43	2.67	2.00	9.96	13.23
2.5th percentile Chi-squared	7.74	7.74	4.03	0.0046	0.01	3.25	4.71
97.5th percentile Chi-squared	38.34	38.34	20.09	12.46	11.37	23.49	31.59
Median *p*-value	0.004	0.004	0.11	0.10	0.16	0.27	0.10
2.5th percentile *p*-value	< 0.001	< 0.001	0.0027	< 0.001	< 0.001	0.0028	< 0.001
97.5th percentile *p*-value	0.26	0.26	0.67	0.95	0.92	0.92	0.79
Median ΔAIC	-7.07	-7.07	1.57	-0.67	0.00056	6.04	2.77
2.5th percentile ΔAIC	-26.34	-26.34	-8.09	-10.46	-9.37	-7.49	-15.59
97.5th percentile ΔAIC	4.26	4.26	7.97	2.00	1.99	12.75	11.29
Median ΔBIC	21.74	21.74	30.08	4.13	4.75	44.46	40.78
2.5th percentile ΔBIC	2.47	2.47	20.42	-5.65	-4.62	30.93	22.42
97.5th percentile ΔBIC	33.07	33.07	36.48	6.80	6.74	51.16	49.30

Figure 26: DHARMa residual diagnostics for temporal models for 1985 (left column) and 2015 (right column). Five randomly selected model refits of type 3.1 are shown per year (the model index is shown above each row). Each row displays a residual-uniformity QQ plot (left) and DHARMa residuals versus predicted values (right). Red symbols indicate observations flagged as outliers by DHARMa. The plots report DHARMa tests for residual uniformity (Kolmogorov–Smirnov), dispersion and outliers. Red test labels denote statistically significant deviations (p < 0.05).

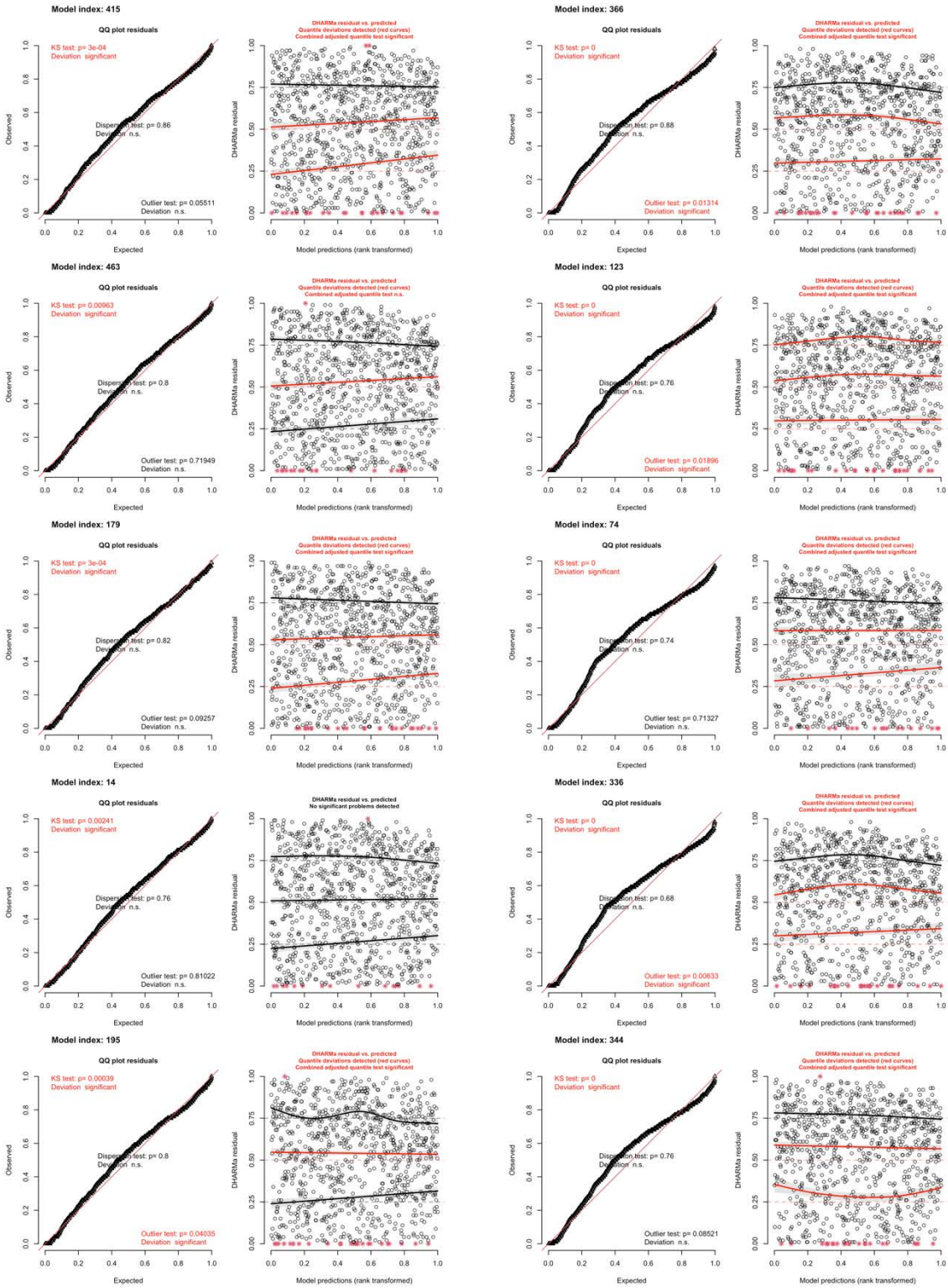

8.4.2 Size-metric models for *Larix decidua* 2015 and 2025

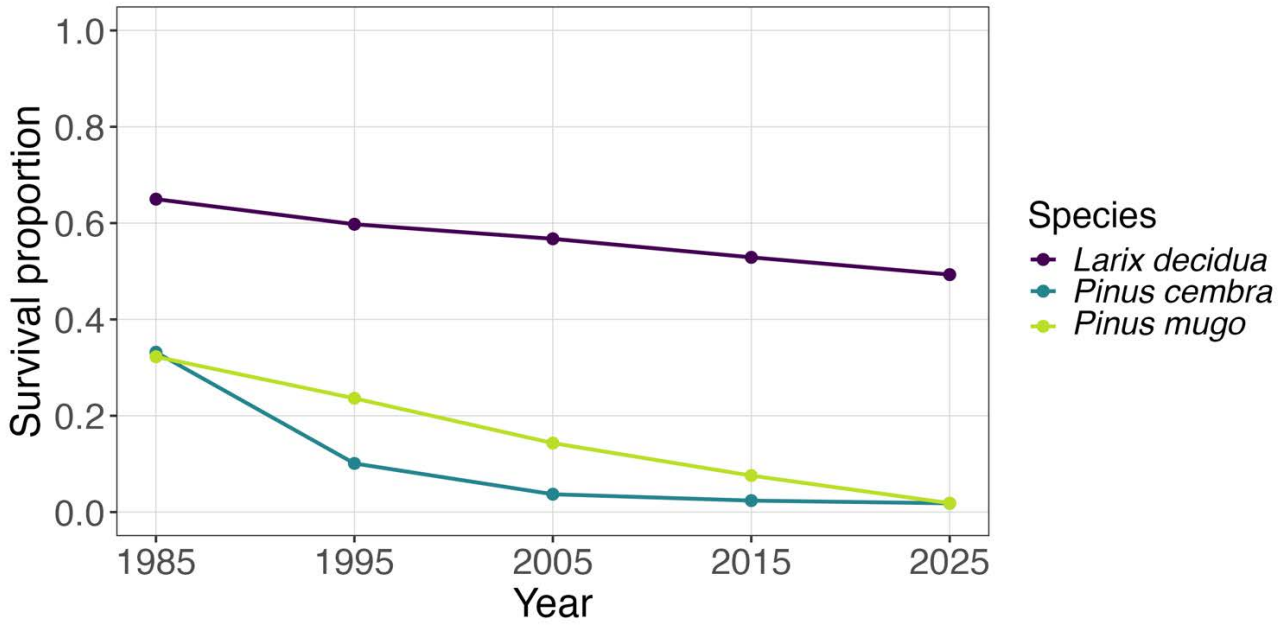

Figure 27: Species-specific survival proportion over time (1985–2025) for the subset dataset. Points and lines show the proportion of individuals alive at each survey year for Larix decidua*,* Pinus cembra *and* Pinus mugo.

Table 27: Overview of model convergence across model refits for each model type for 2015 and 2025. For each model type and year, the corresponding proportion of non-converged model refits is reported.

Model type	Year	Proportion of models with convergence issues
1.2	2015	0.04
1.2	2025	0.03
2.2	2015	0.02
2.2	2025	0.03
3.2	2015	0.02
3.2	2025	0.03
4.2	2015	0.12
4.2	2025	0.04
5.2	2015	0.11
5.2	2025	0.04

Table 28: Overview of isSingular warnings for size-metric model refits for 2015 and 2025.
For each model type and year, the total number of model refits, the number and proportion of model refits that produced warnings, and a breakdown of warning sources are reported. Warning sources are categorised according to whether they are related to the plot-level random intercept (1|plot number), related to the tree-level random intercept (1|tree ID), or unrelated to the random-effects terms. The final column reports the proportion of warning cases attributable to the plot-level random effect.

Model type	Year	Total nr. of models fitted	Total nr. of models with warnings	Proportion of models with warning	Nr. of warnings due to (1|plot number)	Nr. of warnings due to (1|tree ID)	Nr. of warnings unrelated to random-effects	Proportion of models that had n plot as issue
1.2	2015	500	20	0.040	19	0	1	0.95
1.2	2025	500	13	0.026	13	0	0	1.00
2.2	2015	500	10	0.020	8	0	2	0.80
2.2	2025	500	13	0.026	12	0	1	0.92
3.2	2015	500	10	0.020	10	0	0	1.00
3.2	2025	500	14	0.028	14	0	0	1.00
4.2	2015	500	59	0.118	51	0	8	0.86
4.2	2025	500	19	0.038	19	0	0	1.00
5.2	2015	500	57	0.114	55	0	2	0.96
5.2	2025	500	20	0.040	17	0	3	0.85

Table 29: Extended summary of model fit (AIC and BIC) for the size-metric models for 2015 and 2025. For each model type and year, the table reports the total number of model refits ('Nr. of models (all)') and the number of model refits without convergence issues ('Nr. of models (nci)'). Median, 2.5th, and 97.5th percentiles of AIC and BIC are shown both across all model refits (all) and for the subset of non-convergence-issue model refits (nci).

Model type	1.2	1.2	2.2	2.2	3.2	3.2	4.2	4.2	5.2	5.2
Year	2015	2025	2015	2025	2015	2025	2015	2025	2015	2025
Nr. of models (all)	500	500	500	500	500	500	500	500	500	500
Nr. of models (nci)	480	483	490	490	490	486	469	479	468	481
Median AIC (all)	524.77	648.03	519.94	641.70	517.72	639.22	501.78	631.51	493.15	611.98
2.5th percentile AIC (all)	436.83	565.11	432.52	560.47	431.16	557.52	416.27	551.02	413.85	532.52
97.5th percentile AIC (all)	611.60	731.80	602.92	726.57	602.68	724.77	579.98	717.05	567.39	699.58
Median BIC (all)	559.10	681.84	558.57	679.73	573.51	694.16	566.15	694.90	591.86	709.19
2.5th percentile BIC (all)	471.16	598.93	471.15	598.51	486.95	612.47	480.65	614.42	512.56	629.73
97.5th percentile BIC (all)	645.94	765.61	641.55	764.61	658.47	779.71	644.35	780.44	666.10	796.79
Median AIC (nci)	524.77	648.81	519.94	641.92	517.72	639.61	501.64	632.01	493.24	612.27
2.5th percentile AIC (nci)	436.07	565.67	432.52	560.38	430.99	556.07	415.47	552.53	413.17	533.83
97.5th percentile AIC (nci)	611.76	732.39	603.26	726.69	603.07	725.66	583.81	717.92	568.90	699.83
Median BIC (nci)	559.10	682.63	558.57	679.96	573.51	694.55	566.01	695.41	591.94	709.48
2.5th percentile BIC (nci)	470.40	599.49	471.14	598.42	486.78	611.02	479.84	615.93	511.88	631.04
97.5th percentile BIC (nci)	646.09	766.20	641.89	764.73	658.86	780.61	648.18	781.31	667.60	797.04

Table 30: Extended results of likelihood-ratio tests for the size-metric models for 2015 and 2025.
For each model comparison, the rows 'Comparison' and 'Year' identify the contrasted model types and year. The rows 'Median Chi-squared' and 'Median p*-value' report the median chi-squared statistic and median* p*-value, together with the 2.5th and 97.5th percentiles across model refits. Significance levels are indicated using asterisks:* $p < 0.05$ *(*),* $p < 0.01$ *(**) and* $p < 0.001$ *(***). The rows 'Median ΔAIC' and 'Median ΔBIC' give the median differences in AIC and BIC between the more complex model and the simpler model. Negative values in 'Median ΔAIC' or 'Median ΔBIC' indicate improved fit with the more complex model. The rows '2.5th percentile ΔAIC/ΔBIC' and '97.5th percentile ΔAIC/ΔBIC' report the 2.5th and 97.5th percentiles of these differences across model refits, summarising uncertainty in the relative model support.*

Comparison of models:	2.2 vs 3.2	2.2 vs 3.2	3.2 vs 4.2	3.2 vs 4.2	4.2 vs 5.2	4.2 vs 5.2
Year	2015	2025	2015	2025	2015	2025
Median Chi-squared	3.84	2.57	25.73	13.90	35.89	44.00
2.5th percentile Chi-squared	0.49	0.39	7.38	3.38	17.66	24.97
97.5th percentile Chi-squared	12.06	8.74	56.59	33.21	59.44	68.62
Median *p*-value	0.43	0.63	< 0.001	< 0.001	< 0.001	< 0.001
2.5th percentile *p*-value	0.02	0.07	< 0.001	< 0.001	< 0.001	< 0.001
97.5th percentile *p*-value	0.97	0.98	0.03	0.18	0.02	0.0016
Median ΔAIC	4.16	5.43	-21.73	-9.90	-19.89	-28.00
2.5th percentile ΔAIC	-4.06	-0.74	-52.59	-29.21	-43.44	-52.62
97.5th percentile ΔAIC	7.51	7.61	-3.38	0.62	-1.66	-8.97
Median ΔBIC	21.33	22.34	-13.14	-1.45	14.44	5.81
2.5th percentile ΔBIC	13.11	16.16	-44.01	-20.76	-9.10	-18.81
97.5th percentile ΔBIC	24.67	24.51	5.21	9.07	32.67	24.84

Figure 28: DHARMa residual diagnostics for size-metric models in 2015 (left column) and 2025 (right column). Five randomly selected model refits of type 5.2 are shown per year (the model index is shown above each row). Each row displays a residual-uniformity QQ plot (left) and DHARMa residuals versus predicted values (right). Red symbols indicate observations flagged as outliers by DHARMa. The plots report DHARMa tests for residual uniformity (Kolmogorov–Smirnov), dispersion and outliers. Red test labels denote statistically significant deviations (p < 0.05).

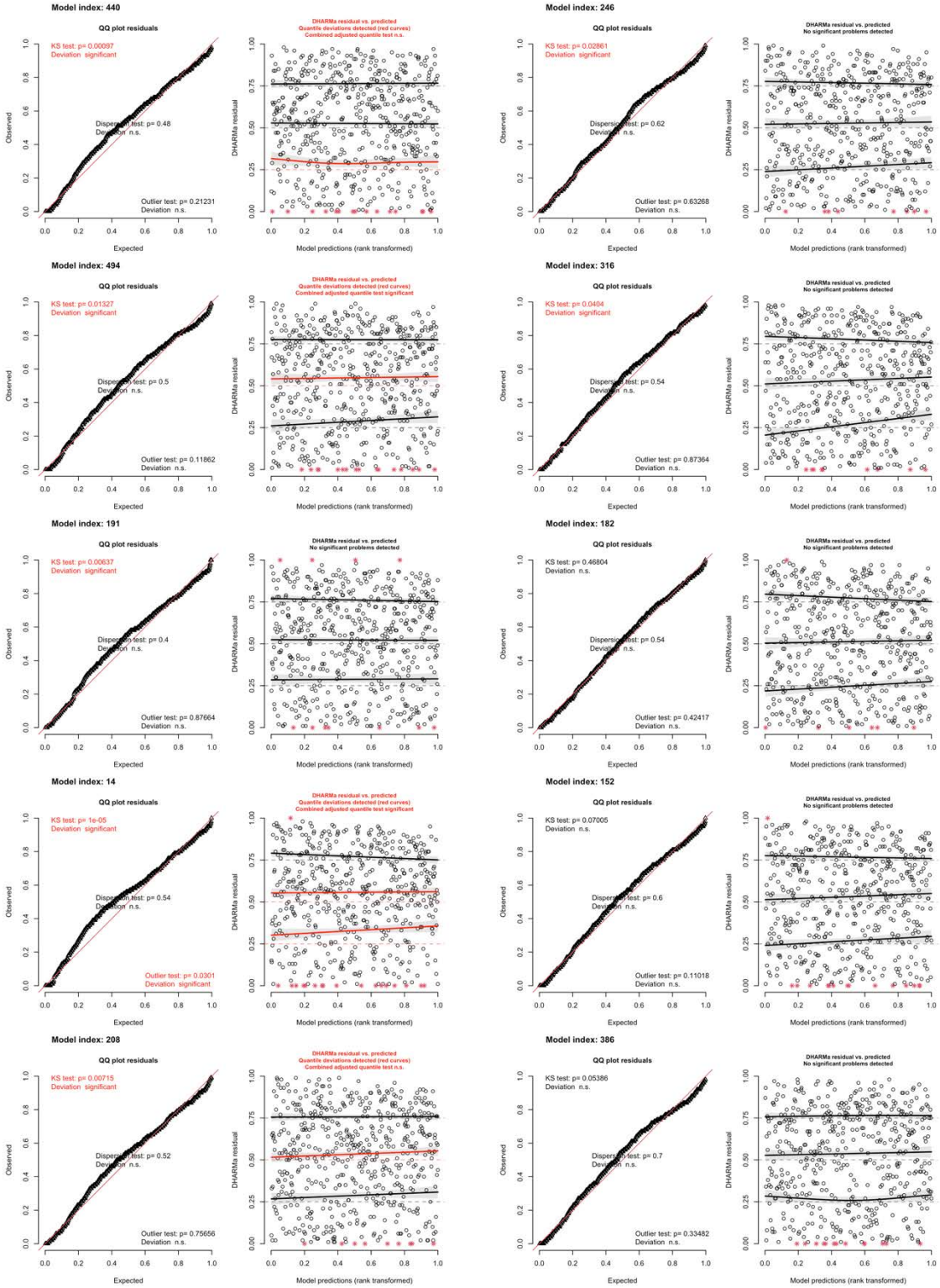

8.4.3 Species models 1985 and 1995

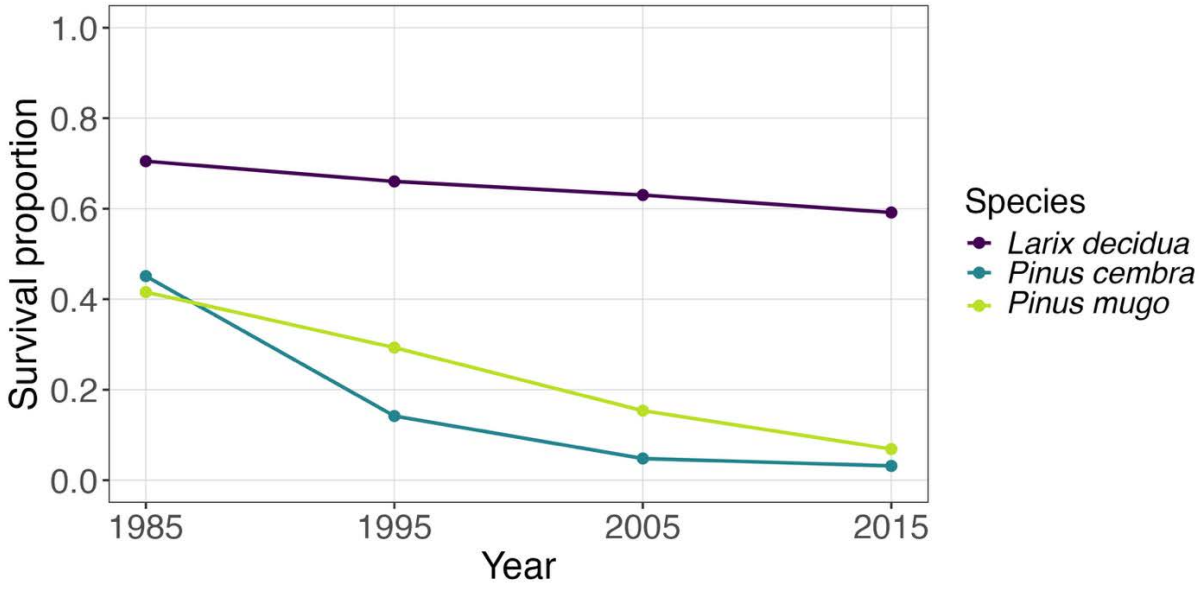

Figure 29: Species-specific survival proportion over time (1985–2015) for the full-area dataset.
Points and lines show the proportion of individuals alive at each survey year for Larix decidua*,* Pinus cembra *and* Pinus mugo*.*

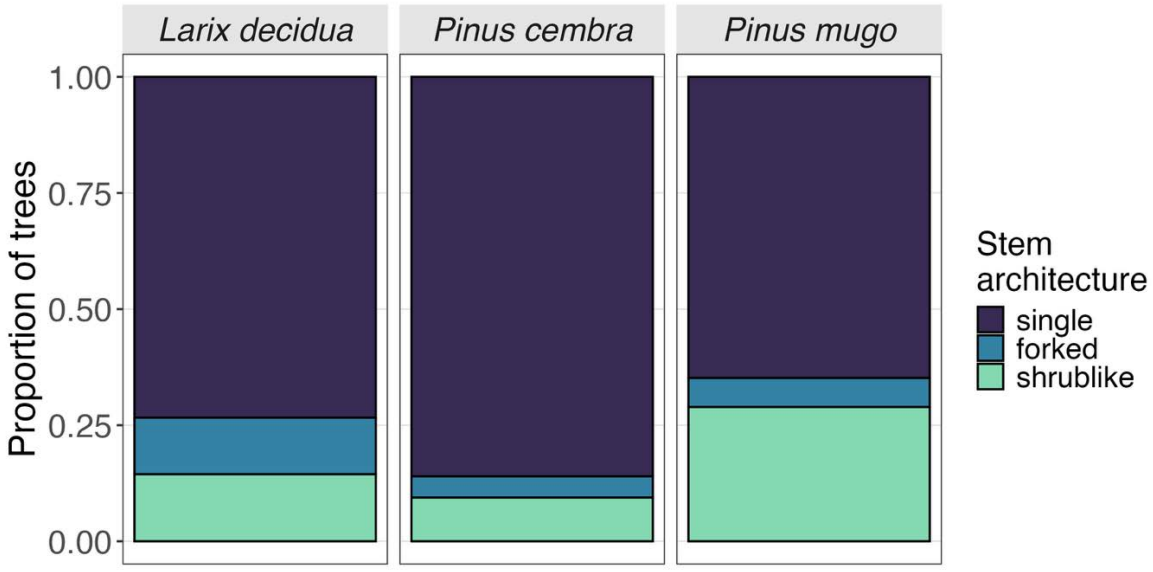

Figure 30: Proportion of trees by stem-architecture category for each species in 1995.
Stacked bars show the relative frequency of single-stemmed, forked and shrublike individuals within Larix decidua*,* Pinus cembra *and* Pinus mugo*. Proportions are calculated within species.*

Table 31: Extended summary of model fits (AIC and BIC) for the species models for 1985 and 1995.
For each model type and year, the median and the 2.5th and 97.5th percentiles of AIC and BIC across all model refits are reported.

Model type	Year	Median AIC	2.5th percentile AIC	97.5th percentile AIC	Median BIC	2.5th percentile BIC	97.5th percentile BIC
1.3	1985	3115.20	2914.55	3311.73	3162.41	2961.76	3358.94
1.3	1995	3068.01	2873.17	3260.48	3114.94	2920.10	3307.41
2.3	1985	3106.37	2904.09	3299.63	3159.48	2957.20	3352.74
2.3	1995	3054.23	2861.05	3247.60	3107.03	2913.85	3300.40
3.3	1985	3112.19	2912.09	3306.60	3188.90	2988.80	3383.31
3.3	1995	3057.10	2866.01	3247.17	3133.36	2942.27	3323.43
4.3	1985	3040.38	2851.61	3231.73	3211.51	3022.74	3402.86
4.3	1995	3036.58	2836.39	3237.22	3206.71	3006.51	3407.34
5.3	1985	2969.42	2765.82	3165.27	3164.15	2960.55	3360.00
5.3	1995	2908.44	2694.42	3116.39	3102.03	2888.01	3309.98

Table 32: Extended results of likelihood-ratio tests for the species models for 1985 and 1995.
For each model comparison, the rows 'Comparison' and 'Year' identify the contrasted model types and year. The rows 'Median Chi-squared' and 'Median p*-value' report the median chi-squared statistic and median* p*-value, together with the 2.5th and 97.5th percentiles across model refits. Significance levels are indicated using asterisks:* p *< 0.05 (*),* p *< 0.01 (**) and* p *< 0.001 (***). The rows 'Median ΔAIC' and 'Median ΔBIC' give the median differences in AIC and BIC between the more complex model and the simpler model. Negative values in 'Median ΔAIC' or 'Median ΔBIC' indicate improved fit with the more complex model. The rows '2.5th percentile ΔAIC/ΔBIC' and '97.5th percentile ΔAIC/ΔBIC' report the 2.5th and 97.5th percentiles of these differences across model refits, summarising uncertainty in the relative model support.*

Comparison of model:	2.3 vs 3.3	2.3 vs 3.3	3.3 vs 4.3	3.3 vs 4.3	4.3 vs 5.3	4.3 vs 5.3
Year	1985	1995	1985	1995	1985	1995
Median Chi-squared	6.41	8.5	120.81	57.24	100.28	159.04
2.5th percentile Chi-squared	1.30	2.21	80.75	33.52	71.87	122.33
97.5th percentile Chi-squared	17.49	19.46	176.01	86.66	134.6	200.85
Median *p*-value	0.17	0.07	< 0.001	< 0.001	< 0.001	< 0.001
2.5th percentile *p*-value	0.0016	< 0.001	< 0.001	< 0.001	< 0.001	< 0.001
97.5th percentile *p*-value	0.86	0.70	< 0.001	0.0063	< 0.001	< 0.001
Median ΔAIC	1.59	-0.50	-88.81	-25.24	-92.28	-151.04
2.5th percentile ΔAIC	-9.49	-11.46	-144.01	-54.66	-126.60	-192.85
97.5th percentile ΔAIC	6.70	5.79	-48.75	-1.52	-63.87	-114.33
Median ΔBIC	25.20	22.97	5.61	68.62	-68.67	-127.57
2.5th percentile ΔBIC	14.12	12.01	-49.60	39.20	-102.99	-169.39
97.5th percentile ΔBIC	30.31	29.26	45.66	92.34	-40.26	-90.86

Figure 31: DHARMa residual diagnostics for species models in 1985 (left column) and 1995 (right column). Five randomly selected model refits of type 5.3 are shown per year (the model index is shown above each row). Each row displays a residual-uniformity QQ plot (left) and DHARMa residuals versus predicted values (right). Red symbols indicate observations flagged as outliers by DHARMa. The plots report DHARMa tests for residual uniformity (Kolmogorov–Smirnov), dispersion and outliers. Red test labels denote statistically significant deviations (p < 0.05).

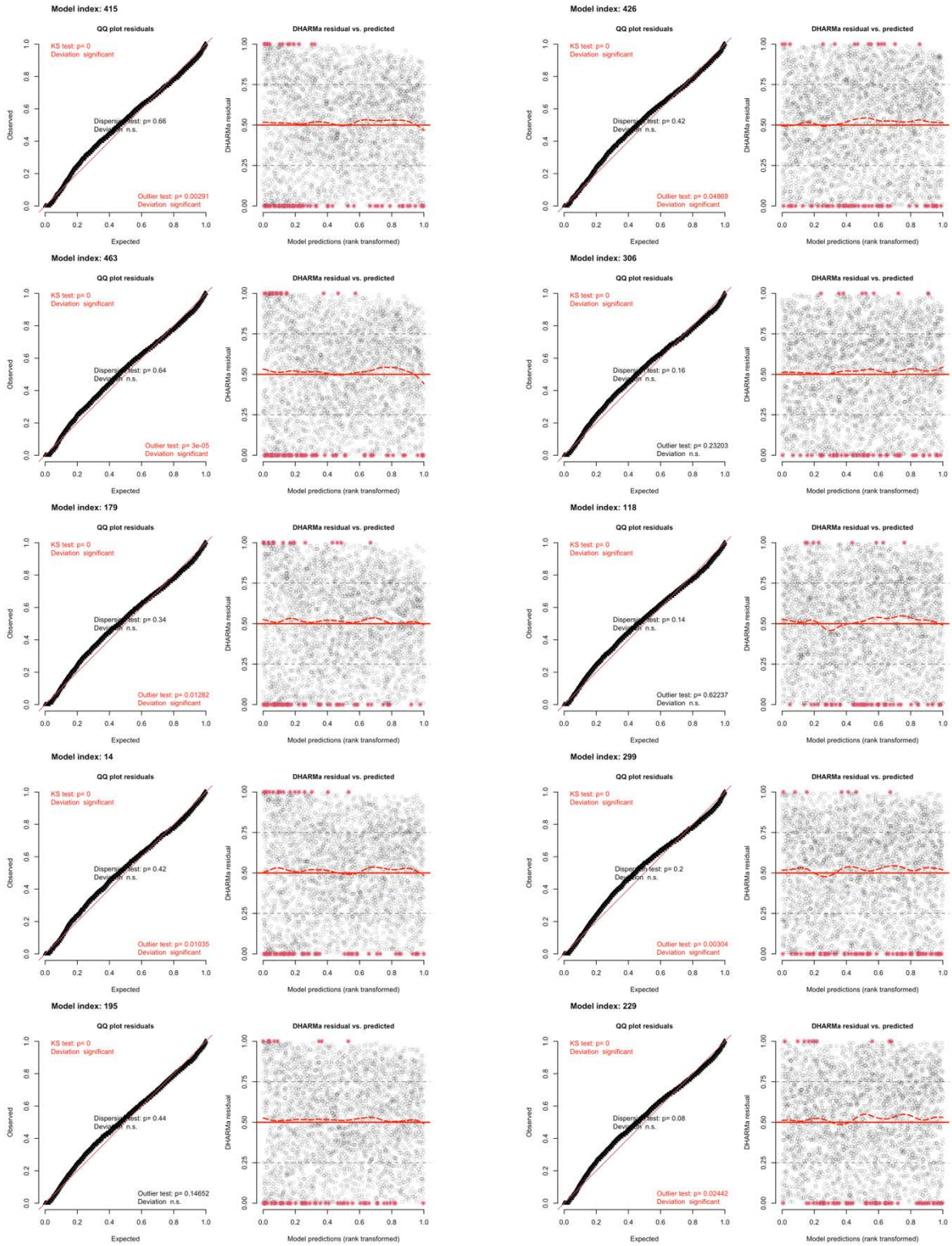

8.5 Extended results

8.5.1 Temporal dimension

8.5.1.1 *Larix decidua* height for 1985–2015

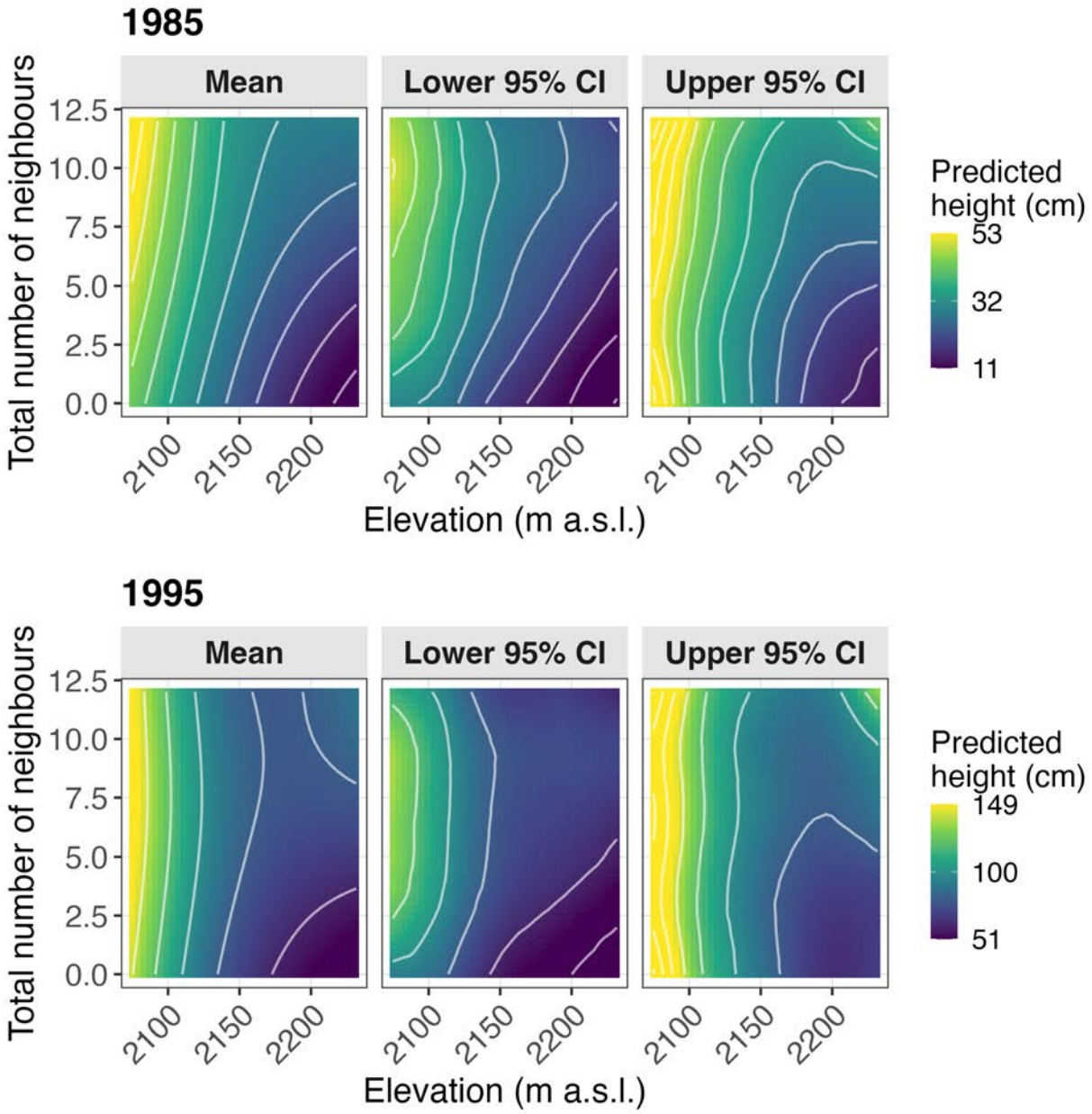

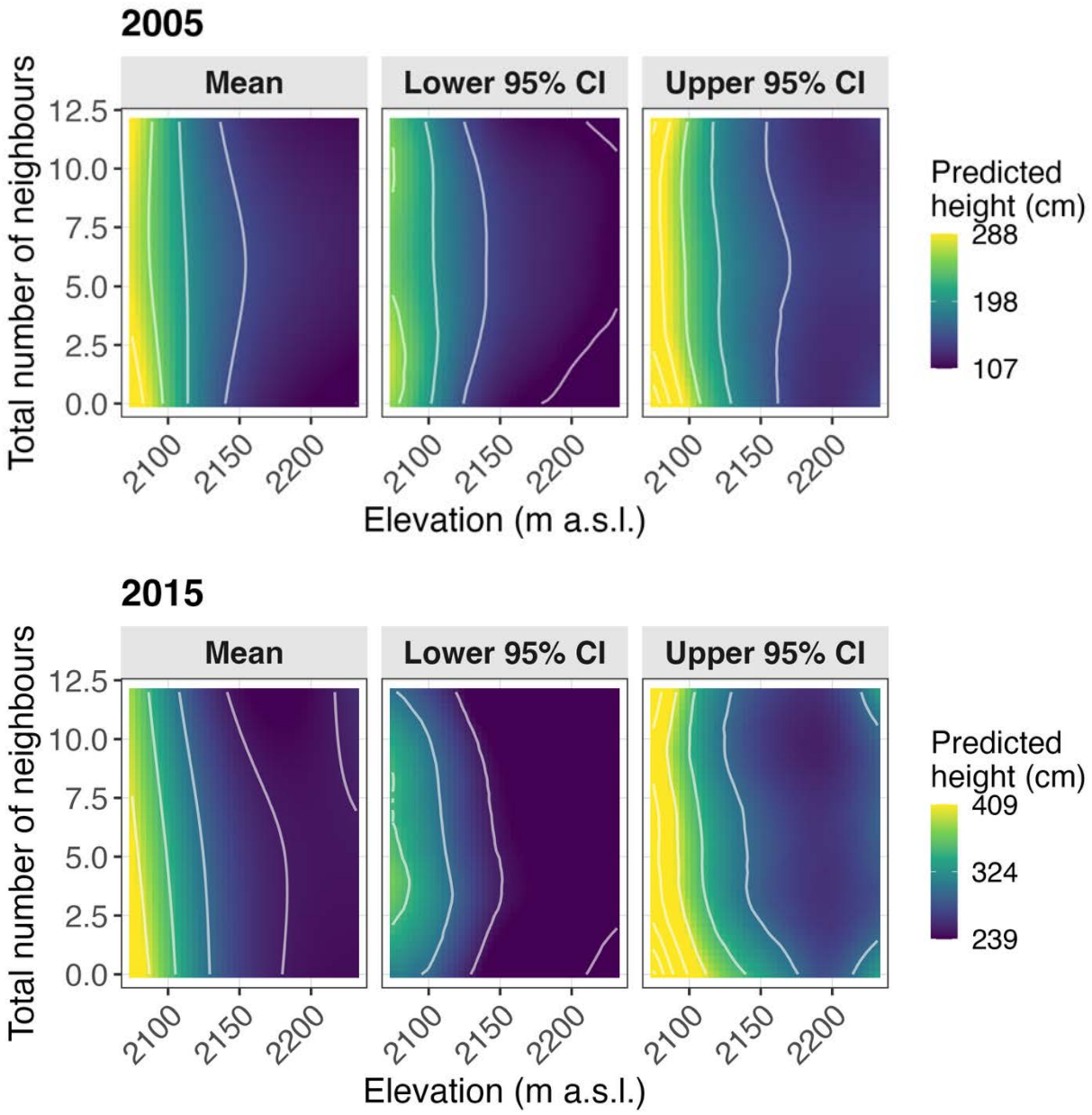
2005
Mean
Lower 95% CI
Upper 95% CI
Total number of neighbours
12.5
10.0
7.5
5.0
2.5
0.0
2100
2150
2200
Elevation (m a.s.l.)
Predicted height (cm)
288
198
107
2015
Mean
Lower 95% CI
Upper 95% CI
Total number of neighbours
Elevation (m a.s.l.)
Predicted height (cm)
409
324
239

8.5.1.2 *Larix decidua* height for 1985–2025

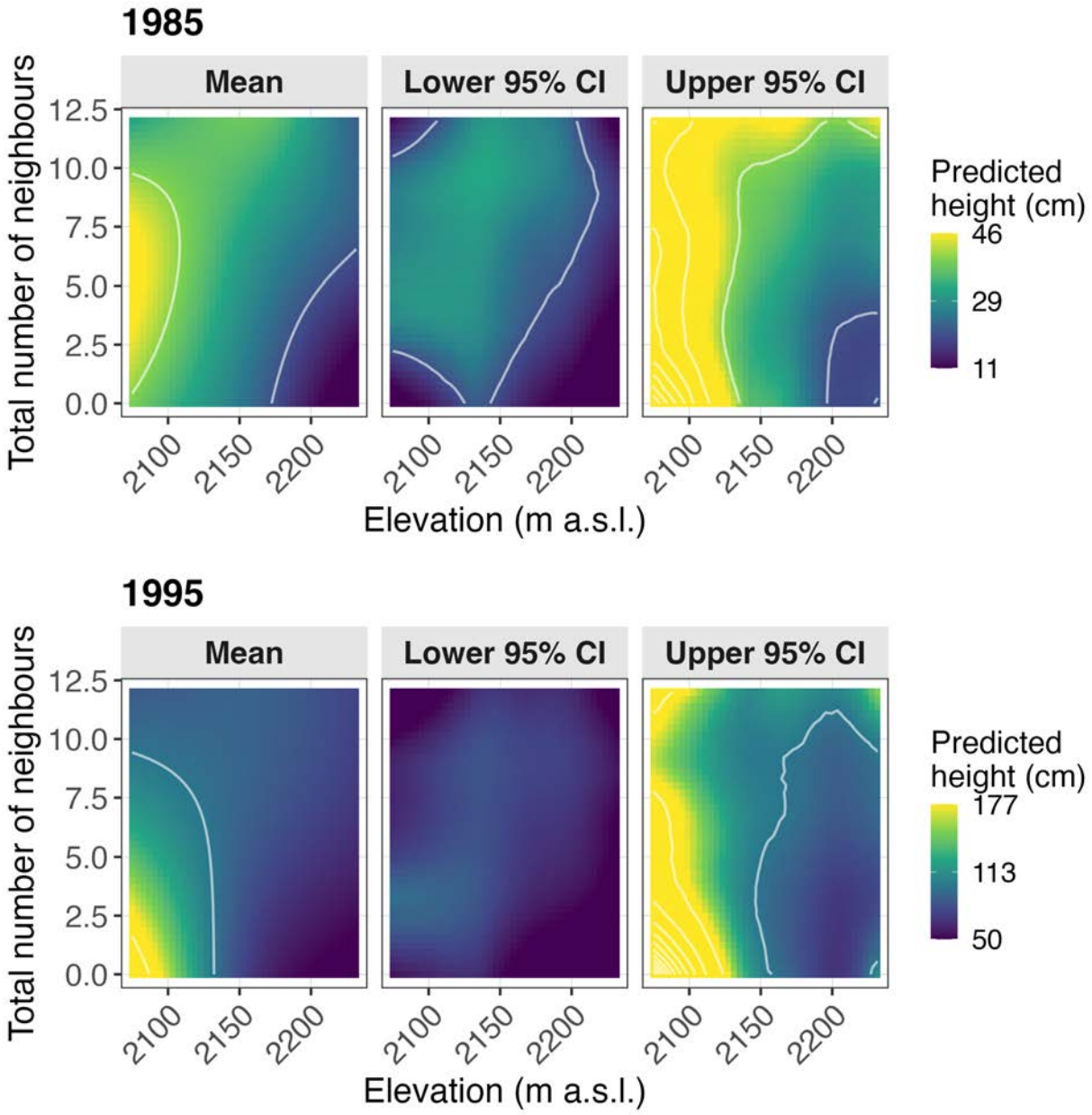

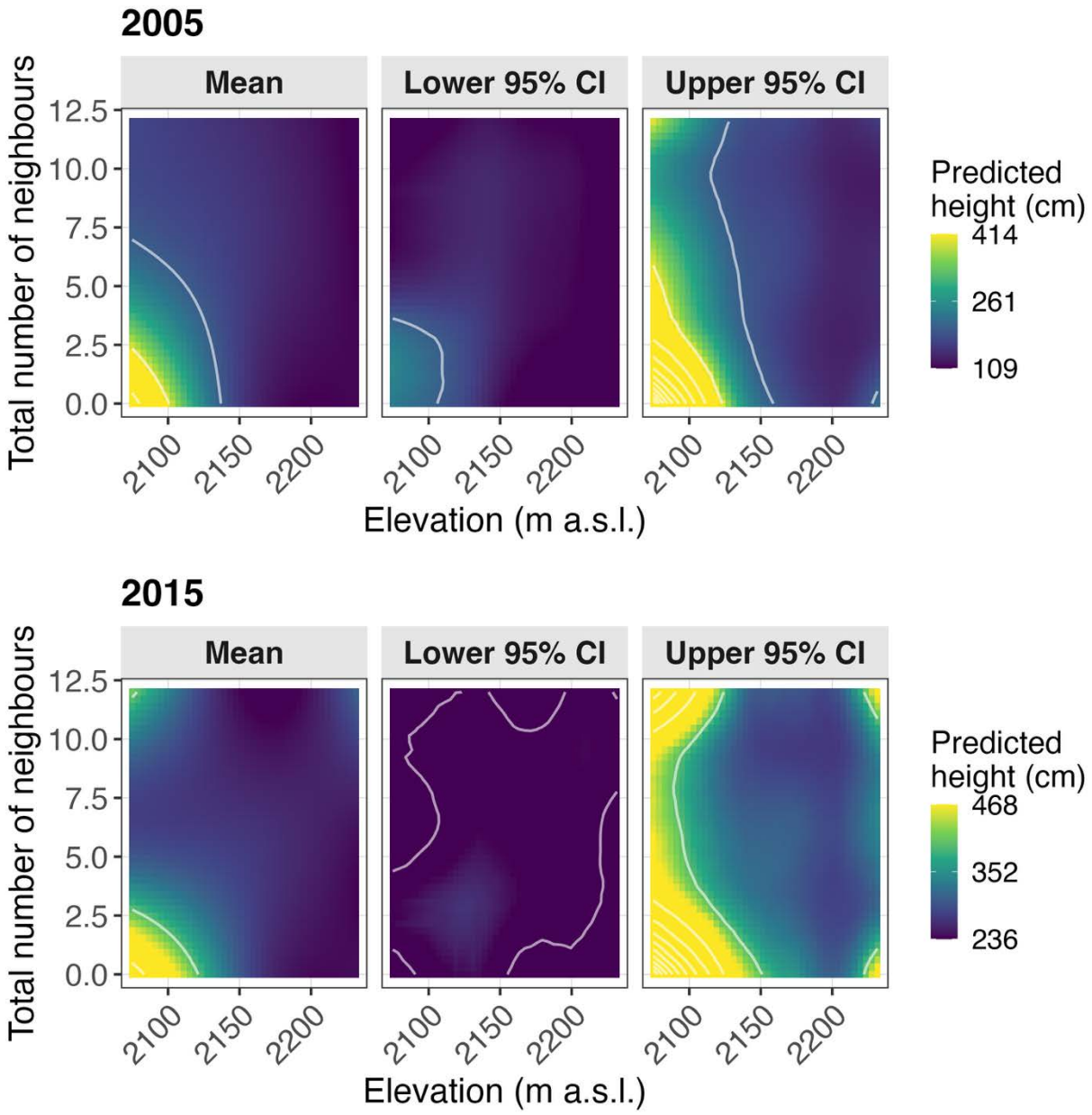
2005
Mean
Lower 95% CI
Upper 95% CI
Total number of neighbours
12.5
10.0
7.5
5.0
2.5
0.0
2100
2150
2200
Elevation (m a.s.l.)
Predicted height (cm)
414
261
109
2015
Mean
Lower 95% CI
Upper 95% CI
Total number of neighbours
Elevation (m a.s.l.)
Predicted height (cm)
468
352
236

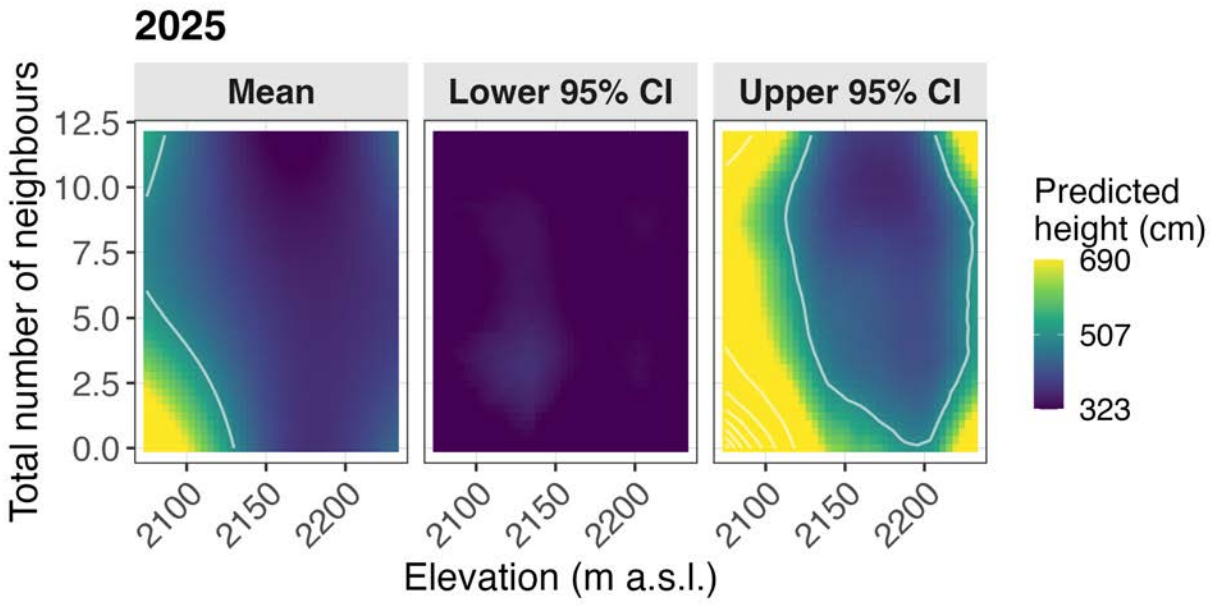

8.5.2 Size-metric dimension

8.5.2.1 *Larix decidua* diameter for 2015 and 2025

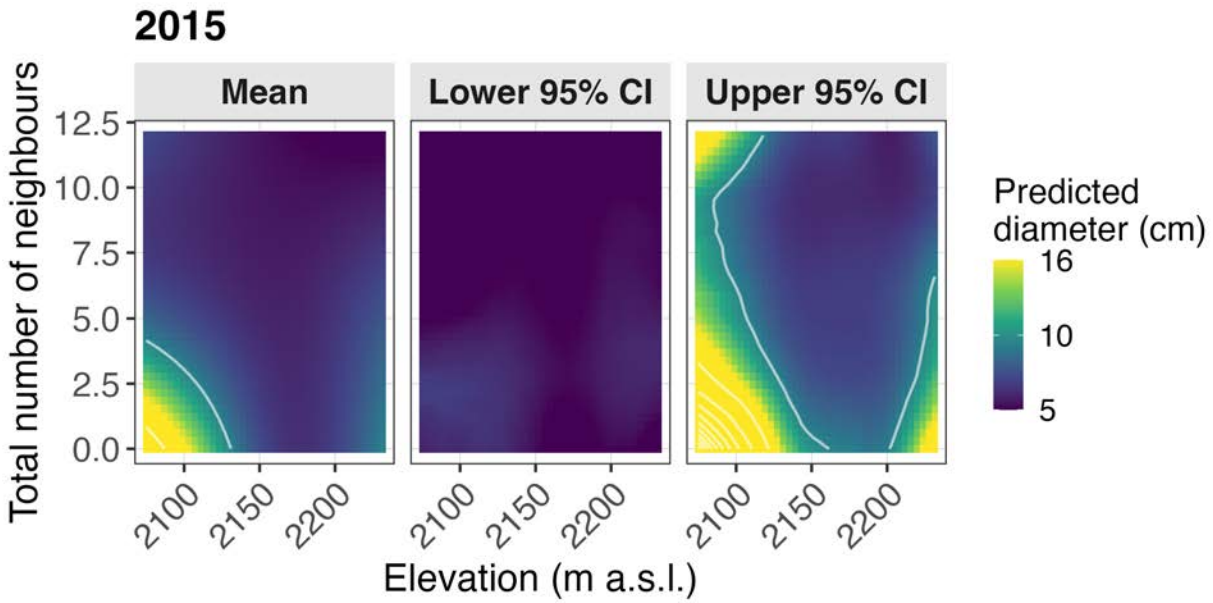

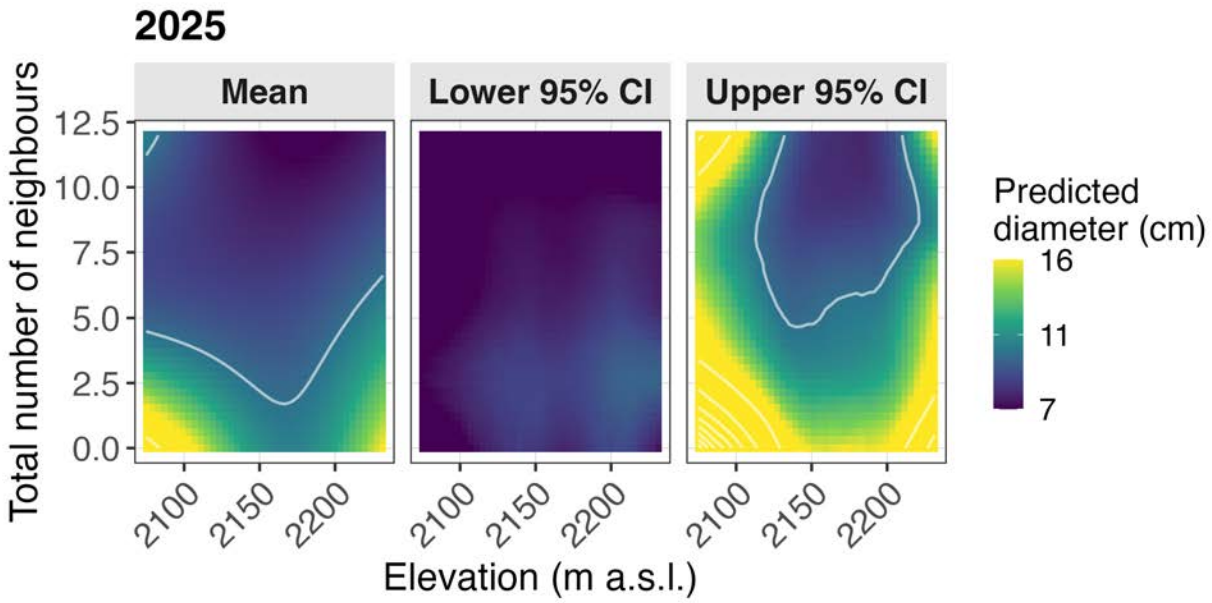

8.5.3 Species dimension

8.5.3.1 *Pinus cembra* height for 1985 and 1995

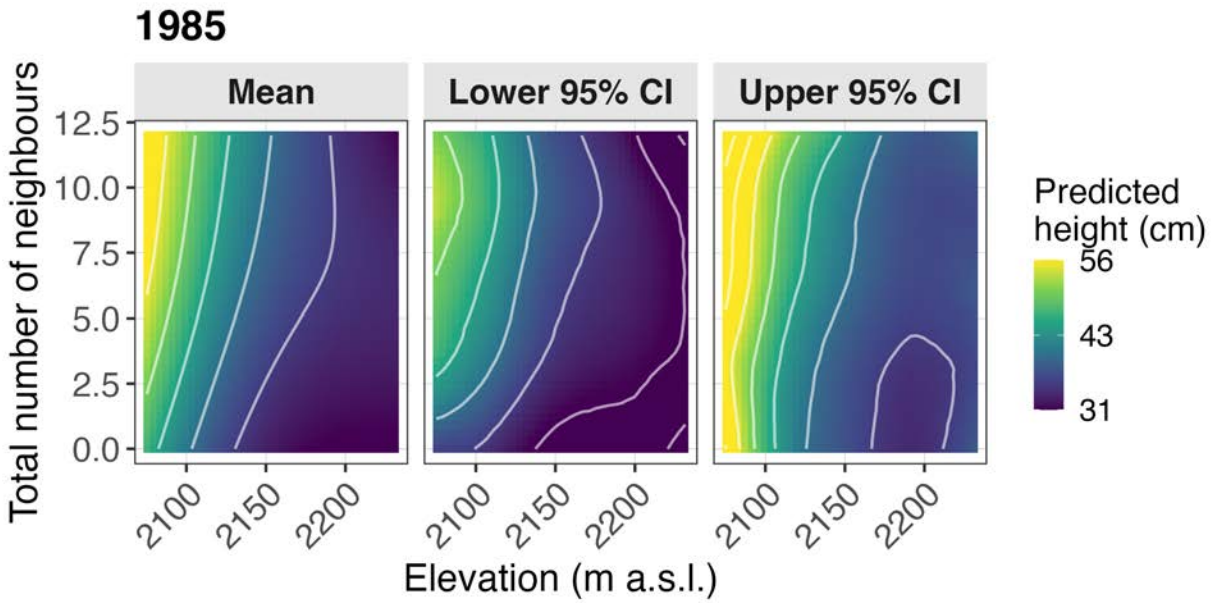

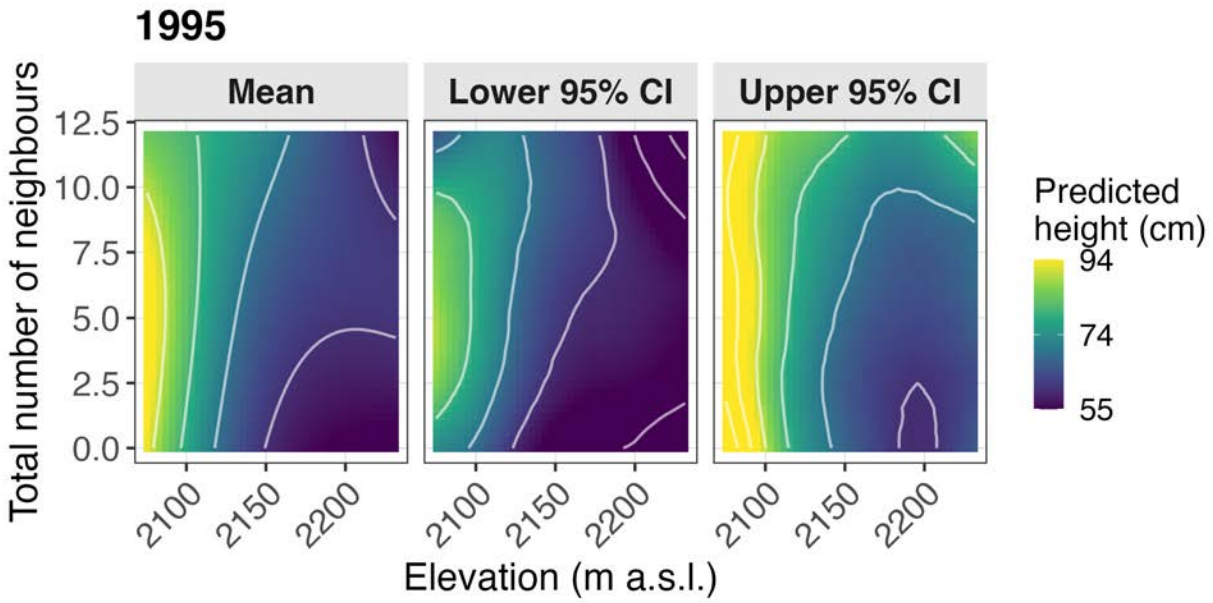

8.5.3.2 *Pinus mugo* height for 1985 and 1995

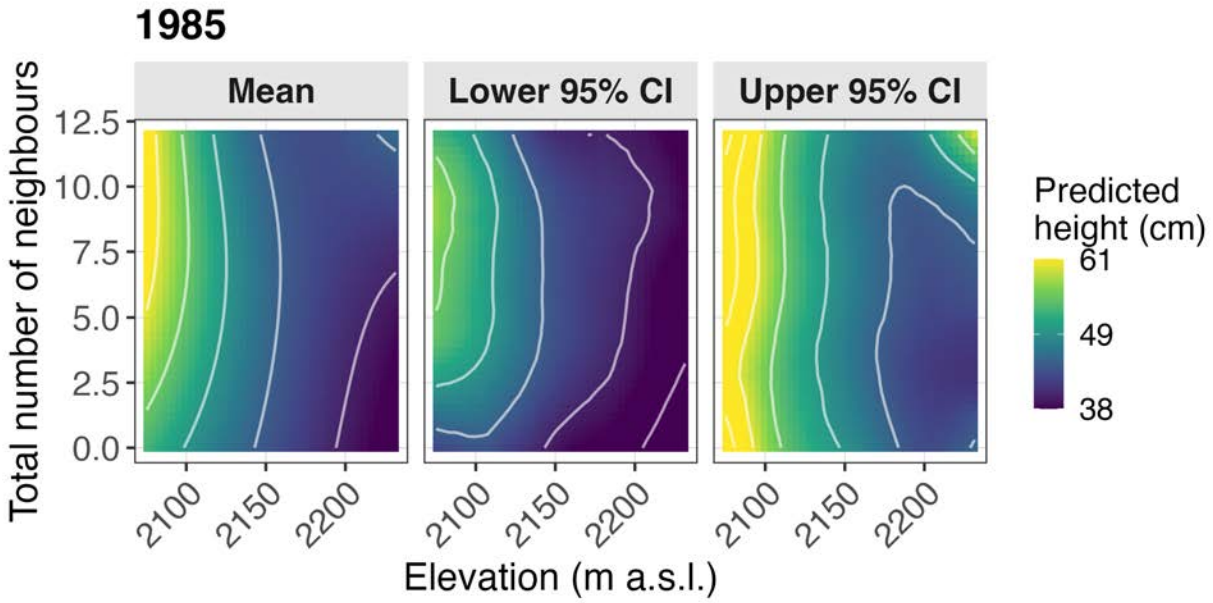

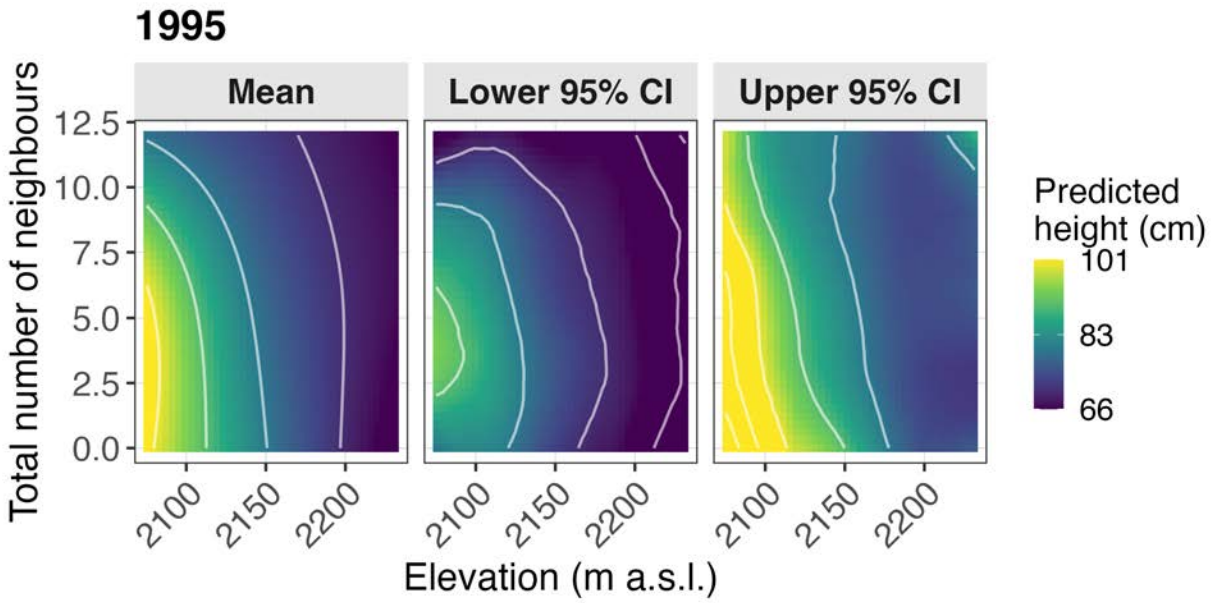
1995
Mean
Lower 95% CI
Upper 95% CI
Total number of neighbours
12.5
10.0
7.5
5.0
2.5
0.0
2100
2150
2200
Elevation (m a.s.l.)
Predicted height (cm)
101
83
66

Eidgenössische Technische Hochschule Zürich
Swiss Federal Institute of Technology Zurich

Declaration of originality

The signed declaration of originality is a component of every written paper or thesis authored during the course of studies. **In consultation with the supervisor**, one of the following two options must be selected:

☐ I hereby declare that I authored the work in question independently, i.e. that no one helped me to author it. Suggestions from the supervisor regarding language and content are excepted. I used no generative artificial intelligence technologies[1].

☒ I hereby declare that I authored the work in question independently. In doing so I only used the authorised aids, which included suggestions from the supervisor regarding language and content and generative artificial intelligence technologies. The use of the latter and the respective source declarations proceeded in consultation with the supervisor.

Title of paper or thesis:

When does the stress-gradient hypothesis hold true in a treeline ecotone?

Authored by:
If the work was compiled in a group, the names of all authors are required.

Last name(s):	**First name(s):**
Gisler	Jamila

With my signature I confirm the following:
- I have adhered to the rules set out in the Citation Guidelines.
- I have documented all methods, data and processes truthfully and fully.
- I have mentioned all persons who were significant facilitators of the work.

I am aware that the work may be screened electronically for originality.

Place, date	**Signature(s)**
Zurich, 16.01.26	JG

If the work was compiled in a group, the names of all authors are required. Through their signatures they vouch jointly for the entire content of the written work.

[1] For further information please consult the ETH Zurich websites, e.g. https://ethz.ch/en/the-eth-zurich/education/ai-in-education.html and https://library.ethz.ch/en/researching-and-publishing/scientific-writing-at-eth-zurich.html (subject to change).